uOttawa

L'Université canadienne
Canada's university

FACULTÉ DES ÉTUDES SUPÉRIEURES ET POSTOCTORALES

u Ottawa

L'Université canadienne
Canada's university

FACULTY OF GRADUATE AND POSDOCTORAL STUDIES

Kelly Anne Hoop
AUTEUR DE LA THÈSE / AUTHOR OF THESIS

M.Sc. (Chemistry)
GRADE / DEGREE

Department of Chemistry
FACULTÉ, ÉCOLE, DÉPARTEMENT / FACULTY, SCHOOL, DEPARTMENT

Novel Bioconjugation Methods for Protein Microarrays and Cell Surface Labelling
TITRE DE LA THÈSE / TITLE OF THESIS

John Pezacki
DIRECTEUR (DIRECTRICE) DE LA THÈSE / THESIS SUPERVISOR

CO-DIRECTEUR (CO-DIRECTRICE) DE LA THÈSE / THESIS CO-SUPERVISOR

Robert Ben

Christopher Boddy

Gary W. Slater
Le Doyen de la Faculté des études supérieures et postdoctorales / Dean of the Faculty of Graduate and Postdoctoral Studies

Novel Bioconjugation Methods for Protein Microarrays and Cell Surface Labelling

Kelly Anne Hoop

Thesis submitted to the
Faculty of Graduate and Postdoctoral Studies
In partial fulfilment of the requirements of the

M.Sc. degree in Chemistry

Department of Chemistry
Ottawa-Carleton Chemistry Institute
Faculty of Science
University of Ottawa

Your file Votre référence
ISBN: 978-0-494-65482-8
Our file Notre référence
ISBN: 978-0-494-65482-8

"Nothing in the world is worth having or worth doing unless it means effort, pain, difficulty..."
-Theodore Roosevelt

Acknowledgements

I would like to thank first and foremost my supervisor, Dr. John Paul Pezacki, for his guidance. Not only is he a brilliant scientist and researcher, he is also a warm, generous and kind man. I will always be grateful for the opportunities that he has extended to me. I would also like to thank him for his encouragement and never-failing belief in me.

The work presented in this thesis would not have been possible without the help of the many brilliant minds present at the National Research Council, and I extend my deepest thanks to all of them. To Malgosia Daroszewska, from the Molecular and Nanomaterials Architecture group at SIMS, for her help in all things analytical; HPLC, HPLC-MS, prep-HPLC and MS. To Donald Leek, from the Materials Structure and Function at SIMS, for his help with the NMR experiments. To Simona Moisa from Surfaces and Interfaces at IMS and Dr. Anne Charrier from the Biosensing and Imaging group at SIMS, for their help with XPS experiments. To Yanouchka Rouleau from the Biosensing and Imaging group at SIMS, for her help with tissue culture. Special thanks to Dr. Greg Lopinski and Trevor Mischki for helping me make the transition from chemistry in a flask to chemistry on a surface, for their patience while teaching me and for the helpful tips and conversations. Special thanks to Dr. Li-Lin Tay from the Surfaces and Interfaces group at IMS and to Dr. David Kennedy from the Biosensing and Imaging group at SIMS, for their time spent helping me sort out the world of nanoparticles. To Li Lin for the tireless hours spent imaging my many samples, and to David, for the time spent brainstorming over experiments with me and his friendship.

I would also like to thank the members of the Pezacki lab, past and present, for making me feel welcome in the in the group; there was never a dull day! I would like to especially thank my fellow graduate students, Dr. Selena Sagan, Ragunath Singaravelu and the chemistry boys,

Craig McKay, Marc Legault, Zimmer Qian and Rodney Lyn. We've shared many laughs over the past two years and I will miss you all. A special note goes out to Rodney, who grew to be a dear friend, who was always there to listen to my stories, good or bad!

To my dear friends, Maxine, Luc, Mel and Campbell, who were always there for me; lending a helping hand and cheering me on tirelessly. Lastly, to my family, there are no words to describe the support and love I have received from them over the course of my studies. Dad, thank you for all the words of encouragement you've always had for me. Mom, pour ta grande présence maternelle. Tu as toujours su quand j'avais besoin de tes mots d'encouragement. Merci de tout mon cœur.

Thank you all.

Abstract

Chemical tools play an important role in research across many fields in science. The development of new tools for use in biology is therefore of the utmost importance. This thesis will discuss the development of two new chemically based tools for the field of biology. In the first part, the development of a new bioconjugation reaction will be discussed. The benzoin condensation was explored as a possible new bioconjugation reaction for the functionalization of surfaces with biomolecules. Using thiamine and other N-heterocyclic carbenes, it was shown that aromatic aldehydes can be tethered to a Si surface bearing a second aromatic aldehyde in aqueous media. In the second part, development of a new imaging technique will be discussed. Surface enhanced Raman scattering was successfully employed to image multiple targets on the surface of a cell. The design and synthesis of various Raman active ligand functionalized Ag nanoparticles allowed for the simultaneous imaging of two membrane proteins present in cardiomyocyte cells.

Table of Contents

List of Abbreviations

Ab	antibody
ABPP	activity based protein profilling
Ag	silver
amide-BA	4-formyl-N-[2-(2-hydroxy-ethoxy)-ethyl]-benzamide
amine-BA	4-[2-(2-hydroxy-ethoxy)ehylamino]-benzaldehyde
APTES	3-aminopropyltriethoxysilane
ATR	attenuated internal reflectance
Au	gold
β_2AR	β2 adrenergic receptor
BA	benzaldehyde
BSA	bovine serum albumin
CF_3-BA	4-(trifluoromethyl)benzaldheyde
CuAAC	copper catalyzed Huisgen azide-alkyne 3+2 cycloaddition
DMMB	deuterated mercaptomethylbenzene
DTSP	dithiobis(succinimidyl propionate)
DTSP-alkyne	DTSP-propargyl amine
DTSP-boron	DTSP-4-boronic acid-phenyl alanine
DTSP-CN	DTSP-4-cyano-phenyl alanine
DTSP-d_2Gly	DTSP-d2-glycine
DTSP-d_5Phe	DTSP-d5-phenyl alanine
DTSP-NO_2	DTSP-4-nitro-phenyl alanine
EGFR	epidermal growth factor receptor
EG_3SH	2-[2-(2-methoxy-ethoxy)-ethoxy]-ethanethiol
F-BA	4-fluorobenzaldehyde

FT-IR	Fourier transform infrared spectroscopy
GFP	green fluorescent protein
HPLC	high pressure liquid chromatography
IgG	Immunoglobulin G
LC-MS	liquid chromatography mass spectrometry
miRNA	microRNA
MMBN	4-(mercaptomethyl)benzonitrile
MMBNO	4-(mercaptomethyl)nitrobenzene
MMByne	4-(mercaptomethyl)ethynylbenzene
NHC	N-heterocyclic carbine
NMR	nuclear magnetic resonance
NO_2-BA	4-nitrobenzaldehyde
NP	nanoparticle
OMe-1-benzoin	2-hydroxy-2-(4-methoxy-phenyl)-1-phenyl-ethanone
OMe-2-benzoin	2-hydroxy-1-(4-methoxy-phenyl)-2-phenyl-ethanone
OMe-BA	4-methoxybenzaldehdye
SERS	surface enhanced Raman scattering
SiO_2	silicon oxide
TEA	triethylamine
XPS	X-ray photoelectron spectroscopy
PBS	phosphate buffered saline solution
Qdots	quantum dots

List of Figures

List of Tables

Chapter 1: Introduction

The work in this thesis concerns bioorthogonal chemical reactions and how they are applied in life sciences. Specifically it will focus on novel methods for the functionalization of microarrays and the labelling of mammalian cells. Orthogonal is defined by the Merriam-Webster dictionary as "statistically independant".[1] The term orthogonal, can be applied to many concepts in chemistry, including protecting group chemistry, stereo and regioselectivity and chiral synthesis. The term is even more relevant when it is applied to chemical biology. Within this realm of chemistry, many experiments are deemed to be bioorthogonal, meaning that they take place within a biological setting, but without interacting with it. When thinking about bioorthogonality, two key concepts will be discussed within this thesis, orthogonal conjugation reactions and orthogonal labelling reactions for cell surface imaging.

1.1 Bioorthogonal Chemical Reactions

Synthetic organic chemists have at their disposal a veritable arsenal of reactions to choose from when designing the synthesis of complex molecules. These reactions have been perfected over the years and much research continues towards the development of novel applications of these reactions. Chemical biologists however are not as lucky. Reactions that are employed within biological systems, or even just in the presence of biomolecules, must rigorously adhere to strict conditions.[2] The reaction must be high yielding, with minimal by products. It must proceed under mild conditions, ideally at neutral pH, 37°C and in water without the need for additional reagents. Most importantly the reactive groups must be benign to the reaction environment. Additionally, if the reaction milieu is within a living system the reaction components must not be cytotoxic. While these restrictions are highly limiting, there

does exist a small number of reactions that are considered to be bioorthogonal. I will briefly discuss the most prominent ones, as well as give examples of their recent uses in the field of chemical biology.

1.1.1 Staudinger Ligation

The Staudinger reaction was originally reported in 1919 by Staudinger and Meyer, where they described the reaction between a tertiary phosphine and an organic azide to produce phospho-azide compounds,[3, 4] which decompose to form a terminal amine and phosphine oxide as stable byproducts when exposed to water. The Bertozzi group was the first to see the potential of the Staudinger reaction as a bioorthogonal reaction, and in 2000 reported their modifications to turn this classic organic reaction into one that could be used within a biological environment to ligate two molecules together.[5, 6] (Figure 1.1 A) When examining the original reaction, we can see why the Staudinger reaction was such an attractive candidate for bioorthogonal chemistry. Both reactive groups, the azide and phosphine, are not functional groups that are typically found in nature and are non-reactive to biological environments.[5] A problem lies however in the aza-ylide intermediate, which is not stable in water, and readily undergoes hydrolysis to yield the amine and phosphine oxide.[7] In order to overcome this stability problem, a phosphine reagent with an electrophilic trap was designed that would trap the unstable aza-ylide in a intramolecular cyclization. By appending a methyl ester group to one of the phenyl groups of tripheylphospine they were able to create a phosphine that, once reacted with the azide to from the aza-ylide, would then undergo cyclization to form an amide. In addition to overcoming the stability issues by trapping the aza-ylide in an amide bond, the ligation aspect of the reaction was also addressed. By additionally decorating the same phenyl group with a molecule of interest, it would then be covalently linked to whatever carried the azide tag.

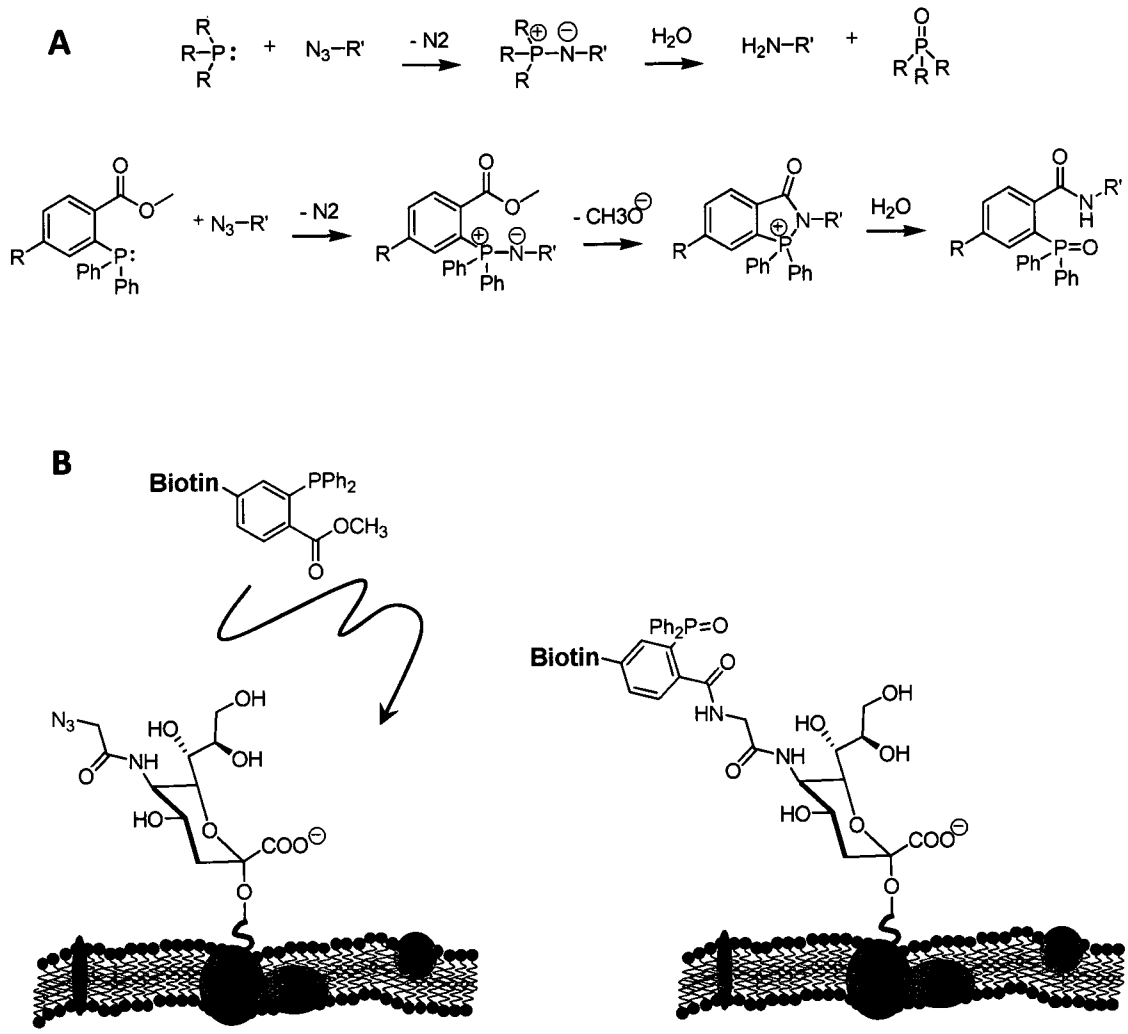

Figure 1.1 Staudinger ligation. **A** Original Staudinger reaction (top) and modified Staudinger ligation (bottom). **B** Example of utility of the Staudinger ligation by Bertozzi for the labelling of cell surface glycans. Adapted from *Science* **2000,** 287, (5460), 2007-2010.[5]

One of the first uses of the Staudinger ligation as a bioorthogonal reaction was in the detection of cell surface glycans. (Figure 1.1 B) The Bertozzi group successfully incorporated an azide tagged sugar onto a cell surface by using the cells own machinery. Then using the modified Staudinger ligation reaction they were able to ligate a biotin molecule to each of these sugar residues bearing an azide.[5] This example is just one of the many that use the Staudinger Ligation as a bioconjugation tool.[8, 9]

1.1.2 Huisgen Azide-Alkyne [3+2] Cycloaddition

Like the Staudinger ligation, the Huisgen [3+2] cycloaddition makes use of the azide functionality as one of its reacting partners; the phosphine reagent is however replaced by a terminal alkyne. The original publication by Huisgen describes the reaction between unactivated alkynes and azides to form substituted triazoles.[10, 11] The reaction may initially seem attractive in terms of bioorthogonality since both reactant groups are just that, orthogonal to biological environments. However the original reaction requires the use of high temperatures or high pressures in organic solvents, making it impossible to use within a delicate biological environment. In 2002 both the Mendal and Sharpless groups reported a copper (I) catalyzed version of the Huisgen azide-alkyne [3+2] cycloaddition.[12, 13] (Figure 1.2 A)

The Mendal group first investigated the Huisgen reaction with copper as a means to mildly and efficiently produce peptidotriazoles by solid phase synthesis.[13] They reported that by reacting a terminal copper acetylide, where the alkyne is part of a modified peptide bound to resin, with an azide they obtained the desired 1,4-substituted 1H-[1,2,3]-triazoles with almost quantitative conversions and purities ranging from 75-99%. Most notably the reaction proceeds at 25°C and was found to be tolerant of most protecting groups used in solid phase synthesis (Fmoc, Boc, tert-butyl, trityl, and Pmc groups), as well as free reactive groups usually found

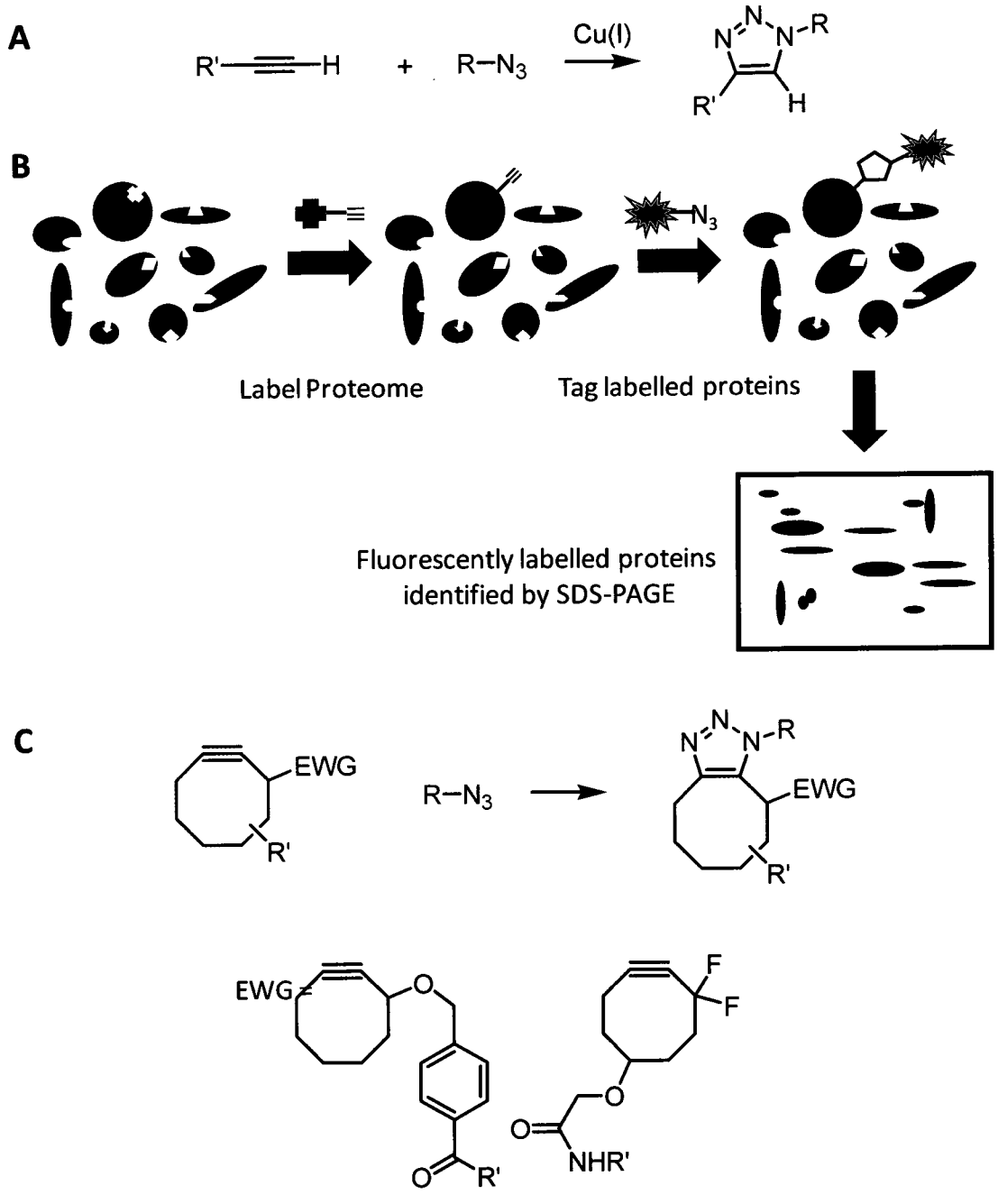

Figure 1.2 The Huisgen [3+2] cycloaddition. **A** The Huisgen [3+2] cycloaddtion catalyzed by copper (CuCAA))as report idependently by Mendal and Sharpless. **B** Example of utlitiy of the CuCAA in activity based protein profiling developed by Cravatt. Adapted from *J. Am. Chem. Soc.* **2003,** 125, (16), 4686-4687.[14] **C** Modification of the Huisgen [3+2] cycloaddtion allowing for the omission of copper for *in vivo* use.

within peptides, including thioethers, esters, amides, ethers, carboxylic acids and amines. The reaction also did not modify sensitive residues such as methionine, tryptophan or cysteine. While the research by the Mendal group proved a step in the right direction by getting rid of the requirement of the elevated pressure and/or temperature and by showing that the reaction is tolerant of most amino functional groups, all their reactions were still conducted in organic solvent.

At the same time as the Mendal paper was published, the Sharpless group also published their findings into a copper catalyzed Huisgen azide-alkyne [3+2] cycloaddition (CuAAC). They reported the same reaction between terminal alkynes and organic azides taking place at ambient temperature, this time using copper (II) salts reduced in situ to provide the copper (I) catalyst.[12] The solvents screened this time include more bio-friendly ones such as aqueous tert-butyl alcohol or ethanol and even water on its own. A high tolerance for functional groups was also reported, but the Sharpless group went one step further towards the eventual use of the reaction in a biological environment to note that reaction proceeds well in human plasma. They proceeded to show in a second paper that the CuAAC can in fact be used in bioconjugation.[15] By first decorating the outer protein shell of the Cowpea mosaic virus with either azides or alkynes they were successful in ligating azide or alkyne tethered dyes to the surface of the virus. They reported that the addition of a copper binding ligand enhanced the rate of the reaction. Also, the ascorbate reducing agent was changed for the milder tris(carboxyethyl)phosphine in order to conserve the integrity of the viral capsid (protein shell). These modifications allowed the Sharpless group to conduct the first bioconjugation by the CuCAA.[15]

The CuAAC has gained most attention for its use in activity based protein profiling (ABPP), a technique pioneered by Benjamin Cravatt.[16, 17] ABPP uses small molecule probes to report on the activity of enzymes within a complex system. (Figure 1.2 B) Previously, ABPP was carried out *in vitro* on cell lysates since the large size of the probes used limited their cellular uptake.[14] Cravatt developed a "tag free" method of ABPP where the small molecule probe and reporter tag are separate from each other.[14] To first test whether the CuAAC conditions were compatible with a complex proteomic mixture, cell lysates were incubated with a phenyl sulfonate ester probe bearing an azide functionality. After incubation, the lysates were treated to the CuAAC reaction conditions developed by Sharpless with a rhodamine-alkyne tag and the proteins separated by SDS-PAGE. Enzymes previously identified using a rhodamine phenyl sulfonate ester probe were similarly identified using the new "tag-free" method. It was also shown that this method was efficient in labelling enzymes *in vivo*, where the probe was first administered to either live cells or live mice. The CuAAC reaction to ligate the tag to the labelled enzyme was preformed *in vitro*, however still the presence of a highly complex biological environment.[14] This technique continues to be used frequently in the field of proteomic research.

While the Sharpless and Cravatt groups have shown that the CuAAC reaction can be used to ligate biomolecules to "tags", there comes a problem when applying the reaction to a fully *in vivo* experiment since the copper catalyst can become toxic to the organism. In 2004, the Bertozzi group reported their preliminary results into the development of reagents for a copper-free Huisgen azide-alkyne [3+2] cycloaddition.[18] (Figure 1.2 C) Using a cyclooctyne derivitized with an electron withdrawing group, they reported the labelling of azide-bearing sugars on the cell surface in live cell experiments. This first generation reagent employed an ether linkage as the electron withdrawing substituent, and also provided the means to

incorporate biotin as the tag. They have since then optimized the cycloalkyne reagent, replacing the ether with two fluorine atoms as an electron withdrawing group and installing a tether at C_6 to incorporate a desired tag, either biotin or a fluorescent molecule.[19] Fluorine was chosen as an electron withdrawing group as opposed to a carbonyl group so as not to create a Michael accepter that could react with various biological nucleophiles, thus maintaining the bioorthogonality of the reagent.

1.2 Probing Living Systems

Many tools have been developed to help us better understand living systems, most of which must be orthogonal to their surrounding milieu in order to gain a true understanding of the system. Examples of rapid and high throughput types of tools include various forms of microarrays including DNA, RNA and protein based arrays that can probe cells and tissues at the genomic or proteomic level. Also, imaging tools including fluorescent proteins and dyes as well as quantum dots and nanoparticles have enabled the visualization of the quantity and localization of specific molecules in living systems. While the body of this thesis discusses the development of new techniques in these fields, highlights of existing techniques will be discussed now.

1.2.1 Microarrays

DNA, RNA and protein microarrays have many different functions and have led to a deeper understanding of many diverse living systems, primarily by measuring the relative quantity of many different molecules simultaneously in a high throughput fashion. For example, in 2000, MacBeath and Schreiber published work towards developing protein microarrays that could be used to probe protein function.[20] They have shown that protein microarrays can be

used to detect protein-protein interactions by successfully visualizing the interaction between two known protein pairs. In their paper, they successfully visualized binding of protein G to immunoglobulin G; and p50 (of the nuclear factor NF-kB complex) to the NF-kB inhibitor IkBa by first immobilizing protein G and p50 onto glass slides and probing the surface with fluorescent conjugates of their pairs.[20] Additionally they were able to show selective binding between the FKBP12-rapamycin binding domain of FKBP-rapamycin–associated protein and the human immunophilin FKBP12 only when rampamycin, a small molecule necessary for binding, is present. By using different fluorophores for each protein pair, they were able to visualize binding of all three protein pairs on the same chip, showing that this technology can be amenable to high throughput screening of many proteins at once.

In 2004, the Cravatt group published their work towards the development of microarray based ABBP, where the pre-labelled proteome is incubated with a microarray of antibodies. The labelled proteins are captured and subsequently identified based on where they bind on the microarray.[21] This microarray based ABPP offers an advantage over traditional ABPP experiments by allowing high throughput. In traditional ABPP, hits are identified first by gel fluorescence experiments and the enzyme identified in a second step by mass spectrometry. This microarray approach combines these two steps into one, allowing multiple proteins to be assessed for activity and identified simultaneously.[21]

Also in 2004, the Croce group published their work into the fabrication of an oligonucleotide microarray that allowed for the quick screening of hundreds of small microRNA (miRNA) sequences to look for changes in expression levels.[22] miRNAs are small non coding RNAs and play a role in gene regulation[23] and some studies suggest that miRNAs play a role in cancer development.[24] Traditional methods used to study RNA are time consuming and require

large sample amounts, and often RNAs with low expression levels can be missed. By using a microarray platform, miRNA expression levels can be studied rapidly and with very little sample. In their microarray design, 368 oligos were designed against 248 miRNAs and 15 tRNAs (as positive controls) found in both humans and mouse and attached them to commercially available polymer coated slides. Total RNA from human and mouse samples were evaluated for expression levels of the miRNA by first labelling the total RNA with biotin and then hybridizing the labelled RNA to the microarray slide. The slide was then processed by treatment with Streptavidin-Alexa647 to fluorescently label any hybridized oligos. Slides were then scanned and signal intesnisty was used to establish relative expression levels of all miRNA in the different samples. This work has shown that microarrays are a usefully tool in the study of miRNA and provide valuable knowledge about miRNA expression levels and their correlation to different cancers.[25-27]

1.2.2 Cellular Imaging

Cellular imaging can be made difficult by the lack of contrast in cells. The easiest way to overcome this contrast issue is to add a label that offers some kind of enhancement. The most common label that is used in cellular imaging is the green fluorescent protein (GFP). The discovery of and its transformation into a molecular biology tool has had such a large impact on science, that its discoverers Osamu Shimomura, Martin Chalfie and Roger Y. Tsien were awarded the 2008 Nobel Prize in Chemistry.[28-30] GFP was first extracted from the jelly fish *Aequorea victoria* in 1961,[31] and its chromaphore identified in 1979[32] by Shimomura and co-workers. GFP is a single peptide chain of 238 amino acid residues folded into cylindrical shape made up of an 11 stranded β barrel wrapped around a α helix, with the fluorescent chromaphore residing in the center of the cylinder made up of the spontaneous reaction of 3 amino acids within the peptide chain; Ser65, Tyr66 and Gly67.[33] (Figure 1.3 A) GFP was first used in imaging when the

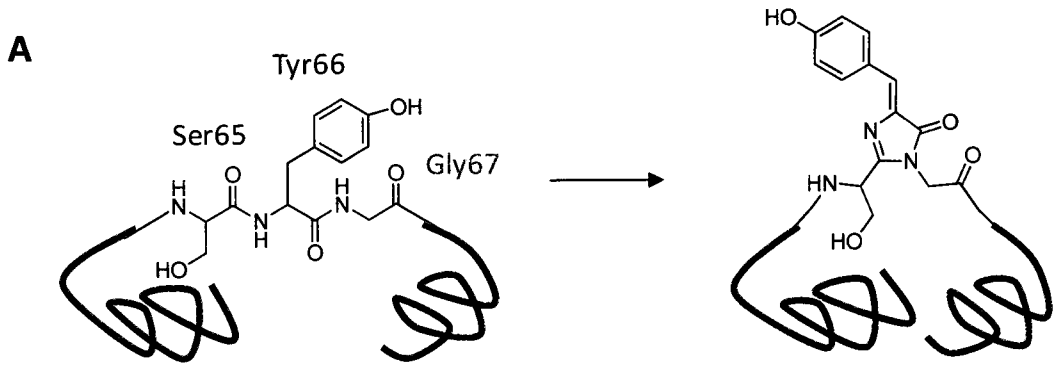

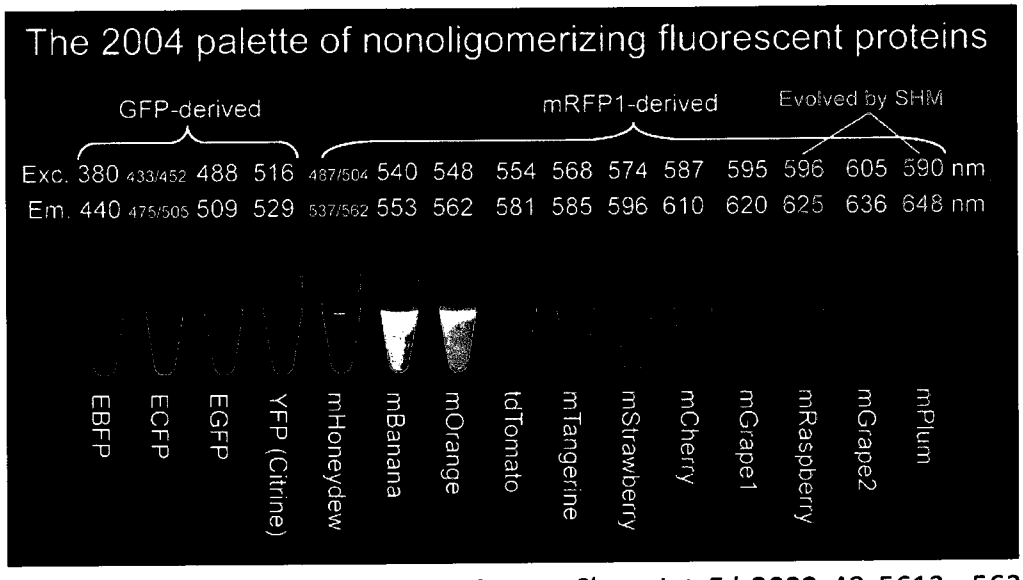

Angew. Chem. Int. Ed. **2009**, 48, 5612 – 5626

Figure 1.3 The green fluorescent protein (GFP). **A** Representation of the chromophore found in GFP. **B** Representive sampling of GFP varients. Protiens were expressed in bacteria and purified. Fluescent emission based on different excitation wavelengths. Taken from *Angew. Chem. Int. Ed.* **2009**, 48, 5612 – 5626.[28]

Chalfie group succeeded in expressing GFP in neuronal cells of the nematode *Caenorhabditis elegans* as a reporter of gene expression.[34] Fusion proteins of GFP were also used to visualize protein location in cells.[35] Work pioneered by the Tsien group, as well as many others, has led to the development of many variants of fluorescent proteins, based on mutations of GFP and red fluorescent protein (isolated from *Discosoma sp*, a form of red coral[36]) with emission spectrums ranging from 440nm to 648nm[28] spanning the colour pallet from blue to red making fluorescent proteins an even more invaluable tool for imaging.[37] (Figure 1.3 B)

While GFP and its variants are still widely used in cellular imaging, new tools are continuously sought after, especially those that can offer advantages over GFP based tools such as increased brightness and increased photostability. Focusing on these two improvements alone would allow for the detection of low abundance targets as well as longer imaging times. The development of quantum dots (Qdots) for imaging is an example of such an improvement. Qdots are single crystals of colloidal semiconductor material, measuring between 2nm to 10nm in diameter, bearing a core/shell composition.[38] The core/shell structure is attributed to Qdots increased brightness as well as their resistance to photobleaching since the shell is a passavating layer, confining excitation by absorption of energy and emission to the core material. The emission wavelengths of Qdots are dependent on their size and the material used, and can range from 400nm to 1350nm.[39] (Figure 1.4) Qdots have been used in many biological imaging applications as the fluorescent tag with great success. Recent work by Tada and co-workers[40] show how the increased photostability of Qdots allows for long term *in vivo* tracking of Qdots mimicking drug delivery to cancerous tumours. Qdots were conjugated to anti-HEGR2 antibodies, which selectively binds human epidermal growth factor receptor 2, a common receptor that is over expressed in many cancer lines. Conjugated Qdots were injected into a mouse model for human breast cancer and the mice were imaged at regular time intervals,

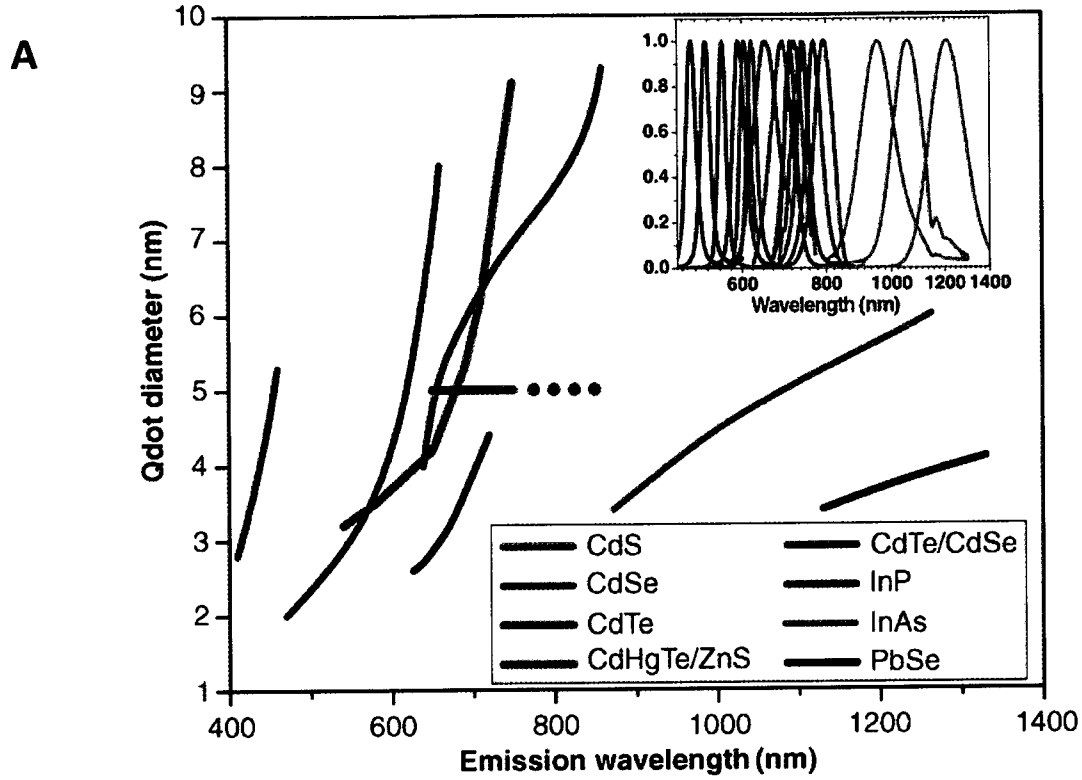

Figure 1.4 Quantum dots (Qdots). Emission and size of various Qdots of different composition. Taken from *Science* **2005** 307, 538 -544.[39]

revealing the specific delivery path of the Qdots from the blood stream to cancer cells.[40] Moving away from fluorescence in imaging is another strategy used to overcome photobleaching. Examples of using Raman active nanoparticles are prevalent in the literature and are discussed in *Chapter 3*.

1.3 Outline

This thesis will discuss the development of two bioorthogonal tools, developed by chemistry to be use to probe biological systems. *Chapter 2* will discuss work towards the development of new surface chemistry techniques for the covalent attachment of proteins to glass for the production of protein microarrays. *Chapter 3* will discuss work towards the development of probes for a multiplex surface enhanced Raman scattering (SERS) system to image multiple cell surface receptors simultaneously.

1.4 Refrences

1. Orthogonal. In *Merriam-Webster Online Dictionary*, 2009.
2. Prescher, J. A.; Bertozzi, C. R., Chemistry in living systems. *Nat. Chem. Biol.* **2005,** 1, (1), 13-21.
3. Staudinger, H.; Jules, M., Über neue organische Phosphorverbindungen III. Phosphinmethylenderivate und Phosphinimine. *Helv. Chim. Acta* **1919,** 2, (1), 635-646.
4. Gololobov, Y. G.; Zhmurova, I. N.; Kasukhin, L. F., 60 Years of Staudinger Reaction. *Tetrahedron* **1981,** 37, (3), 437-472.
5. Saxon, E.; Bertozzi, C. R., Cell surface engineering by a modified Staudinger reaction. *Science* **2000,** 287, (5460), 2007-2010.
6. Saxon, E.; Armstrong, J. I.; Bertozzi, C. R., A "traceless" Staudinger ligation for the chemoselective synthesis of amide bonds. *Org. Lett.* **2000,** 2, (14), 2141-2143.
7. Gololobov, Y. G.; Kasukhin, L. F., Recent advances in the staudinger reaction. *Tetrahedron* **1992,** 48, (8), 1353-1406.
8. Maja, K.; Rolf, B., The Staudinger Ligation - A Gift to Chemical Biology. *Angew. Chem. Int. Ed.* **2004,** 43, (24), 3106-3116.
9. Hackenberger, C. P. R.; Schwarzer, D., Chemoselective Ligation and Modification Strategies for Peptides and Proteins. *Angew. Chem. Int. Ed.* **2008,** 47, (52), 10030-10074.
10. Rolf, H., 1,3-Dipolar Cycloadditions. Past and Future. *Angew. Chem. Int. Ed. in English* **1963,** 2, (10), 565-598.
11. Huisgen, R., Kinetics and Mechanism of 1,3-Dipolar Cycloadditions. *Angew. Chem. Int. Ed. in English* **1963,** 2, (11), 633-645.
12. Rostovtsev, V. V.; Green, L. G.; Fokin, V. V.; Sharpless, K. B., A stepwise Huisgen cycloaddition process: Copper(I)-catalyzed regioselective "ligation" of azides and terminal alkynes. *Angew. Chem. Int. Ed.* **2002,** 41, (14), 2596-2599.
13. Tornoe, C. W.; Christensen, C.; Meldal, M., Peptidotriazoles on solid phase: [1,2,3]-triazoles by regiospecific copper(I)-catalyzed 1,3-dipolar cycloadditions of terminal alkynes to azides. *J. Org. Chem.* **2002,** 67, (9), 3057-3064.
14. Speers, A. E.; Adam, G. C.; Cravatt, B. F., Activity-based protein profiling in vivo using a copper(I)-catalyzed azide-alkyne [3+2] cycloaddition. *J. Am. Chem. Soc.* **2003,** 125, (16), 4686-4687.
15. Wang, Q.; Chan, T. R.; Hilgraf, R.; Fokin, V. V.; Sharpless, K. B.; Finn, M. G., Bioconjugation by copper(I)-catalyzed azide-alkyne [3+2] cycloaddition. *J. Am. Chem. Soc.* **2003,** 125, (11), 3192-3193.
16. Cravatt, B. F.; Sorensen, E. J., Chemical strategies for the global analysis of protein function. *Curr. Opin. Chem. Biol.* **2000,** 4, (6), 663-668.
17. Adam, G. C.; Sorensen, E. J.; Cravatt, B. F., Chemical Strategies for Functional Proteomics. *Mol. Cell. Proteomics* **2002,** 1, (10), 781-790.
18. Agard, N. J.; Prescher, J. A.; Bertozzi, C. R., A strain-promoted [3+2] azide-alkyne cycloaddition for covalent modification of blomolecules in living systems. *J. Am. Chem. Soc.* **2004,** 126, (46), 15046-15047.
19. Baskin, J. M.; Prescher, J. A.; Laughlin, S. T.; Agard, N. J.; Chang, P. V.; Miller, I. A.; Lo, A.; Codelli, J. A.; Bertozzi, C. R., Copper-free click chemistry for dynamic in vivo imaging. *Proc. Natl. Acad. Sci. U. S. A.* **2007,** 104, (43), 16793-16797.

20. MacBeath, G.; Schreiber, S. L., Printing Proteins as Microarrays for High-Throughput Function Determination. *Science* **2000,** 289, (5485), 1760-1763.
21. Sieber, S. A.; Mondala, T. S.; Head, S. R.; Cravatt, B. F., Microarray Platform for Profiling Enzyme Activities in Complex Proteomes. *J. Am. Chem. Soc.* **2004,** 126, (48), 15640-15641.
22. Liu, C.-G.; Calin, G. A.; Meloon, B.; Gamliel, N.; Sevignani, C.; Ferracin, M.; Dumitru, C. D.; Shimizu, M.; Zupo, S.; Dono, M.; Alder, H.; Bullrich, F.; Negrini, M.; Croce, C. M., An oligonucleotide microchip for genome-wide microRNA profiling in human and mouse tissues. *Proc. Natl. Acad. Sci. U. S. A.* **2004,** 101, (26), 9740-9744.
23. Bartel, D. P., MicroRNAs: Genomics, Biogenesis, Mechanism, and Function. *Cell* **2004,** 116, (2), 281-297.
24. Calin, G. A.; Sevignani, C.; Dumitru, C. D.; Hyslop, T.; Noch, E.; Yendamuri, S.; Shimizu, M.; Rattan, S.; Bullrich, F.; Negrini, M.; Croce, C. M., Human microRNA genes are frequently located at fragile sites and genomic regions involved in cancers. *Proc. Natl. Acad. Sci. U. S. A.* **2004,** 101, (9), 2999-3004.
25. Lujambio, A.; Calin, G. A.; Villanueva, A.; Ropero, S.; Sánchez-Céspedes, M.; Blanco, D.; Montuenga, L. M.; Rossi, S.; Nicoloso, M. S.; Faller, W. J.; Gallagher, W. M.; Eccles, S. A.; Croce, C. M.; Esteller, M., A microRNA DNA methylation signature for human cancer metastasis. *Proc. Natl. Acad. Sci. U. S. A.* **2008,** 105, (36), 13556-13561.
26. Li, W.; Ruan, K. C., MicroRNA detection by microarray. *Anal. Bioanal.Chem.* **2009,** 394, (4), 1117-1124.
27. Kong, W.; Zhao, J. J.; He, L.; Cheng, J. Q., Strategies for Profiling MicroRNA Expression. *J. Cell. Physiol.* **2009,** 218, (1), 22-25.
28. Tsien, R. Y., Constructing and Exploiting the Fluorescent Protein Paintbox (Nobel Lecture). *Angew. Chem. Int. Ed.* **2009,** 48, (31), 5612-5626.
29. Osamu, S., Discovery of Green Fluorescent Protein (GFP) (Nobel Lecture). *Angew. Chem. Int. Ed.* **2009,** 48, (31), 5590-5602.
30. Chalfie, M., GFP: Lighting Up Life (Nobel Lecture). *Angew. Chem. Int. Ed.* **2009,** 48, (31), 5603-5611.
31. Osamu, S.; Frank, H. J.; Yo, S., Extraction, Purification and Properties of Aequorin, a Bioluminescent Protein from the Luminous Hydromedusan, *Aequorea*. *J. Cell. Comp. Physiol.***1962,** 59, (3), 223-239.
32. Shimomura, O., Structure of the chromophore of *Aequorea* green fluorescent protein. *FEBS Lett.***1979,** 104, (2), 220-222.
33. Ormö, M.; Cubitt, A. B.; Kallio, K.; Gross, L. A.; Tsien, R. Y.; Remington, S. J., Crystal Structure of the *Aequorea victoria* Green Fluorescent Protein. *Science* **1996,** 273, (5280), 1392-1395.
34. Chalfie, M.; Tu, Y.; Euskirchen, G.; Ward, W. W.; Prasher, D. C., Green fluorescent protein as a marker for gene expression. *Science* **1994,** 263, (5148), 802-805.
35. Wang, S.; Hazelrigg, T., Implications for *bcd* mRNA localization from spatial distribution of *exu* protein in *Drosophila* oogenesis. *Nature* **1994,** 369, (6479), 400-403.
36. Matz, M. V.; Fradkov, A. F.; Labas, Y. A.; Savitsky, A. P.; Zaraisky, A. G.; Markelov, M. L.; Lukyanov, S. A., Fluorescent proteins from nonbioluminescent *Anthozoa* species. *Nat. Biotech.* **1999,** 17, (10), 969-973.
37. Zhang, J.; Campbell, R. E.; Ting, A. Y.; Tsien, R. Y., Creating new fluorescent probes for cell biology. *Nat. Rev. Mol. Cell. Biol.* **2002,** 3, (12), 906-918.
38. Walling, M.; Novak, J.; Shepard, J. R. E., Quantum Dots for Live Cell and In Vivo Imaging. *I Int. J. Mol. Sci.* **2009,** 10, (2), 441-491.

39. Michalet, X.; Pinaud, F. F.; Bentolila, L. A.; Tsay, J. M.; Doose, S.; Li, J. J.; Sundaresan, G.; Wu, A. M.; Gambhir, S. S.; Weiss, S., Quantum dots for live cells, in vivo imaging, and diagnostics. *Science* **2005,** 307, (5709), 538-544.
40. Tada, H.; Higuchi, H.; Wanatabe, T. M.; Ohuchi, N., In vivo Real-time Tracking of Single Quantum Dots Conjugated with Monoclonal Anti-HER2 Antibody in Tumors of Mice. *Cancer Res.* **2007,** 67, (3), 1138-1144.

Chapter 2: Surface Functionalization using the Benzoin Condensation:
Towards Oriented Protein Microarrays

2.1 Introduction

Biosensors are devices that use biomolecules to detect a specific analyte within a given sample, and are used in many areas ranging from food science for the detection of food born pathogens[1] to defence for the detection of biological and chemical warfare agents[2] and also include DNA, RNA and protein microarrays. The development of new biosensors is a rapidly growing field. Synthesis of silicon-based biosensor devices, where the silicon components comprise the sensor or the coating (silicon oxide) where sensor elements for detecting biomolecules for sensing are attached.[3] Despite this, there exist only a very limited number of chemical strategies for the bioconjugation and specific orientation of probe molecules such as oligonucleotides and proteins to silicon surfaces that are biocompatible and can proceed in aqueous media. This chapter describes the development of methodology involving thiamine and N-heterocyclic carbene (NHC) catalyzed cross coupling of aldehydes on silicon surfaces.

Much research has gone into developing stable platforms to use in biosensors, specifically hydrogen terminated silicon and silicon-oxide platforms. The most common techniques for the formation of monolayers on hydrogen terminated silicon, include UV irradiation of alcohols and aldehydes, radical reactions of olefins using radical initiator (such as TEMPO) and also reactions with acylchlorides which can then be further fucntionlized.[4] Silanes have been used for many years as a means to attach organic molecules to silicon oxide, or glass and remain an important reagent in the fabrication modified surfaces.[5] Three different types of

silanes exist; chlorosilanes, alkoxysilanes and aminosilanes, all of which react with the surface hydroxides forming Si-O bonds to covalently attach to the surface. Monolayers formed with silanes bearing various functional groups at the terminal end are often used as the starting point in the fabrication of devices, and are often further modified as needed.

Currently the techniques available to functionalize surfaces with proteins are limited. These strategies span 3 major categories: physical immobilization, bioaffinity immobilization and covalent immobilization.[6] (Figure 2.1 A) Physical immobilization implies the non-specific absorption of proteins on to a surface. Intermolecular forces, such as ionic bonds or hydrophobic/hydrophilic interactions, provide the binding force in this immobilization. This leads to a heterogeneous surface of randomly oriented proteins, thus limiting its usefulness since only some proteins will have accessible active sites on these surfaces. Bioaffinity immobilization offers an advantage over physical immobilization since it can allow for the specific orientation of the protein to the surface and provides for a more complete and reproducible coverage of the surface. Bioaffinity immobilization makes use of naturally occurring affinities, most commonly the adivin-biotin system[7] or the histidine-nickel system[8]. Both of these examples necessitate the introduction of a relatively large group (biotin or histidine tag) which can potentially alter the structure of the protein and diminish its activity. Covalent immobilization, where the protein is directly attached to the surface via newly formed covalent bond, offers similar advantages to that of bioaffinity immobilization as it allows for specific orientation and homogenous surface coverage. However, unlike bioaffinity immobilization, the coupling partners employed in covalent immobilization are relatively small, thus minimizing the chance that they will affect the structure and activity of the protein. Covalent immobilization approaches typically make use of bioorthognal chemical reactions. While this technique offers many advantages, there only exists a handfull of reactions that can

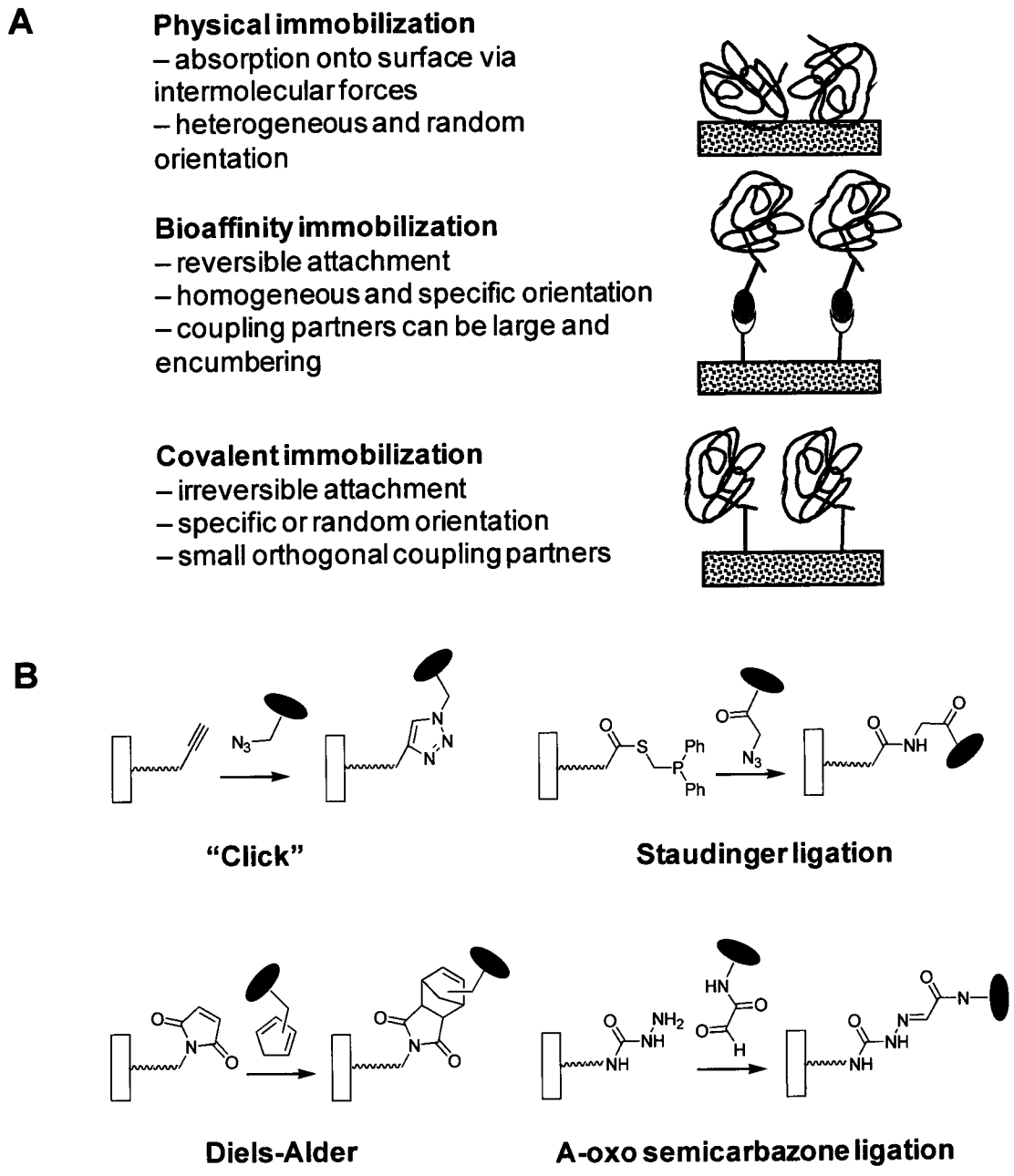

Figure 2.1 Physical and chemical methods for microarray patterning. **A** Schematic for the most common methods for biomolecule immobilization on glass surfaces. **B** Common reactions used for the covalent immobilization of biomolecules. Adapted from *Biomacromolecules* **2007,** 8, (6), 1775.[6]

be employed in a bioorthogonal manner (Figure 2.1 B).[6] The benzoin condensation, originally published in 1919, involves the coupling of two aromatic aldehydes to form an alpha-hydroxy ketone via activation by cyanide.[9] Later on, it was discovered that thiamine, a naturally occurring vitamin, could catalyze that same reaction.[10] (Figure 2.2) Current research into benzoin type reactions has shown that many other N-heterocylic carbenes (NHC) similar to thiamine can also catalyze the reaction in polar protic solvents.[11, 12] These new developments now make the benzoin condensation a good candidate for a new bioorthogonal reaction for covalent immobilization since the catalyst would not be toxic and aromatic aldehydes are functional groups not found in biology.

Conveniently there are a number of approaches for the site-specific incorporation of aldehyde functionality into proteins. For example, unnatural organisms (bacteria) can be created in the laboratory setting that use a 21 amino acid complement, including a new tRNA and tRNA synthase specific for unnatural amino acids. This has been applied broadly for the site-specific incorporation of numerous unnatural amino acids including ketones.[13] Another approach involved the genetic incorporation of a peptide tag which can be post-translationly modified into an aldehyde. This 6 amino acid cystine-containing tag is a substrate for formylglycine-generating enzyme (FGE) which oxidizes cysteine into formylglycine.[14] The site specific incorporation of an aldehyde-bearing unnatural amino acid provides a handle for specific chemical functionalization and possible orientation of proteins onto silicon surfaces.

This chapter will demonstrate that thiamine as well as other NHCs can catalyze the cross-coupling of aromatic aldehydes on both silicon oxide (glass) and on hydrogen terminated silicon surfaces in aqueous media.

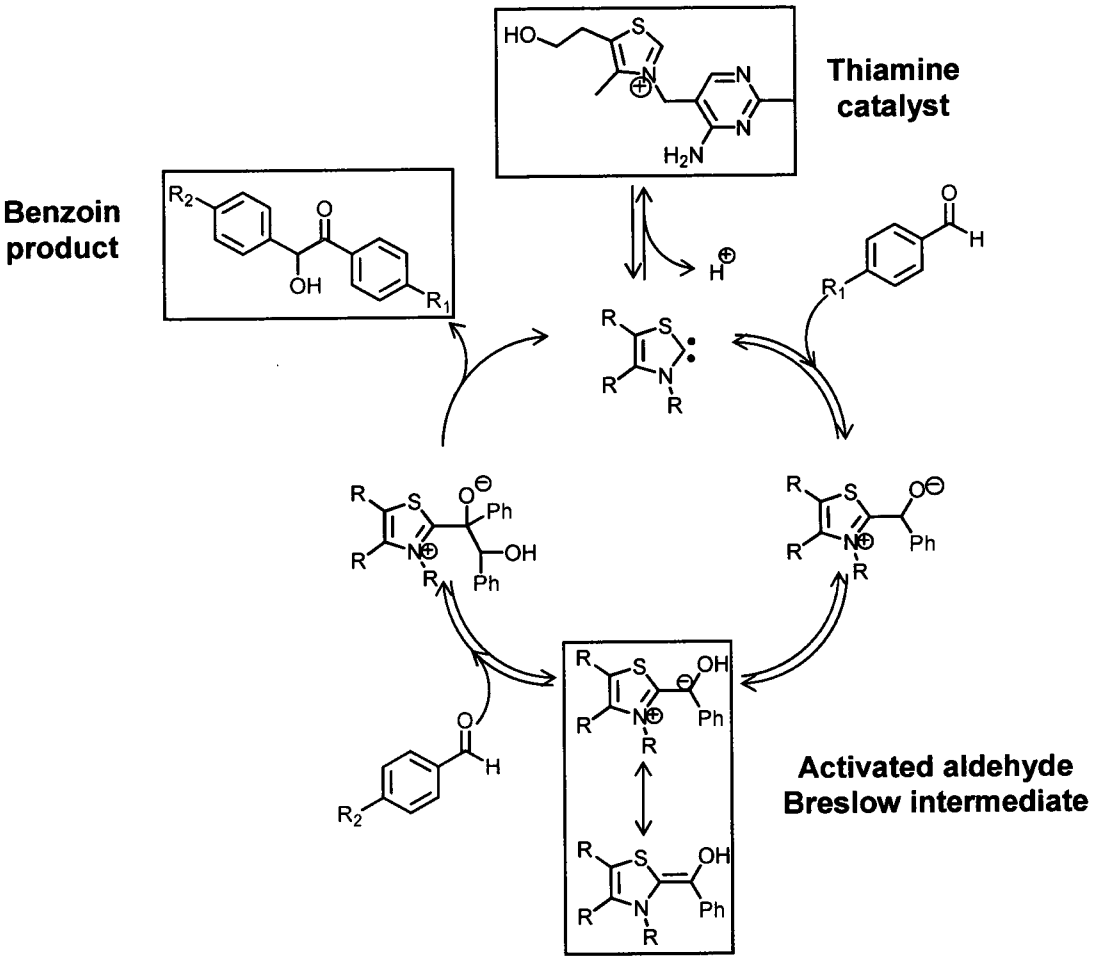

Figure 2.2 Mechanism of the thiamine catalyzed benzoin condensation.

2.2 Results

2.2.1 Solution Optimization of Benzoin Condensation Reactions

Reaction conditions for the cross-coupling in aqueous media were first developed in solution, using as a model the classic benzoin condensation with thiamine as catalyst and high pressure liquid chromatography (HPLC) as the monitoring method. Numerous areas of the reaction were optimized, including solvent, NHC catalyst, NHC catalyst loading, reaction time, base and temperature. The ideal solvent for a bioconjugation reaction is water however this is often problematic since many reactants involved in organic reactions are not soluble in water. Surfactants were initially employed to help solubilise the reaction components by forming micelles, however it was quickly discovered that this addition did not aid the reaction, and that the reaction readily took place in water. A total of 11 NHCs[15-22] were screened, all of which were already known catalysts of umpolung chemistry in organic media (Figure 2.3). At optimal conditions (0.6 mol eq NHC, 0.6 mol eq of triethylamine (TEA), in water at room temperature), 4 NHCs were identified that yielded between 70-90% conversion of benzaldehyde to benzoin in water after 48 hours. HPLC profiles of reaction solutions carried out at higher temperatures were not as clean as those preformed at room temperature. Since a higher temperature did not translate to a significant increase in conversion rate or decrease in reaction time, the ideal temperature for the reaction was left at room temperature.

A small substrate screen was also preformed where 3 different aromatic aldehydes were used to test whether or not substitution at the para position would affect the rate of the reaction. Benzaldehyde (BA) was used as the neutral aldehyde, 4-nitrobenzaldehyde (NO_2-BA) as the electron deficient aldehyde and 4-methoxybenzaldehdye (OMe-BA) as the electron rich

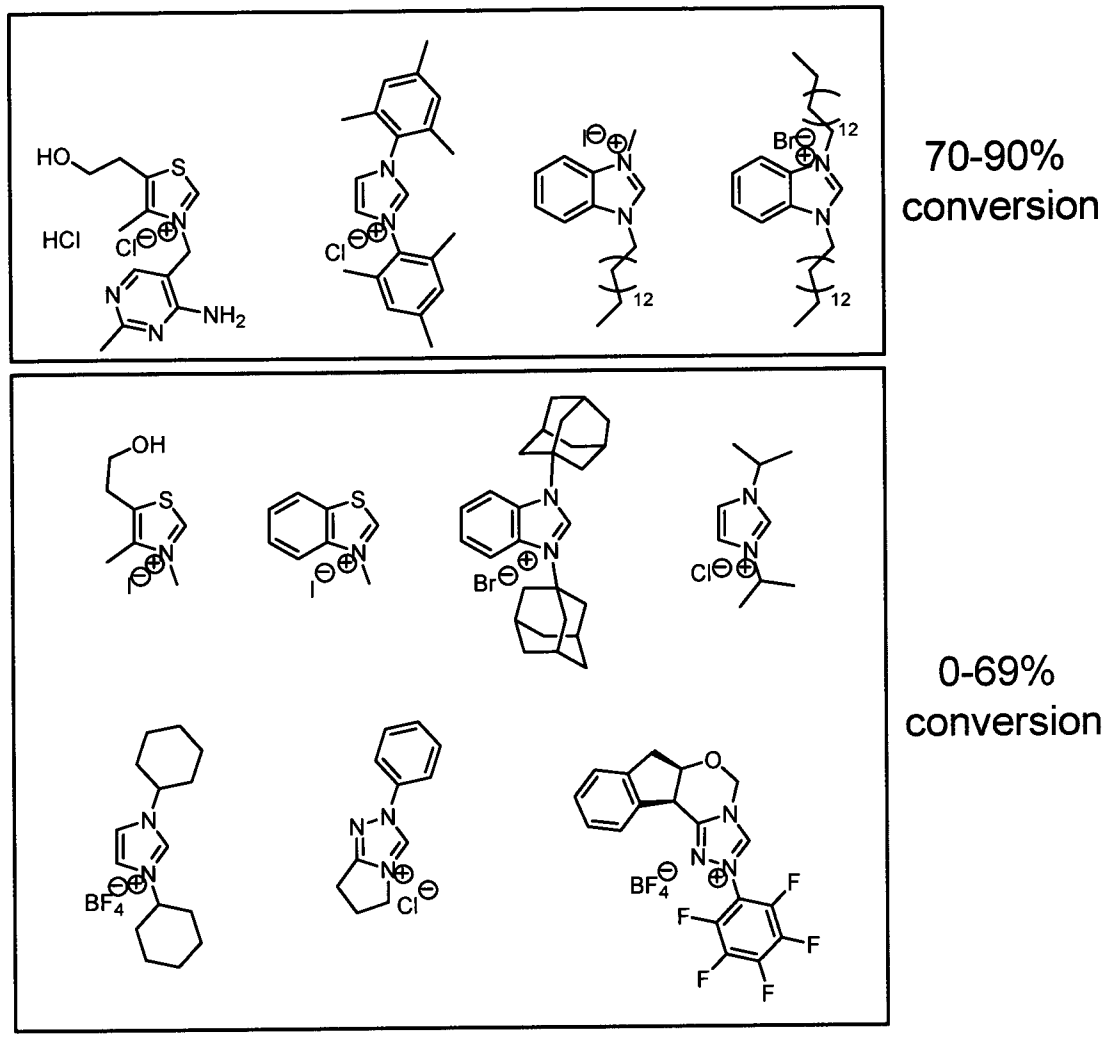

Figure 2.3 N-heterocyclic carbenes (NHCs) in optimization experiments. The structures in the blue box represent NHCs that yielded a greater than 70% conversion rate. The structures in the green box represent NHCs that yielded less than 70% conversion rate.

aldehyde. Reactions were set up to monitor by liquid chromatography-mass spectrometry (LC-MS) the formation of cross products in the neutral/deficient, neutral/rich and deficient/rich systems. Additionally self-coupling within each system was also monitored. The reactions between BA and NO_2-BA (neutral/deficient) and between OMe-BA and NO_2-BA (rich/deficient) yielded no cross-coupling products and only self-coupling of BA and OMe-BA was observed. The reaction between BA and OMe-BA (neutral/rich) yielded 4 products by LC-MS with masses corresponding to the cross-coupling products as well as the self-couplings (Table 2.1 A). A second test was developed using benzaldheyde modified at the para position with a short tether to generate both an electron rich and deficient aldehyde (4-[2-(2-hydroxy-ethoxy)ehylamino]-benzaldehyde (amine-BA) and 4-formyl-N-[2-(2-hydroxy-ethoxy)-ethyl]-benzamide (amide-BA)). Similar results were seen where no self coupling was observed with amide-BA (deficient) but was observed with amine-BA (rich). Interestingly, cross coupling was observed between amine-BA and amide-BA (Table 2.1 B).

2.2.2 FT-IR of Authentic Benzoin Samples on SiO_2

Samples of both isomers of 4-methoxybenzoin (2-hydroxy-1-(4-methoxy-phenyl)-2-phenyl-ethanone (OMe-2-benzoin) and 2-hydroxy-2-(4-methoxy-phenyl)-1-phenyl-ethanone (OMe-1-benzoin)) were prepared. Pure samples were each physisorbed onto a silicon oxide (SiO_2) attenuated internal reflectance (ATR) chips to obtain Fourier transform infrared (FT-IR) spectra (Figure 2.4). Both provided clean spectra, with OMe-2-benzoin showing peaks at 1687cm^{-1} and 1600cm^{-1} corresponding to the C=O stretching vibration and phenyl rings respectively and OMe-1-benzoin showing peaks at 1683cm^{-1} and 1598cm^{-1} corresponding to the C=O stretching vibration and phenyl rings respectively. When comparing the energy of the carbonyl stretching vibration of both compounds to values for other benzoin derivatives found in the literature[23, 24], it is apparent that this value is variable, depending on the substituents on

Table 2.1 A Identification of benzoin products using electron neutral, rich and poor bezaldehdye systems.

Reacting System	Product Identified					
	self coupling			cross coupling		
	neutral[b]	*rich*[c]	*deficient*[d]	*neutral/ rich*	*neutral/ deficient*	*rich/ deficient*
neutral / neutral	yes					
neutral / rich	yes	yes		yes		
neutral / deficient	yes		no		no	
rich / deficient		yes	no			no
deficient / deficient			no			
rich / rich		yes				

a – Identified by MS or LCMS
b – benzaldehyde
c – 4-methoxybenzaldehyde
d – 4-nitrobenzaldehyde

Table 2.1 B Identification of benzoin products using electron rich and poor tethered bezaldehdye systems.

Reacting System	Product Identified[a]			
	self coupling		cross coupling	
	rich[e]	*deficient*[f]	*neutral/ deficient*	*rich/ deficient*
rich / deficient	yes	no		yes
deficient / deficient		no		
rich / rich	yes			

a – Identified by MS or LCMS
e – 4-[2-(2-hydroxy-ethoxy)ehylamino]-benzaldehyde
f – 4-formyl-N-[2-(2-hydroxy-ethoxy)-ethyl]-benzamide

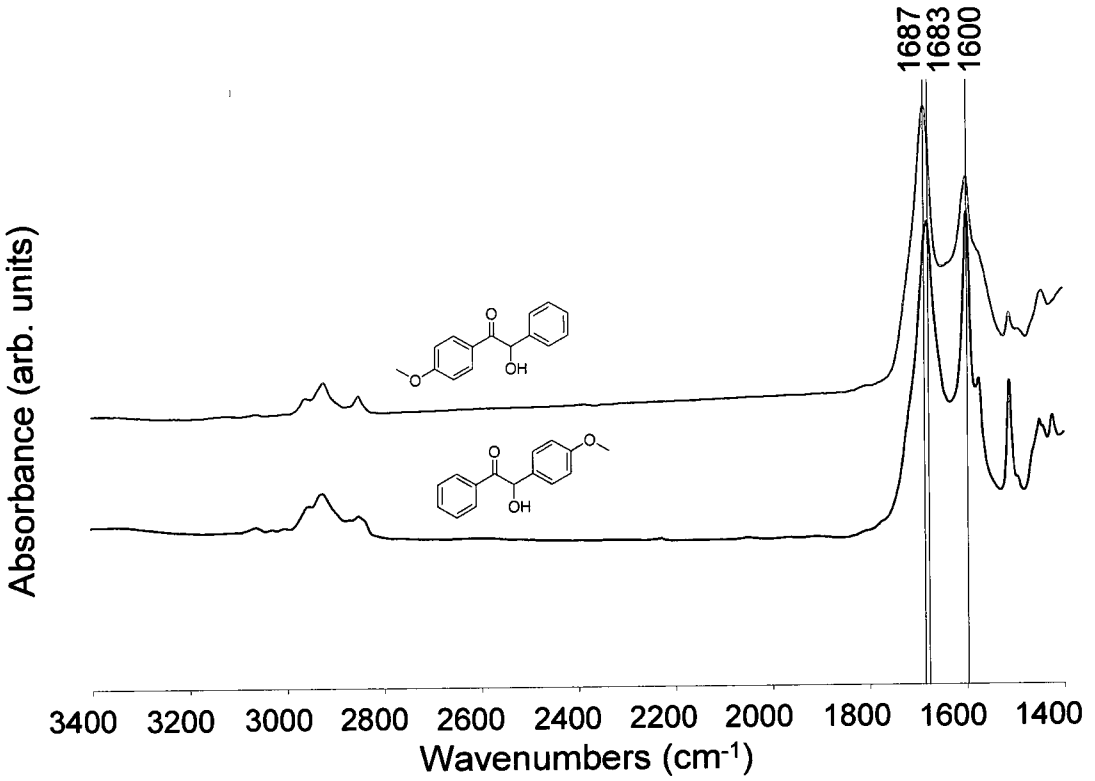

Figure 2.4 FT-IR spectrum of 4-methoxybenzoin samples physisorbed on SiO_2.

the phenyl ring. This apparent variability of the carbonyl peak will become important when analyzing upcoming spectra.

2.2.3 SiO_2 functionalization

2.2.3.1 FT-IR characterization of thiamine catalyzed coupling of OMe-BA to a model surface

A Si ATR chip was prepared as described in *Chapter 4 Material and Methods*. The surface was aldehyde terminated by first reacting the native oxide with 3-aminopropyltriethoxysilane (APTES) to form a terminal amine, followed by reaction with terephthalaldehyde to form an imine, yielding the terminal aldehyde (subsequently referred to as the imine-linker aldehyde surface Figure 2.5A). Peaks in the FT-IR spectrum (Figure 2.6 A) of this surface agreed with the proposed structure, with peaks at 2929cm^{-1} and 2854cm^{-1} corresponding to methylene C-H stretching[25] and the peak at 1645cm^{-1} corresponding to the imine C=N stretching[25]. The small peak observed at 1610cm^{-1} is associated with the phenyl ring and the peak at 1703cm^{-1} corresponds to the C=O stretching of the benzaldheyde[25]. The ATR chip was submitted to the optimized reaction conditions with thiamine and OMe-BA and the reaction progress was monitored by FT-IR (Figure 2.6 A). After 4 hours, the aldehyde peak at 1703cm^{-1} had been drastically reduced and after 24 hours was no longer visible and the peak at 1610cm^{-1} had grown considerably, which is to be expected for the additional phenyl ring in the benzoin product. Control experiments (Figure 2.6 B) were carried out where aldehyde terminated ATR chips were immersed in benzoin reaction conditions, without the NHC (OMe-BA and TEA in water). After 4 hours of reaction time, the FT-IR spectrum showed no significant change. The native oxide was submitted to the same treatment to rule out non-specific absorption. Again no new significant peaks were observed in the FT-IR spectrum.

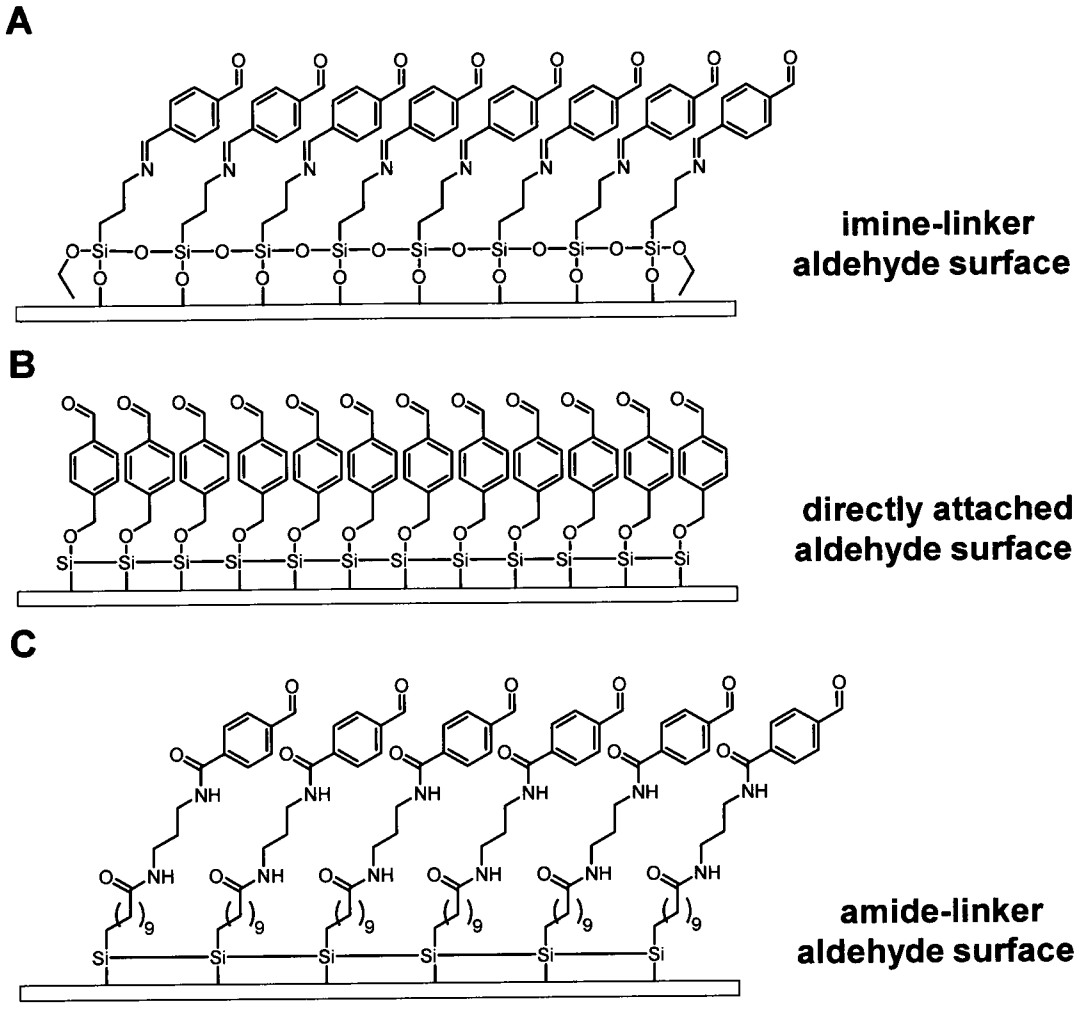

Figure 2.5 Schematic of different surfaces used throughout Chapter 2. **A** Imine-linker aldehyde surface on silicon oxide. **B** Directly attached aldehyde surface on Si(111). **C** Amide-linker aldehyde surface on Si(111).

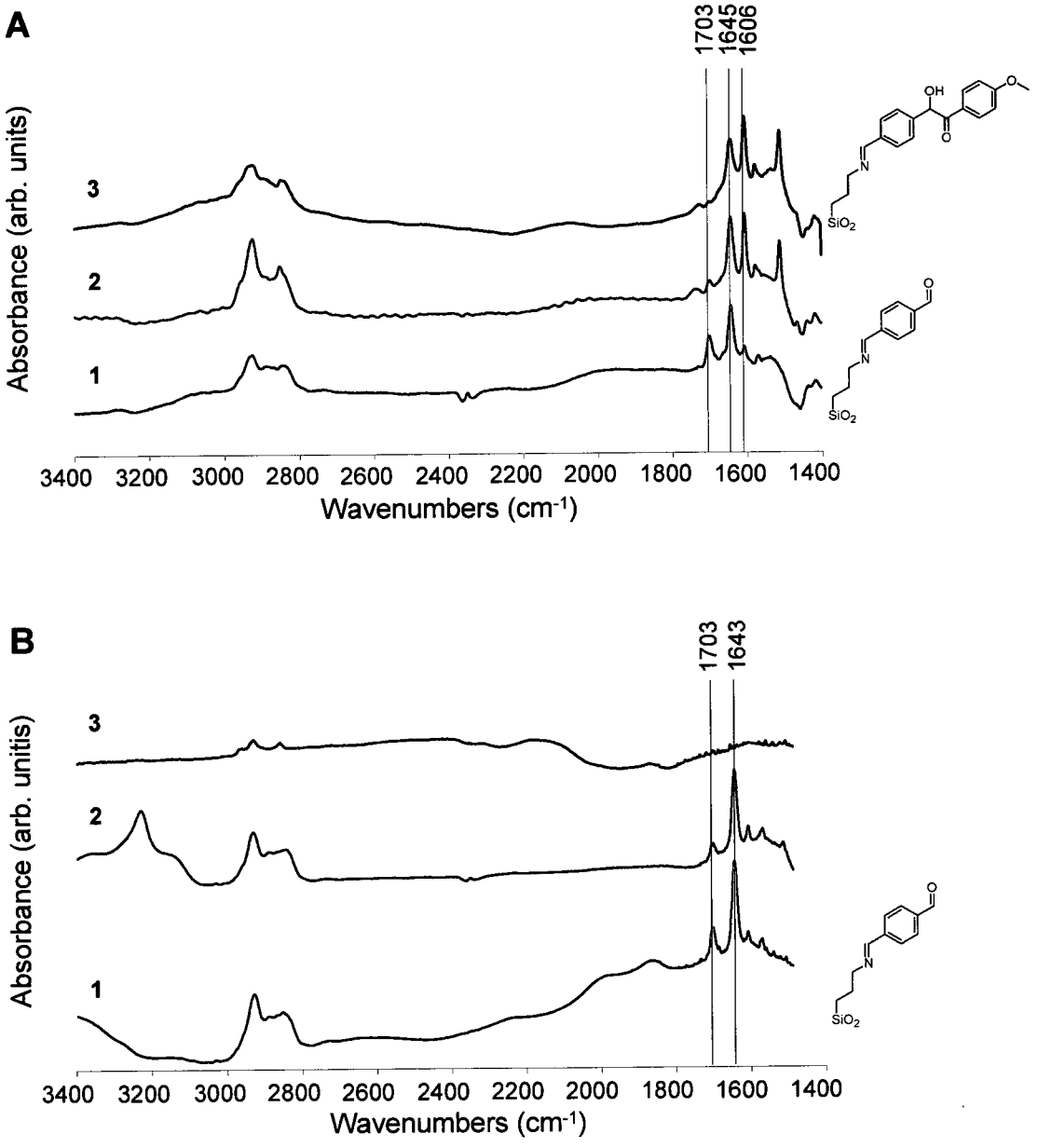

Figure 2.6 FT-IR characterization of thiamine catalyzed coupling of OMe-BA to a model surface. **A** Reaction progression at 0hr (1), 4hrs (2) and 24hrs (3) of conjugation reaction using thiamine as catalyst. **B** Control reactions (no catalyst added) on model surface at 0hr (1) and 4hrs (2) and on native oxide surface at 4hrs (3).

2.2.3.2 FT-IR characterization of thiamine catalyzed coupling of amine-BA to a model surface

In order to test whether a bulkier group would be tolerated at the para position, a tether bearing electron rich benzaldehyde (amine-BA) was used in the same conditions as previously described. The reaction proceeded at a similar rate to that with OMe-BA. The aldehyde carbonyl peak at 1703cm^{-1} greatly reduced after 4 hours and no longer visible after 24 hours. A peak at 1605cm^{-1} corresponding to the phenyl group is also present.

2.2.3.3 FT-IR characterization of NHC catalyzed coupling of OMe-BA to a model surface

During the solution optimization, other NHCs were identified and tested as to whether they would also efficiently catalyze the reaction at the surface. 1,3-Bis(2,4,6-trimethylphenyl) imidazolium chloride was used with the imine-linker aldehyde surface. Reaction conditions in this case were adjusted as only one equivalent of base was needed to fully deprotonate the NHC. The reaction was monitored by FT-IR and was observed to be complete after only 4 hours since the aldehyde carbonyl peak at 1703cm^{-1} was no longer visible and the phenyl peak at 1606cm^{-1} had dramatically increased in intensity.

2.2.3.4 FT-IR characterization of thiamine catalyzed coupling of F-BA to a model surface

4-Fluorobenzaldehyde (F-BA) was used in place of OMe-BA to test whether an electron deficient aldehyde would affect the rate of the reaction as seen in the solution based optimization experiments. The imine-linker aldehyde terminated surface was employed once again and the reaction progression was monitored by FT-IR (Figure 2.7 A). In agreement with

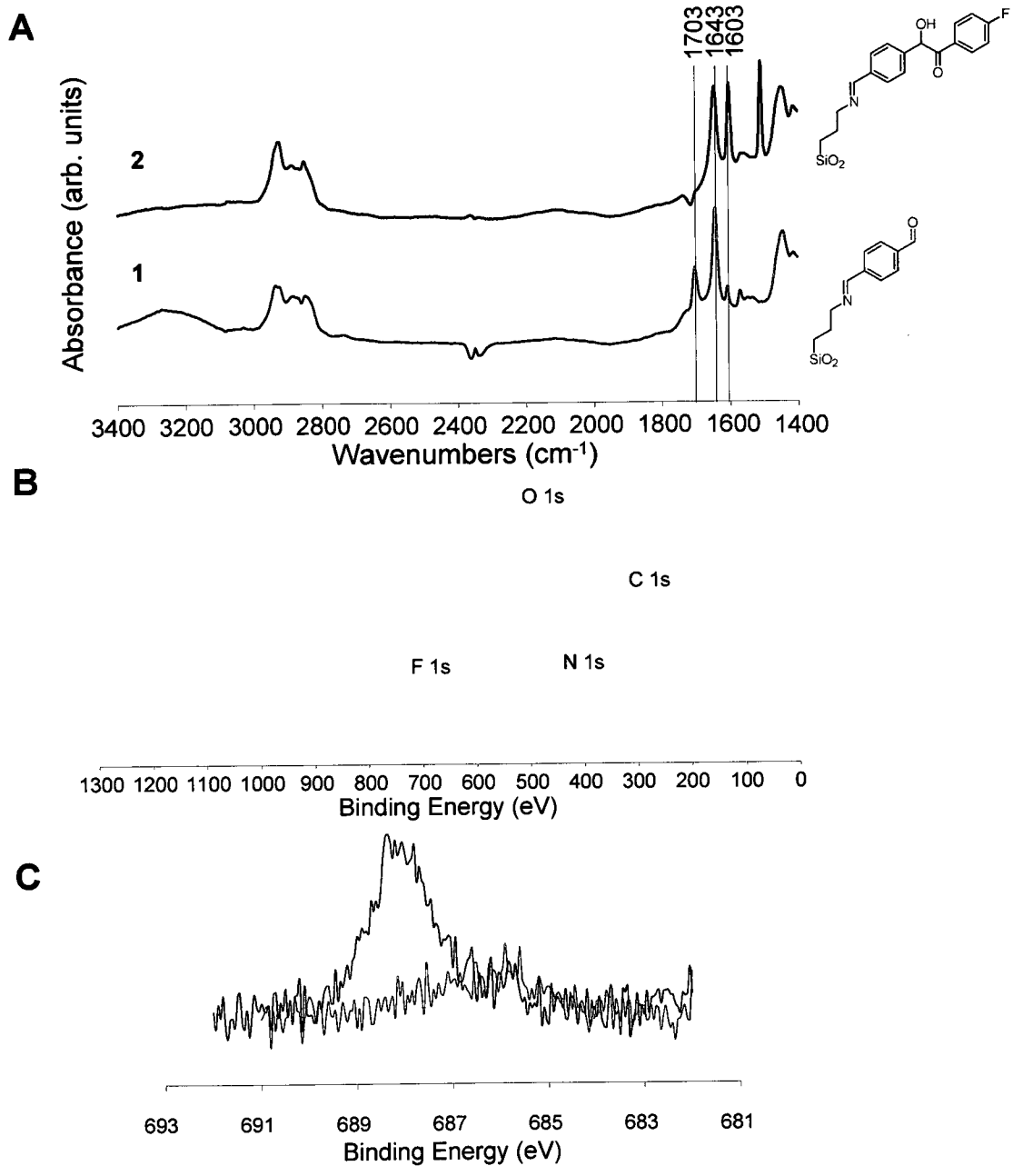

Figure 2.7 Characterization of thiamine catalyzed coupling of F-BA to a model oxide surface. **A** FT-IR characterization at 0hrs (1) and at 24hrs (2). **B** XPS survey scan.(red: control, no catalyst; blue: reaction after 24hrs). **C** XPS high resolution of F 1s region. (red: control, no catalyst; blue: reaction after 24hrs).

the solution based experiments, the reaction proceded much slower with an electron deficient aldehyde. After 18 hours the peak at 1703cm^{-1}, corresponding to the aldehyde carbonyl, while diminished, was still present. Only after 24 hours of reaction time was the peak no longer visible. The phenyl peak had grown in at 1603cm^{-1}.

2.2.3.5 XPS characterization of thiamine catalyzed coupling of F-BA to a model surface

The use of F-BA allowed not only for the study of the effects of electronics on the reactions, but also provided an excellent detection label for X-ray photoelectron spectroscopy (XPS) studies. Scans of the imine-linker aldehyde surface after 24 hours of reaction (Figure 2.7 B) showed the appearance of an F 1s signal at approximately 688 binding eV that is absent in the starting material. A control experiment, where the surface was exposed to reaction conditions without the NHC, was carried out where only a small amount of fluorine was detected, which was determined to be within background levels. In order to determine the amount of benzoin product formed on the surface, the N/F ratio of the final surface was determined. In order to calculate this ratio, sensitivity factors relative to carbon for both nitrogen (1.68) and fluorine (4) had to be considered.[26] Ratios are obtained by multiplying the observed intensity ratio from high resolution scans by the inverse ratio of the sensitivity factors. The N/F ratio was found to be 4.7 for the benzoin coated wafer (where the theoretical ratio should be 1) and 10.0 for the control wafer.

2.2.3.6 XPS characterization of thiamine catalyzed coupling of CF_3-BA to a model surface

In order to enhance the fluorine reporter signal, 4-(trifluoromethyl)benzaldehyde (CF_3-

BA) was used in place of F-BA (Figure 2.8). In the survey scan of the reacted surface, the F 1s signal at 688 binding eV was much larger than previously observed with F-BA. A high resolution scan of the F 1s region showed that the reacted surface had a 4 fold increase of fluorine emission over the control. When calculating the N/F ratio value of 1.4 (where the theoretical ratio should be 0.33) was obtained and 2.5 for the control wafer. Additionally, a high resolution scan of the C 1s region showed an additional signal at 294 biding eV which can be associated to a CF_3 carbon. An F/C_{CF3} of 3 was calculated which agrees with the theoretical value. Using the entire C 1s region between 282 and 295 binding eV, the calculated C/F ratio was 11.5 compared to a theoretical ratio of 6.3 for the benzoin product.

2.2.4 Si(111) Functionalization

Other surfaces were also tested to see whether the reaction would be suitable to use in other applications where the use of glass or SiO_2 was not appropriate. A Si(111) ATR chip was prepared as described in *Chapter 4 Materials and Methods* to provide a hydrogen terminated surface. The surface was aldehyde terminated by first reacting with undecylenic acid, followed by NHS activation of the terminal acid and coupling to N-(3-amino-propyl)-4-[1,3]dioxolan-2-yl-benzamide. Deprotection yielded the aldehyde terminated Si(111) surface (subsequently referred to as the amide-linker aldehyde surface (Figure 2.5B). The amide linker was chosen for its stability and ease of formation. The FT-IR spectrum of the aldehyde terminated slide was in agreement with the structure, with peaks at 3277cm^{-1} corresponding to N-H stretching, 2924cm^{-1} and 2853cm^{-1} corresponding to methylene C-H stretching, 1648 cm^{-1} and 1545cm^{-1} indicative of an amide group. The peak at 1710cm^{-1} corresponds to the C=O stretching of the benzaldehyde. This new surface was submitted to the same reaction conditions as in the initial experiment with the imine-linker aldehyde surface and the progression was monitored by FT-IR (Figure 2.9 A).

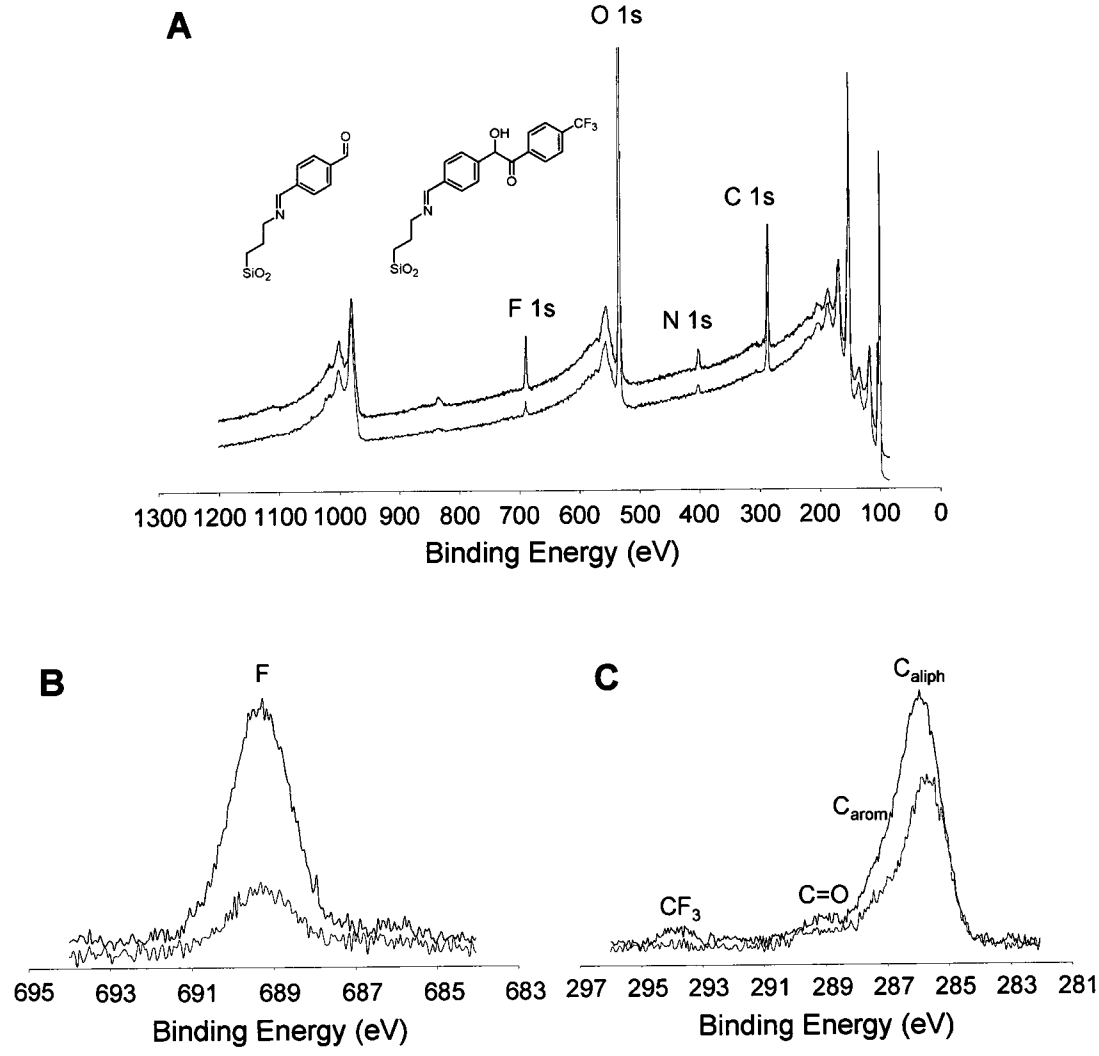

Figure 2.8 XPS characterization of thiamine catalyzed coupling of CF_3-BA to a model surface. (red: control, no catalyst; blue: reaction after 24hrs) **A** Survey scan, relevant peaks are highlighted. **B** High resolution scans of the F 1s region. **C** High resolution scans of the C 1s region.

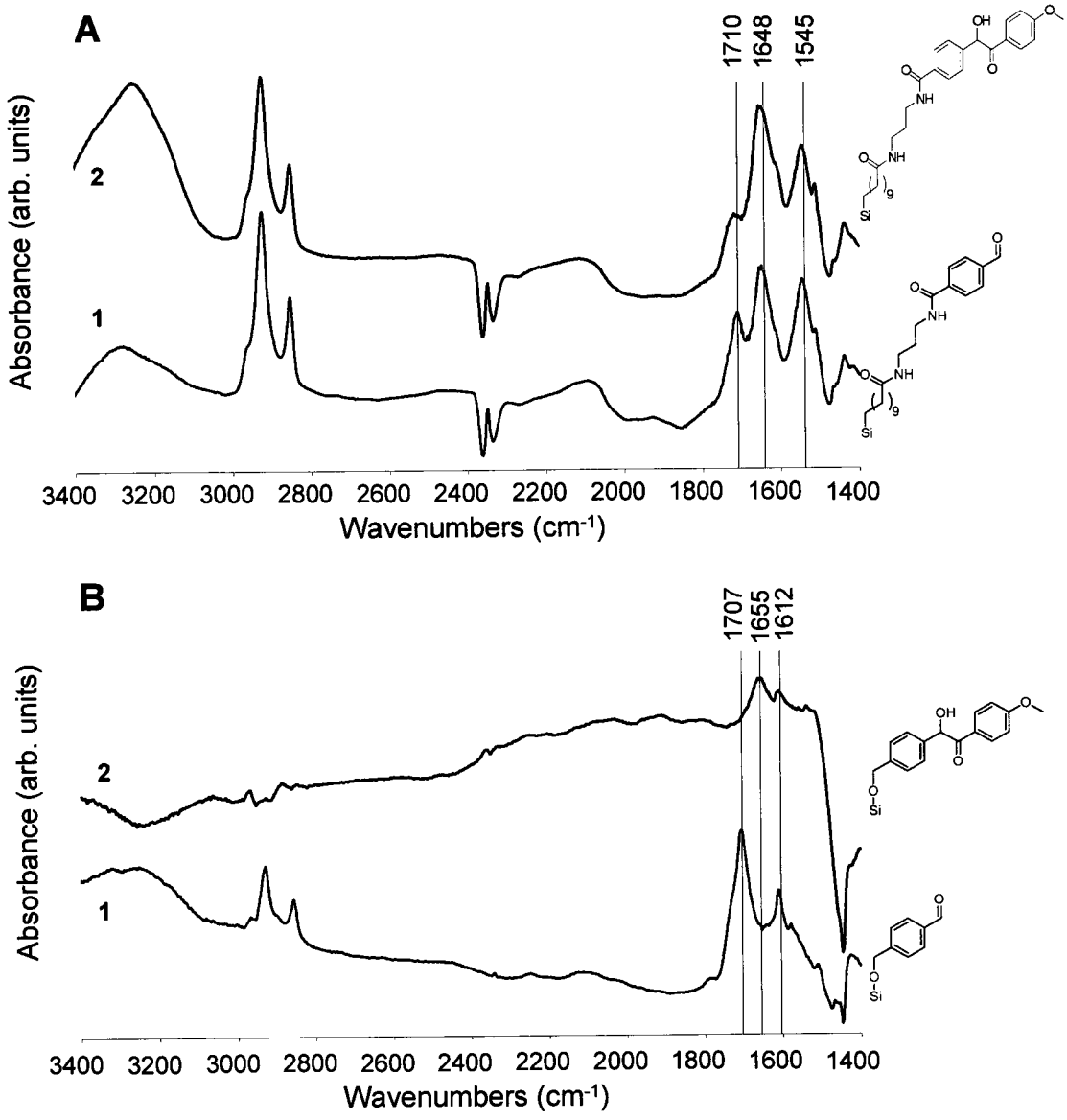

Figure 2.9 FT-IR characterization of thiamine catalyzed coupling of OMe-BA to Si(111) surfaces. **A** Amide-linker aldehyde surface, reaction progression at 0hr (1) and 24hrs (2) **B** Directly attached aldehyde surface, reaction progression at 0hr (1) and 24hrs (2)

After 24 hours the peak at 1710cm^{-1} was no longer visible, however no new peaks were visible. It is hypothesised that the peaks corresponding to the phenyl rings and the benzoin carbonyl were being masked by the large and broad amide I and II peaks. This surface was not pursued any further.

A new surface was sought to minimize the background peaks of the amide, and so terephthaldialdehyde was directly attached to the H-terminated Si(111) surface (subsequently referred to as the directly attached aldehyde surface). (Figure 2.5 C) This would eliminate the amide I and II peaks in the IR and hopefully allow the peaks from the benzoin product to be observed. The initial aldehyde terminated surface provided a clean IR spectrum, with peaks at 2928 cm^{-1} and 2856cm^{-1} corresponding to methylene C-H stretching, a peak at 1707cm^{-1} corresponding to the C=O stretching of the benzaldheyde and the peak at 1608cm^{-1} assigned to the phenyl now present. The new directly attached aldehyde surface was submitted to the same reaction conditions and monitored by FT-IR (Figure 2.9 B). Though the spectrum of the reaction progression did not afford clear sharp peaks, it was possible to see that after 4 hours, the aldehyde carbonyl peak at 1707cm^{-1} had been significantly reduced and a new peak at 1668cm^{-1} had appeared, which was assigned to the C=O stretching of the benzoin carbonyl. After 24 hours the aldehyde peak was no longer visible.

2.3 Discussion

2.3.1 Solution Optimization

The benzoin condensation is usually carried out in organic solvent, typically because of solvent compatibility of the reactants. Therefore in order for it to be utilized in the presence of bio-molecules, the reaction must be adapted to be carried out in water. A common problem

encountered when converting organic reactions for use in water is the lack of solubility of the reactants in water. In order to try and circumvent this problem, the possibility of using micellar catalysis was explored. Common detergents such as SDS and CTAB are often employed for this purpose.[27] Made up of a polar head group and non-polar chains, these detergents can self-organize to form spheres with the polar head group acting as a shell exposed to the water solvent, where as the non-polar chains point inwards towards the core. Reactants that would normally not be soluble in water will often readily solublize in the core of micelles. Manabe *et al.* have reported that micelles readily form by centrifuging surfactant solution and that centrifugation accelerates some types of reactions.[28] It was this strategy that was first explored to expand the scope of the benzoin condensation in water.

It was discovered however, that instead of forming micelles, centrifuging the reaction solution resulted in the formation of a density gradient within the reaction vessel forcing the reaction to take place in the bottom of the vessel, mimicking phase transfer conditions. This was found to be necessary for the reaction to proceed, since when the reaction solution was stirred under similar conditions no product was obtained. This observation was found to be fortuitous since these conditions mimic the eventual reaction environment of surface chemistry, at the interface between the surface and the solution. Since no micelles were being formed, the detergent was omitted from the reaction conditions, without any adverse effect on the formation of product.

An important phenomenon was observed during solution optimization involving substitution of the phenyl ring; the rate of the reaction is dependent on whether electron withdrawing groups or electron donating groups are present para to the aldehyde. When electron withdrawing groups such as nitro are present, the aldehyde becomes electron

deficient. Coupling between two electron deficient aldehydes was rarely observed. This could be explained by looking at the reactivity of the intermediate in the reaction, the activated aldehyde (Breslow intermediate). It is possible that the activated aldehyde species formed by condensing thiamine or other NHC to the electron deficient aldehyde is not activated sufficiently to act as nucleophile in the reaction. However, when electron donating groups are present, the aldehyde becomes electron rich. In this case, when the activated aldehyde species is formed, it becomes more reactive due to the greater electron density present at the $C_{2\alpha}$ reactive site, thus increasing the rate of the reaction. With these two observations in hand, one can devise a system to take advantage of the differing reactivities of the different species formed. By using both electron rich and electron deficient aldehydes, not only can the rate of the reaction be increased, but the formation of undesired couplings can be minimized, favouring cross couplings. Since the activated aldehyde species formed from the condensation of an electron deficient aldehyde to the catalyst will be less reactive, it is more likely to revert back to its individual components. The activated aldehyde species formed from an electron rich aldehyde will be more likely to react with another aldehyde to form the benzoin product. Additionally, activated aldehydes formed with electron rich aldehydes are more likely to react with electron deficient aldehydes since the difference in electron density is greater in this case.[29] When considering the application of this reaction for surface functionalization, this observation can be exploited. By designing the system in such a way that the electron deficient aldehyde is on the surface, the amount of attachments made to the surface will increase since it is unlikely that sites at the surface would be used up in self couplings. Also any homo couplings between the electron rich aldehydes could easily be washed away. The ability to design experiments in this manner makes the benzoin condensation ideally suited for surface functionalization.

2.3.2 SiO_2 Surface Functionalization

2.3.2.1 FT-IR analysis

For examining the ability of the benzoin condensation reaction to attach biomolecules to surfaces, a model system was used. SiO_2 was chosen as the base substrate since it is a common substrate in microarrays and has been extensively studied in such applications. SiO_2 lends itself well to many spectroscopic techniques, however for this work, only three were employed: FT-IR, XPS and ellipsometry (data not shown). A simple linker was designed in order to introduce an aromatic aldehyde as the terminal functionality of the SiO_2. APTES was chosen as the attachment molecule as it is a commonly used amino silane in the field.[30, 31] While it is commonly used, it also has a complex reactive profile, because of its three reactive ethoxy groups. It can undergo the desired reaction of covalent attachment with the surface through one, two or three of the ethoxy groups, however there exist an additional two reaction modes, either vertical or horizontal polymerization (Figure 2.10 A).[32] The latter, horizontal polymerization, can still be useful in surface functionalization since it is possible that there is one ethoxy group still present and able to react with the SiO_2 even once polymerized, and anchor the pre-assembled layer to the surface. Not only can APTES react in three different ways with either itself or the surface, but it can form many hydrogen bonds to orient itself in several different ways on the surface (Figure 2.10 B).[32] This complex reactivity explains the difficulties encountered when attempting to create stable and reproducible monolayers of APTES on SiO_2 as seen by the varying ellipsometry data (data note shown).

For future work, a different silane may be investigated, however for these experiments, APTES proved ideal because of its ease of reactivity with SiO_2. It has been previously shown that APTES reacts with the surface quickly at ambient temperature and pressure, without the need of

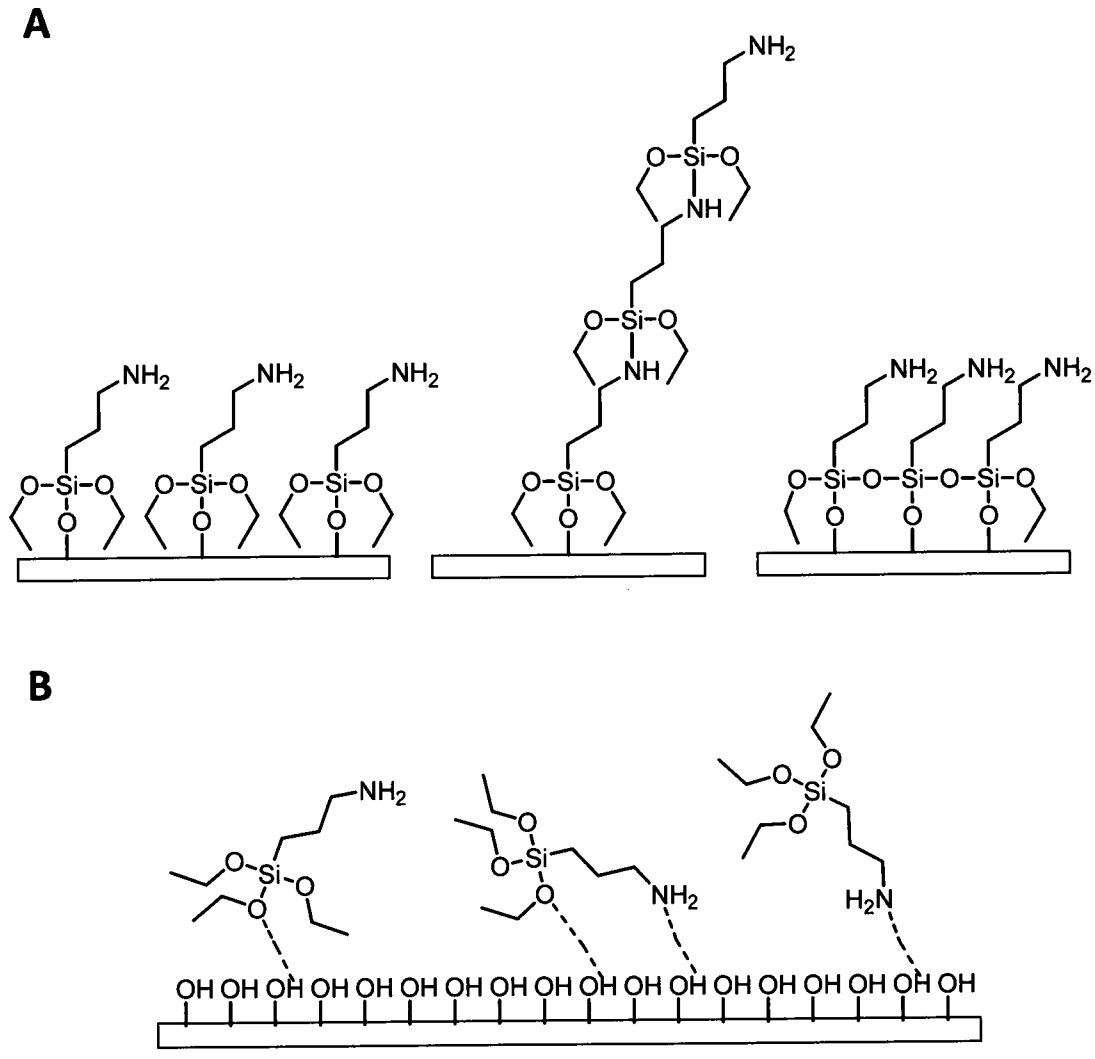

Figure 2.10 APTES interactions with surfaces. **A** Different modes of reactivity of APTES, covalent attachment, vertical polymerization and horizontal polymerization followed by covalent attachment. **B** Different modes of orientation of APTES based on hydrogen bonding with a hydroxy terminated surface. Adapted from *Langmuir* **2008,** 24, (21), 12405-12409.[32]

any additional reagents or solvents.[33] An advantage to using ambient temperature and pressure vapour deposition is that we did not have to worry about excess water in the solvent causing uncontrollable polymerization of APTES. Reaction of the surface with APTES resulted in amine terminated surface. To install the terminal aromatic aldehyde, a simple procedure was sought. Reaction with an aqueous solution of terephthaldialdehyde as described by Rozkiewicz *et al.*[25] provided an efficient means of reaching the terminal aldehyde without excess reagents as well as providing a clean FT-IR spectrum with a clearly visible aldehyde peak at ~1703 cm^{-1}.

OMe-BA was used to react with the imine-linker aldehyde surface to form the benzoin product. This aldehyde was chosen because the methoxy group provides a good mimic for the eventual incorporation of a tethered biomolecule and provides the electron density required to ensure that the aldehyde is electron rich. By monitoring certain peaks in the FT-IR spectrum, we could follow the reaction progression. The shrinking of peak at 1703cm^{-1} which corresponds to the C=O stretching of the terminal aldehyde allowed us visualize the consumption of the initial surface. The peak at 1606cm^{-1} which corresponds to the vibration of the phenyl rings is present in the initial aldehyde, but its intensity increases dramatically once the surface is reacted, which is consistent with a benzoin product. When compared to authentic 4-methoxybenzoins (Figure 2.4) and terephthaldialdehyde (appendix A) samples on SiO_2, we can see that the benzoins have a strong peak in the region around 1610cm^{-1} whereas with terephthaldialdehyde the peak is very weak. Also, the peak at 1643cm^{-1} which corresponds to the C=N stretching of the imine remains unchanged after the benzoin reaction, evidence that the imine-linker is still intact. Together, these observations suggest that the benzoin product is being formed on the surface.

It is interesting to note that while the spectra of the authentic benzoin samples include a peak at ~1685cm^{-1}, there is no observable peak present after the reaction with OMe-BA, nor

with any of the other benzaldehydes tested. One possible explanation for this is that the imine is being hydrolysed in the aqueous conditions of the reaction to regenerate the terminal amine and that OMe-BA is reacting with the latter to form an imine and not the benzoin product. This pathway can be disregarded based on the results of the control experiment which shows that without catalyst, the surface remains the same. If the imine was in fact being exchanged, we would see the loss of the 1703cm^{-1} peak would happen on the same time scale as with catalyst, and a dramatic increase in the intensity of the 1610cm^{-1} peak would be expected since it is present as a very strong peak in the FT-IR spectrum of 4-methoxybenzaldehyde (appendix A). Similar observations to the initial experiment with OMe-BA were seen when amine-BA or F-BA was used, as well as when the alternative NHC was used. More evidence that a benzoin product is being formed can be taken from the experiments with the directly attached aldehyde surface, where a peak at 1668cm^{-1} corresponding to the C=O stretching of the benzoin carbonyl was present. This helps to form the hypothesis that in the imine-linker aldehyde surface the benzoin carbonyl peak is being masked by the imine peak.

It is interesting to note that when amine-BA is used, the reaction proceeds on the same time scale as the initial experiment however, when 1,3-Bis(2,4,6-trimethylphenyl) imidazolium chloride is used in place of thiamine, the 1703cm^{-1} peak is no longer detectable after only 4 hours (compared to 24 hours with thiamine). This may be due to the increased stability and reactivity of the carbene formed after the deprotonation of the C_2 hydrogen. The presence of a phenyl ring on both hetero atoms as compared to only one with thiamine provide additional electron density to the C_2 site, stabilizing the resulting carbene.[12] The same system was also tested using an electron poor aldehyde, F-BA. Based on results seen in the solution based experiments, it was believed that this benzaldehyde would not yield any product since the activated aldehyde species formed would not be reactive enough. Fortuitously this was not the

case, and we did see reduction of the 1703cm^{-1} peak and emergence of a peak at 1603cm^{-1} which was assigned to the additional phenyl ring was seen, however this change in the spectrum was only apparent after 24 hours. This observation does support our initial hypothesis that the electronics of the benzaldehydes play a role in determining the sequence of events in the reaction. More evidence that the activated aldehyde species is forming with the electron rich aldehyde is that when the imine-linker aldehyde terminated surface is reacted with only catalyst and base, there is little change in the surface spectrum, where the 1703cm^{-1} peak is only slightly decreased, but no additional peaks are observed.

2.3.2.1 XPS analysis

The XPS data obtained from reactions involving aldehydes with fluorine substituents suggests that the main pathway for the incorporation of the fluoro signal at 688 binding eV is from the formation of the benzoin product on the surface. With reaction involving F-BA, the observed N/F ratio of 4.7 shows that under the reaction conditions, approximately 1 in 5 amines carried a benzoin product. The presence of a small fluorine peak in the control can be attributed to either cross contamination or to F-BA reacting with free amines from unreacted APTES. With CF_3-BA, the observed N/F ratio of 1.4 corresponds to approximately 1 in 4 amines carrying a benzoin product, which was very similar to the results in the previous system. The additional signal at 294 binding eV corresponding to the carbon of the CF_3 group and the observed F/C_{CF3} ratio of 3 confirms that the entire fluorine signal is associated with the incorporation of CF_3-BA on to the surface. When considering the entire carbon region, the observed C/F ratio of 11.5 was much higher than the theoretical ratio of 6.3 for the benzoin product or 3.7 for imine formation between unreacted APTES at the surface and CF_3-BA . Since unreacted terminal aldehyde will increase the carbon content, this could indicate that only

about 50% of the terminal aldehydes undergo benzoin condensation. The higher C/F ratio also indicated that the direct coupling of unreacted APTES at the surface and CF_3-BA must be a negligible reaction pathway.

2.4 Summary and Future Work

The results gathered after FT-IR and XPS analysis all suggest that the aldehyde terminated surface has in fact been modified with benzoin products using model systems of small non-peptidic benzaldehydes. With these results in hand, further experiments are planned using small peptides bearing aromatic aldehyde functionalities to see whether they too will be incorporated into benzoin products on surfaces using the developed conditions.

2.5 References

1. Leonard, P.; Hearty, S.; Quinn, J.; O'Kennedy, R., A generic approach for the detection of whole *Listeria monocytogenes* cells in contaminated samples using surface plasmon resonance. *Biosens. Bioelectron.* **2004,** 19, (10), 1331-1335.
2. Uithoven, K. A.; Schmidt, J. C.; Ballman, M. E., Rapid identification of biological warfare agents using an instrument employing a light addressable potentiometric sensor and a flow-through immunofiltration-enzyme assay system. *Biosens. Bioelectron.* **2000,** 14, (10-11), 761-770.
3. Mukundan, H.; Anderson, A.; Grace, W. K.; Grace, K.; Hartman, N.; Martinez, J.; Swanson, B., Waveguide-Based Biosensors for Pathogen Detection. *Sensors* **2009,** 9, (7), 5783-5809.
4. Boukherroub, R., Chemical reactivity of hydrogen-terminated crystalline silicon surfaces. *Current Opinion in Solid State and Materials Science* 9, (1-2), 66-72.
5. Ruckenstein, E.; Li, Z. F., Surface modification and functionalization through the self-assembled monolayer and graft polymerization. *Adv. Colloid Interface Sci.* **2005,** 113, (1), 43-63.
6. Rusmini, F.; Zhong, Z.; Feijen, J., Protein Immobilization Strategies for Protein Biochips. *Biomacromolecules* **2007,** 8, (6), 1775.
7. Smith, C.; Milea, J.; Nguyen, G., Immobilization of Nucleic Acids Using Biotin-Strept(avidin) Systems. In *Top. Curr. Chem.*, 2005; Vol. 261, pp 63-90.
8. Zhen, G.; Falconnet, D.; Kuennemann, E.; Vörös, J.; Spencer, N. D.; Textor, M.; Zürcher, S., Nitrilotriacetic Acid Functionalized Graft Copolymers: A Polymeric Interface for Selective and Reversible Binding of Histidine-Tagged Proteins. *Adv. Funct. Mater.* **2006,** 16, (2), 243-251.
9. Lapworth, A., Reactions involving the addition of hydrogen cyanide to carbon compounds. *Journal of the Chemical Society* **1903,** 83, 995-1005.
10. Breslow, R., On the Mechanism of Thiamine Action. IV.1 Evidence from Studies on Model Systems. *J. Am. Chem. Soc.* **2002,** 80, (14), 3719-3726.
11. Enders, D.; Balensiefer, T., Nucleophilic Carbenes in Asymmetric Organocatalysis. *Acc. Chem. Res.* **2004,** 37, (8), 534.
12. Nair, V.; Bindu, S.; Sreekumar, V., N-Heterocyclic Carbenes: Reagents, Not Just Ligands! *Angew. Chem. Int. Ed.* **2004,** 43, (39), 5130-5135.
13. Zhang, Z.; Smith, B. A. C.; Wang, L.; Brock, A.; Cho, C.; Schultz, P. G., A New Strategy for the Site-Specific Modification of Proteins *in Vivo Biochemistry* **2003,** 42, (22), 6735-6746.
14. Carrico, I. S.; Carlson, B. L.; Bertozzi, C. R., Introducing genetically encoded aldehydes into proteins. *Nat. Chem. Biol.* **2007,** 3, (6), 321-322.
15. Breslow, R., Rapid Deuterium Exchange in Thiazolium Salts. *J. Am. Chem. Soc.* **2002,** 79, (7), 1762-1763.
16. Reynolds, N. T.; Rovis, T., Enantioselective Protonation of Catalytically Generated Chiral Enolates as an Approach to the Synthesis of Î±-Chloroesters. *J. Am. Chem. Soc.* **2005,** 127, (47), 16406-16407.
17. Chan, A.; Scheidt, K. A., Conversion of α,β-Unsaturated Aldehydes into Saturated Esters: An Umpolung Reaction Catalyzed by Nucleophilic Carbenes. *Org. Lett.* **2005,** 7, (5), 905-908.
18. Iwamoto, K.-i.; Hamaya, M.; Hashimoto, N.; Kimura, H.; Suzuki, Y.; Sato, M., Benzoin reaction in water as an aqueous medium catalyzed by benzimidazolium salt. *Tetrahedron Lett.* **2006,** 47, (40), 7175-7177.

19. Murry, J. A.; Frantz, D. E.; Soheili, A.; Tillyer, R.; Grabowski, E. J. J.; Reider, P. J., Synthesis of Î±-Amido Ketones via Organic Catalysis: Thiazolium-Catalyzed Cross-Coupling of Aldehydes with Acylimines. *J. Am. Chem. Soc.* **2001,** 123, (39), 9696-9697.
20. Mattson, A. E.; Bharadwaj, A. R.; Zuhl, A. M.; Scheidt, K. A., Thiazolium-Catalyzed Additions of Acylsilanes: A General Strategy for Acyl Anion Addition Reactions. *J. Org. Chem.* **2006,** 71, (15), 5715-5724.
21. Kano, T.; Sasaki, K.; Konishi, T.; Mii, H.; Maruoka, K., Highly efficient trialkylsilylcyanation of aldehydes, ketones and imines catalyzed by a nucleophilic N-heterocyclic carbene. *Tetrahedron Lett.* **2006,** 47, (27), 4615-4618.
22. Arduengo, A. J.; Harlow, R. L.; Kline, M., A stable crystalline carbene. *J. Am. Chem. Soc.* **1991,** 113, (1), 361-363.
23. Linghu, X.; Potnick, J. R.; Johnson, J. S., Metallophosphites as Umpolung Catalysts: The Enantioselective Cross Silyl Benzoin Reaction. *J. Am. Chem. Soc.* **2004,** 126, (10), 3070-3071.
24. Xin, L.; Jeffrey, S. J., Kinetic Control in Direct α-Silyloxy Ketone Synthesis: A New Regiospecific Catalyzed Cross Silyl Benzoin Reaction13. *Angew. Chem. Int. Ed.* **2003,** 42, (22), 2534-2536.
25. Rozkiewicz, D. I.; Ravoo, B. J.; Reinhoudt, D. N., Reversible Covalent Patterning of Self-Assembled Monolayers on Gold and Silicon Oxide Surfaces. *Langmuir* **2005,** 21, (14), 6337-6343.
26. C. D. Wagner, L. E. D., M. V. Zeller, J. A. Taylor, R. H. Raymond, L. H. Gale,, Empirical atomic sensitivity factors for quantitative analysis by electron spectroscopy for chemical analysis. *Surf. Interface Anal.***1981,** 3, (5), 211-225.
27. Torsten, D.; Eckhard, P.; Günther, O., Reactions in Micellar Systems. *Angew. Chem. Int. Ed.* **2005,** 44, (44), 7174-7199.
28. Manabe, K.; Mori, Y.; Wakabayashi, T.; Nagayama, S.; Kobayashi, S., Organic Synthesis Inside Particles in Water: Lewis Acid-Surfactant-Combined Catalysts for Organic Reactions in Water Using Colloidal Dispersions as Reaction Media. *J. Am. Chem. Soc.* **2000,** 122, (30), 7202-7207.
29. Kevser Göçmen, T.; Canan, U.; Viktorya, A., Computational study of the synthesis of benzoin derivatives from benzil. *Int. J. Quantum Chem.* **2006,** 106, (7), 1596-1610.
30. Pasternack, R. M.; Rivillon Amy, S.; Chabal, Y. J., Attachment of 3-(Aminopropyl)triethoxysilane on Silicon Oxide Surfaces: Dependence on Solution Temperature. *Langmuir* **2008,** 24, (22), 12963-12971.
31. Simon, A.; Cohen-Bouhacina, T.; Porté, M. C.; Aimé, J. P.; Baquey, C., Study of Two Grafting Methods for Obtaining a 3-Aminopropyltriethoxysilane Monolayer on Silica Surface. *J. Colloid Interface Sci.* **2002,** 251, (2), 278-283.
32. Smith, E. A.; Chen, W., How To Prevent the Loss of Surface Functionality Derived from Aminosilanes. *Langmuir* **2008,** 24, (21), 12405-12409.
33. Xu, D. X.; Densmore, A.; Delage, A.; Waldron, P.; McKinnon, R.; Janz, S.; Lapointe, J.; Lopinski, G.; Mischki, T.; Post, E.; Cheben, P.; Schmid, J. H., Folded cavity SOI microring sensors for high sensitivity and real time measurement of biomolecular binding. *Opt. Express* **2008,** 16, (19), 15137-15148.

Chapter 3: Probes for Multiplex Cell Surface Receptor Labelling

3.1 Introduction

While surface enhanced Raman scattering (SERS) spectroscopy is a relatively old tool, there has been a recent spike in interest, focusing on the application of SERS in the biological sciences.[1-4] Many different structures have been developed that are amenable to different uses, typically employing silver (Ag) or gold (Au) for their favorable plasmonic characteristics. These structures can be divided into 3 different categories: structured arrays of nanoparticles (NPs), structured surfaces and free NPs.[5] Structured arrays of NPs are the easiest to fabricate. This category can be subdivided again, into clustered or linked NPs and NP patterned surfaces. The clustering of NPs allows for enhancement factors of up to 10^{14}.[6] While structured surfaces are equally easy to fabricate, they don't offer the same enhancement factor as clustered particles, only ranging from 10^4 - 10^6.[7,8] NPs can be used for single molecule detection with enhancement factors of up to 10^{15}, and can be made in a variety of shapes including spheres, rods and ellipses[9,10] and sizes, ranging from 10s to 100s of nanometers, with each size offering varying degrees of enhancement.[11]

The diverse range of NP structures can each be uniquely exploited for different applications. For example, structured arrays can be used for the detection and identification of pathogens. It was shown that by using Ag nanorod arrays, one could easily identify samples of purified adenovirus, rhinovirus, and human immunodeficiency virus and clearly make the differentiation between these three viruses, based on their unique SERS spectrum.[12] Additionally, SERS can also be used to identify respiratory syncytial virus infected cells among

other non-infected cells based on specific bands which are unique to the virus and visible above the background of the cell.[12] While there are many other examples of this type of SERS detection assay, identifying different pathogens or materials based on their unique spectrum, SERS platforms can be designed to act as tags with highly specific binding. A recent example of this type of SERS assay was recently published in Nature Biotechnology.[13] It was shown that Au spherical NPs, functionalized with Raman reporter molecules as well as epidermal growth factor receptor (EGFR) antibodies (Abs) can be used to tag and identify cells where EGFRs are over expressed, namely cancer cells. In the study, 60nm Au NPs were coated with polyethylene glycol (PEG) thiol which was found to protect the particles from degradation in a variety of harsh conditions. In addition, the PEG coating aids in the water solubility and the bio-distribution of the NPs in *in vivo* studies. The Raman reporter chosen for this study was the organic dye diethylthiatricarbocyanine which offers a strong, unique SERS signal once conjugated to the NP. When compared to quantum dots, which are often used for tagging and identification experiments[14], the NPs used offered more a brighter and sharper SERS emission spectrum then the fluorescence spectrum emitted by quantum dots under the same experimental conditions.

Recent work from the Pezacki group[15] has focused on adapting the technique described above to the imaging of cell surface receptor aggregation, specifically the β_2 adrenergic receptor (β_2AR) in cardiomyocyte cells. B_2ARs are known to form multiprotein signalling platforms that play a role in the regulation of the beat rate of the heart. Using small 15nm Ag NPs, functionalized with 4-(mercaptomethyl)benzonitrile as the Raman report molecule and a secondary anti-body for secondary detection of β_2AR we were able to visualize aggregation events using SERS as well as other spectroscopic methods including Rayleigh light scattering, scanning electron microscopy and luminescence imaging to gain important information into β_2AR signalling platforms and their distribution in the cell.[15] This chapter discuses work towards

developing a multiplex SERS imaging technique, were multiple cell surface receptors can be detected and identified using small Ag NPs functionalized with different Raman reporter molecules, each bearing a unique SERS spectrum.

3.2 Results

3.2.1 Spectra

3.2.1.1 Ligands

Two sets of reporter ligands were synthesized as described in *Chapter 4 Materials and Methods* and tested for their Raman activity. For the first set of ligands dithiobis(succinimidyl propionate) (DTSP) was reacted with either a modified amino acid or a short amine compound bearing the Raman reporter group, subsequently referred to as DTSP based ligands. Included in this set were DTSP-4-cyano-phenyl alanine (DTSP-CN), DTSP-d5-phenyl alanine (DTSP-d_5Phe), DTSP-d2-glycine (DTSP-d_2Gly), DTSP-4-boronic acid-phenyl alanine (DTSP-boron), DTSP-4-nitro-phenyl alanine (DTSP-NO_2) and DTSP-propargyl amine (DTSP-alkyne) (Figure 3.1 A). All peaks were assigned based on data from *The Handbook of infrared and Raman characteristic frequencies of organic molecules*.[17] DTSP-NO_2 did not provide a clean Raman spectrum (spectrum not shown) while DTSP-boron only had one strong resolvable peak at 1612cm^{-1} (amide I stretching) and weak poorly resolved peaks in the 1300cm^{-1} - 1400cm^{-1} region where C–B vibrations are typically found and so both compounds were excluded from further testing. Each of the remaining ligands provided unique Raman spectra with sharp peaks that could later be used for Raman markers for identification. (Figure 3.2 A) Focusing in on the region between 1000cm^{-1} and 2800cm^{-1} the remaining DTSP-based ligands had peaks between 1600cm^{-1} -

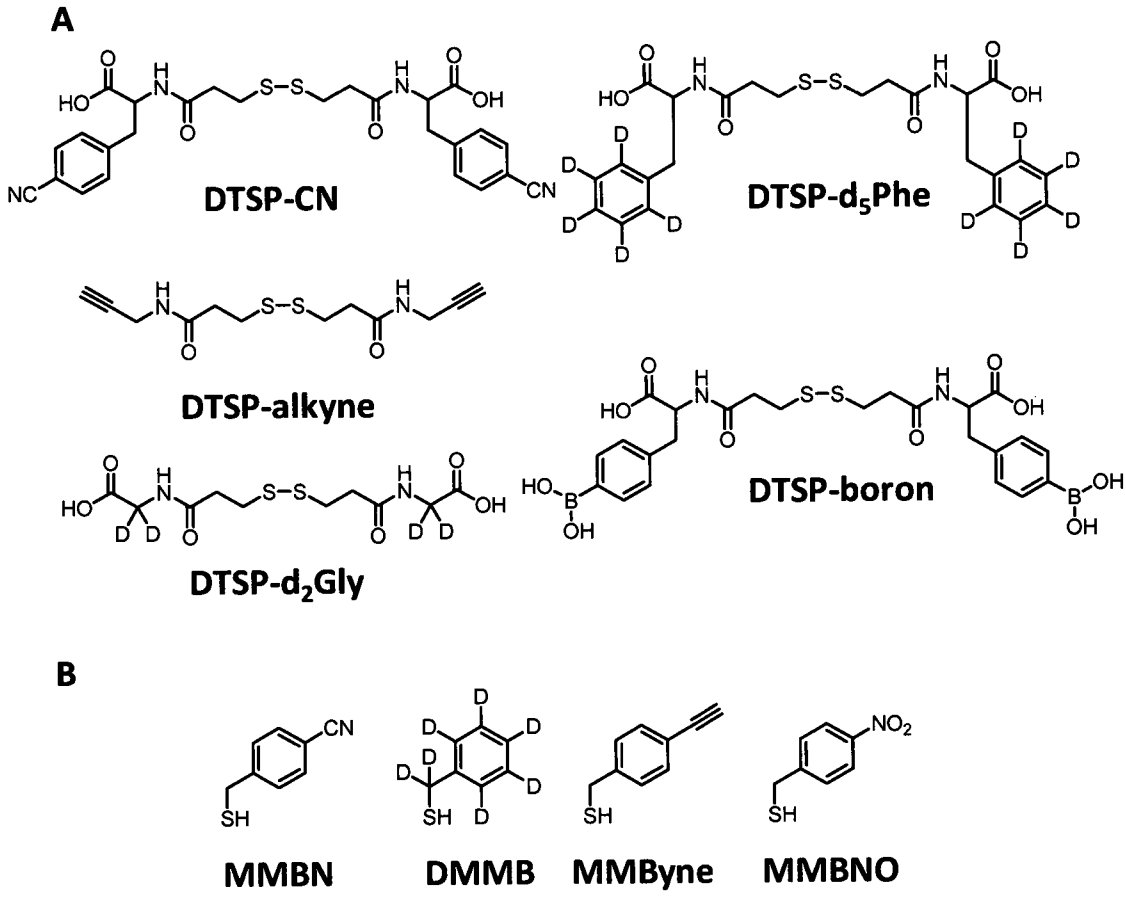

Figure 3.1 Raman reporter lignads. **A** DTSP based ligands. **B** Benzyl thiol ligands.

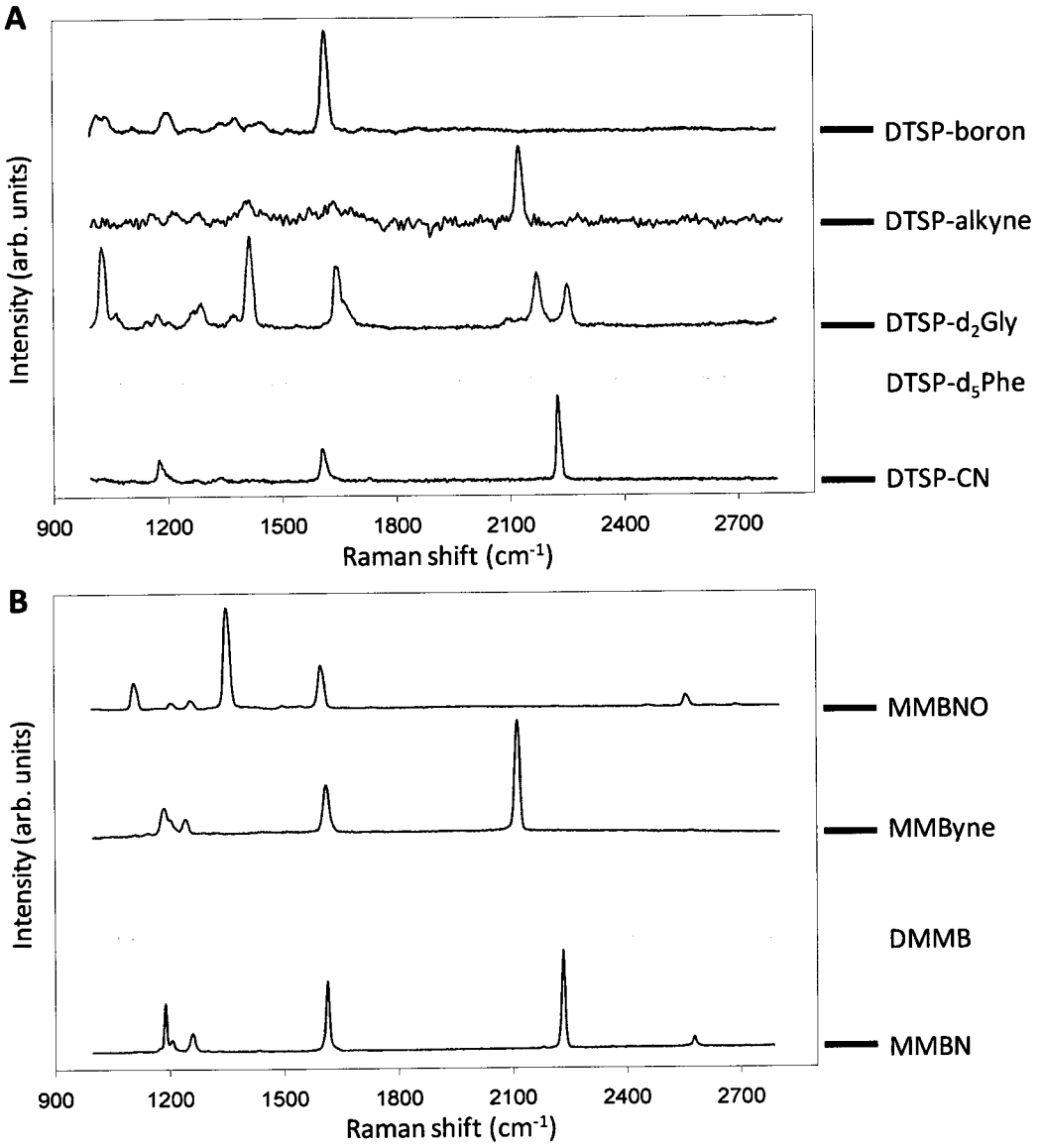

Figure 3.2 Raman spectra of Raman reporter ligands. **A** DTSPbased ligands. **B** Benzyl thiol based ligands.

1650cm^{-1} (amide I stretching and phenyl ring deformation) and 1150cm^{-1} - 1200cm^{-1} (amide III stretching and phenyl ring C–H bending) though for some ligands (DTSP-alkyne and DTSP-d_5Phe) these peaks were barely distinguishable from the background. DTSP-alkyne had one prominent peak at 2121cm^{-1} (C≡C stretching), DTSP-d_2Gly had 4 prominent stretches, 1025cm^{-1} (C–C skeletal stretching), 1413cm^{-1}(C–H stretching), and two peaks at 2169cm^{-1} and 2247cm^{-1} (C–D stretching), DTSP-d_5Phe had a broad peak at 2290cm^{-1} (C–D stretching) and DTSP-CN had a large peak at 2224cm^{-1} (C≡N stretching).

In the second ligand set, similar Raman reporter groups were employed, however simple benzyl thiol ligands were synthesized (subsequently referred to as benzyl thiol based ligands) in order to have the Raman reporter closer to the surface to the nanoparticle and take advantage of the notably increased enhancement from aryl conjugated reports such as 4-nitrobenzyl thiol.[16] Included in this second generation set were 4-(mercaptomethyl)benzonitrile (MMBN), deuterated mercaptomethyl benzene (DMMB), 4-(mercaptomethyl)ethynylbenzene (MMByne) and 4-(mercaptomethyl)nitrobenzene (MMBNO) (Figure 3.1 B). Raman spectra were collected for all ligands (Figure 3.2 B). Focusing in on the region between 1000cm^{-1} and 2800cm^{-1} all ligands had peaks between 1570cm^{-1} - 1620cm^{-1} (phenyl ring deformation), 1100cm^{-1} - 1200cm^{-1} (phenyl ring C–H bending) and 2550cm^{-1} - 2580cm^{-1} (S–H stretching). The Raman spectrum of the MMByne displayed a prominent peak at 2112cm^{-1} (C≡C stretching), MMBN had prominent peaks at 2234cm^{-1} (C≡N stretching); DMMB had prominent peaks at 1047cm^{-1} (phenyl C–D bending) and two peaks at 2168cm^{-1} and 2287cm^{-1} (C–D stretching); MMBNO had prominent peaks at 1352cm^{-1} (NO_2 symmetric stretching) and 1599cm^{-1} (NO_2 asymmetric stretching).

3.2.1.2 Nanoparticles

Ag NPs were synthesized and assembled as described in *Chapter 4 Materials and Methods* (Figure 3.3) utilizing a mixture of DTSP, 2-[2-(2-methoxy-ethoxy)-ethoxy]-ethanethiol (EG_3SH), and Raman reporter ligand in a 2:5:5 ratio and blocking with bovine serum albumin (BSA). NPs were synthesized using the different ligands described above and SERS spectra were collected for each set. (Figure 3.4 A) NPs synthesized using the DTSP based ligands provided SERS spectra that were not as sharp as the corresponding Raman spectra for the free ligand. Peaks within the region spanning $1000cm^{-1}$ and $1800cm^{-1}$ were not resolvable. However it was still possible to distinguish the Raman reporter groups peaks for most of the NPs. The SERS spectrum of DTSP-CN based NPs had a sharp resolved reporter peak at $2216cm^{-1}$ (C≡N stretching). DTSP-d_5Phe based NPs had an easily distinguishable but less sharp reporter peak at $2279cm^{-1}$ (C-D stretching) while the DTSP-d_2Gly based NPs had a mass of poorly resolved reporter peaks between $2100cm^{-1}$ and $2300cm^{-1}$ (C-D stretching) in contrast to the two sharp resolved peaks in the same region in the corresponding ligand spectrum. DTSP-alkyne NPs provided an interesting SERS spectrum, with two resolved peaks at $2011cm^{-1}$ and $2112cm^{-1}$ (C≡C stretching region) while the ligand spectrum only had one peak in this region. This double peak is characteristic of the Fermi resonance found in alkynes though the frequency is slightly lower than expected.[17]

SERS spectra obtained from NPs synthesized with benzyl thiol based ligands provided much sharper and better resolved peaks than those of the DTSP based ligand set NPs. (Figure 3.4 B) Additionally, the region between $1000cm^{-1}$ and $1800cm^{-1}$ remained clean and peaks are sharp and easily resolvable. All benzyl thiol based ligand NP SERS spectra contain a peak between $1160cm^{-1}$ - 1180^{-1} which is associated with the phenyl ring (in plane C–H bending)

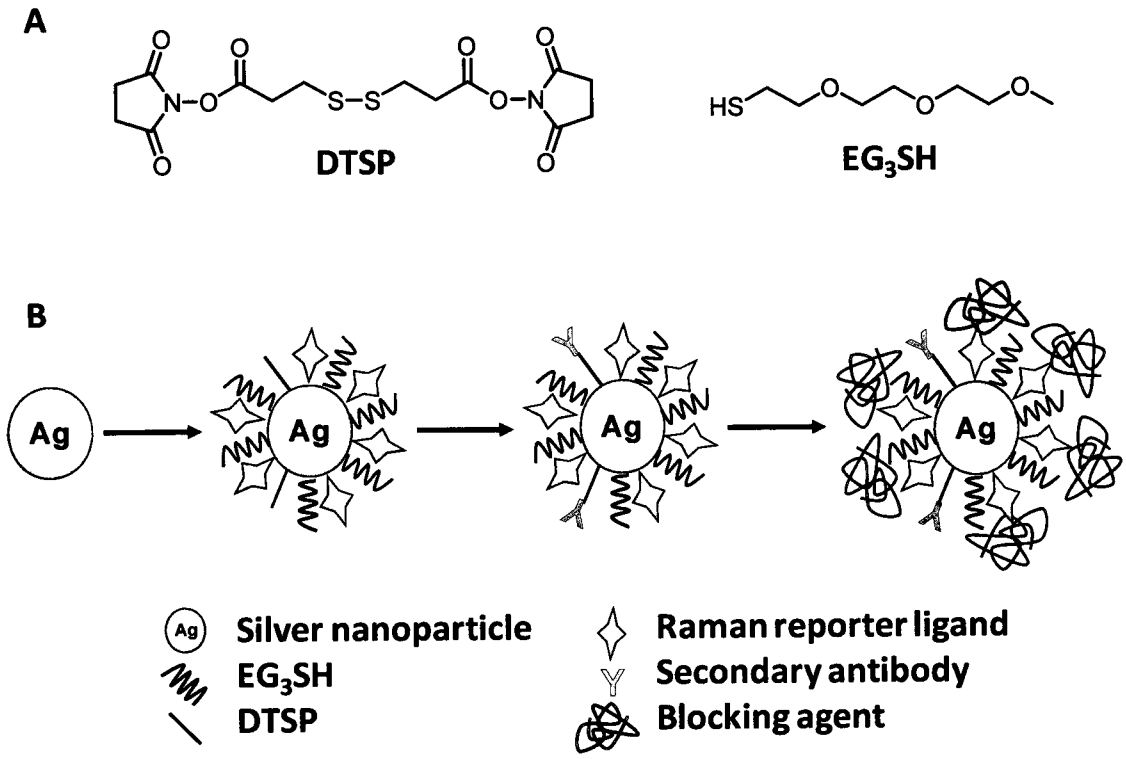

Figure 3.3 Assembly of NPs. **A** DTSP and EG_3SH ligands used for Ab attachment and water solubilization. **B** Order of reaction for assembly of NPs.

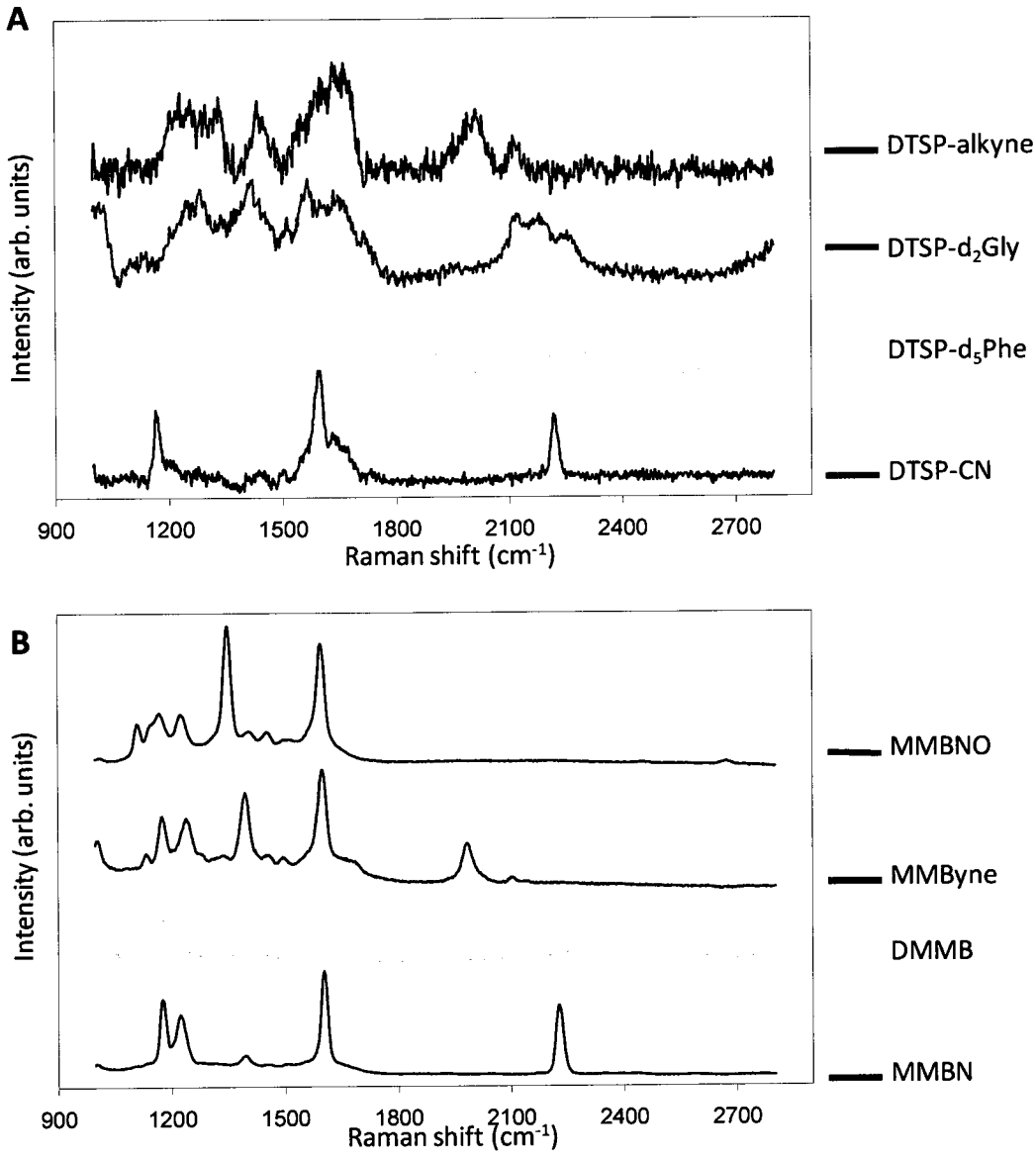

Figure 3.4 SERS spectra of Ag NPs with Raman reporter ligands. **A** Ag NPs with DTSP based ligands. **B** Ag-NPs with benzyl thiol based ligands.

as well as two peaks between 1340cm^{-1} - 1400cm^{-1} and 1560cm^{-1} - 1610cm^{-1} which are associated with ring deformation. Raman reporter group peaks were resolved, sharp and easily distinguishable for most the NPs. The SERS spectrum of MMBN NPs showed a sharp peak at 2226cm^{-1} (C≡N stretching) and the SERS spectrum of DMMB NPs showed two peaks at 2146cm^{-1} at 2283cm^{-1} (C–D stretching) with the double peak being characteristic of deuterated compounds[18], with both spectra resembling their corresponding ligand spectra. The MMByne NP was synthesized using crude ligand (50% purity, contaminated by the corresponding chloride intermediate) however; the SERS spectrum had a resolved peak at 1983cm^{-1} (C≡C stretching) similar to the spectrum of ethynyl benzyl alcohol. In addition to this peak, a second small peak in the same region (2101cm^{-1}) is also observed. This double peak is similar to the SERS spectrum of the DTSP-alkyne NPs previously mentioned. The SERS spectrum of MMBNO NPs showed the characteristic peaks of NO_2 at 1347cm^{-1} and 1594cm^{-1}, however these two peaks overlap and are indistinguishable from the ring deformation peaks of the phenyl.

3.2.2 Imaging

In preparation for cell labelling experiments, H9c2 cells (rat cardiomyocytes) were plated, fixed and treated with primary Abs against β_2AR proteins (derived in rabbits) and caveolin proteins (derived in goats). Cell labelling experiments were carried out using DMMB and MMBN NPs, each additionally functionalized with a secondary Ab specifically chosen to bind the primary Abs already on the surface. (Figure 3.5)

In the first set of experiments (full conditions described in *Chapter 4 Materials and Methods*), DMMB NPs were additionally functionalized with a donkey anti rabbit secondary Ab, which binds the β_2AR primary Ab, while MMBN NPs carried a donkey anti goat secondary Ab, which binds the caveolin primary Ab. After treatment with an equal mixture of the two types of

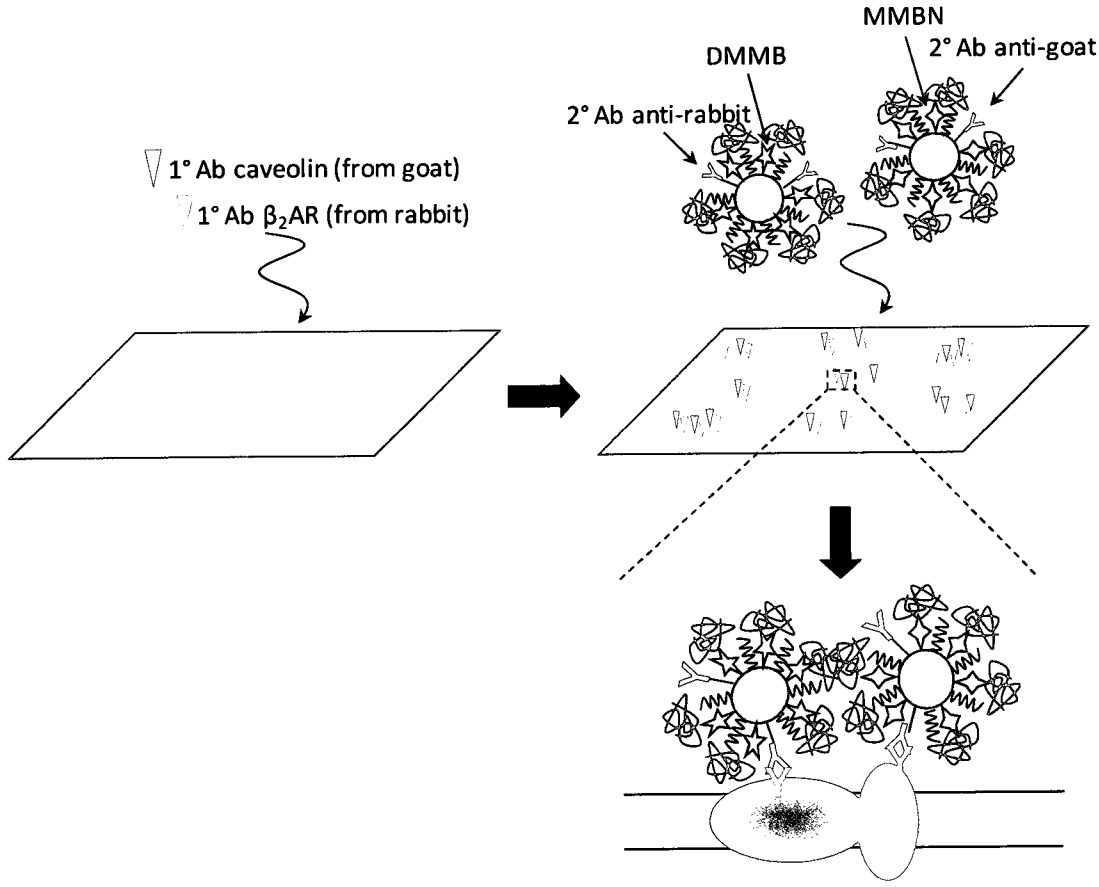

Figure 3.5 Schematic representation of imaging experiments. H9c2 cells are treated with primary Abs for β2AR and caveolin for 24 hours. After Ab treatment, cells are treated with a mixture of DMMB and MMBN NPs for 24hs. NPs bind to either the β2AR or caveolin primary Ab through their secondary Ab.

NPs, cells were ready for imaging, where single cells were selected and scanned, where an entire SERS spectrum was acquired for each pixel in the image of the cell. Two deconvolution SERS intensity maps (Figure 3.6 A) were obtained for the cell, one focussing on the region around 1039cm^{-1} (1021cm^{-1} - 1074cm^{-1}) to highlight the DMMB NPs and the other focussing on the region around 2230cm^{-1} (2208cm^{-1} - 2258cm^{-1}) to highlight the MMBN NPs. Multivariant deconvolution intensity maps (Figure 3.7) were also obtained for the same cell, where the entire SERS spectrum was taken into consideration. In these maps, the red color is assigned to spectral features of MMBN while the color green is assigned to spectral features of DMMB NPs. An overlay of the two multivariant deconvolution maps allowed us to visualize regions that contain spectral features of both MMBN and DMMB. These regions show up as a mixture of red and green, varying in color depending on the percent contribution from the individual spectra. Control experiments, where H9c2 cells without primary Abs were subjected to the same NP treatment show no significant SERS signal.

3.3 Discussion

3.3.1 Ligand and NP Design

When searching for Raman reporter groups, three key features were taken into consideration. First the reporter groups must provide a unique Raman spectrum, to allow the different particles to be identified and distinguished from each other. Secondly, characteristic bands must be resolvable above the background signals coming from the cellular environment. Cells are made up primarily of lipids and proteins, and so it is not surprising that when examining the Raman spectrum of an unlabeled cell (Figure 3.8), we see that it contains many

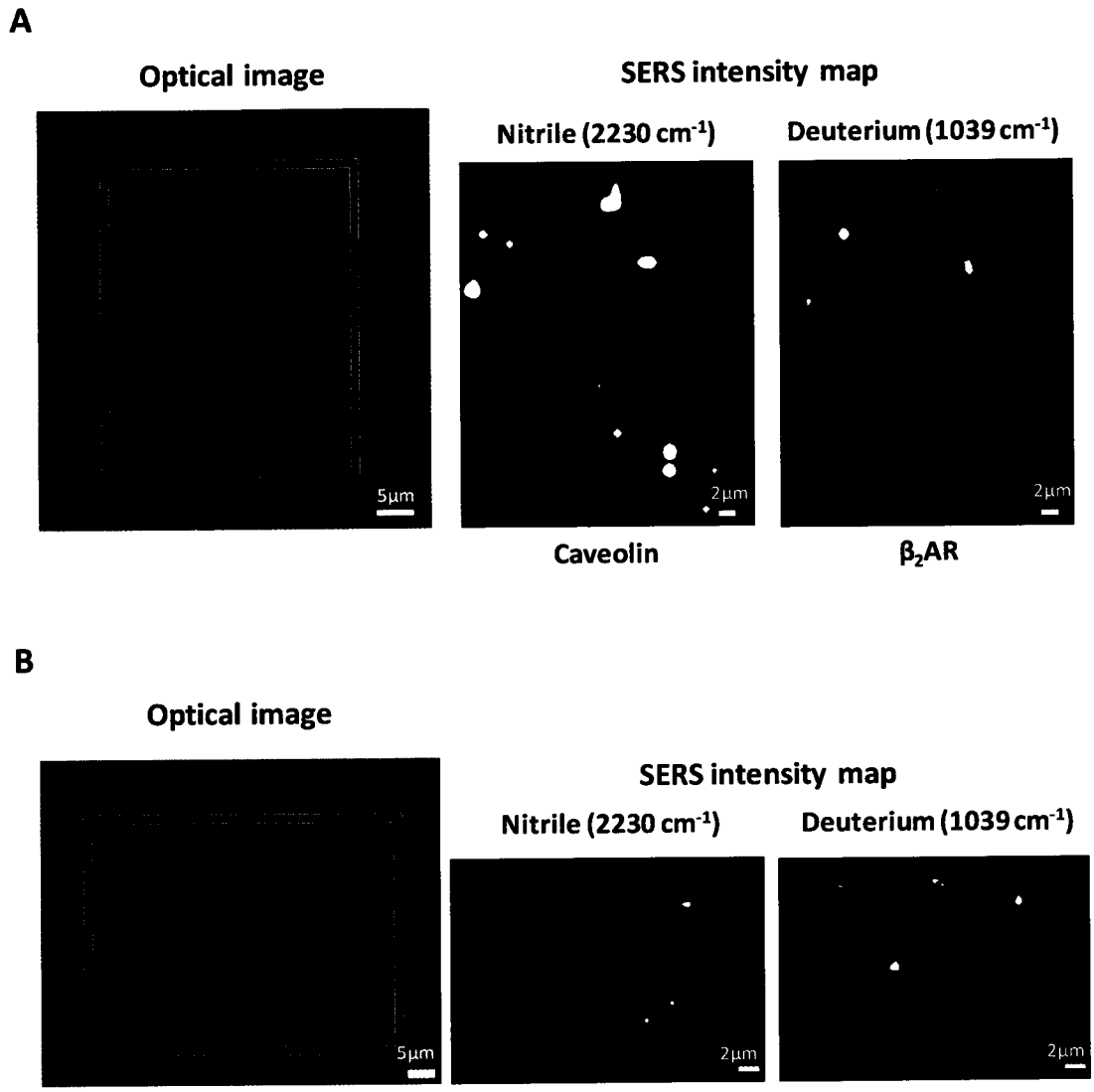

Figure 3.6 Images of cells after NP treatment. **A** H9c2 cell with caveolin and β2AR primary Abs after 24hr treatment with MMBN and DMMB NPs. **B** Negative control. H9c2 cell without primary Ab after 24hr treatment with MMBN and DMMB NPs.

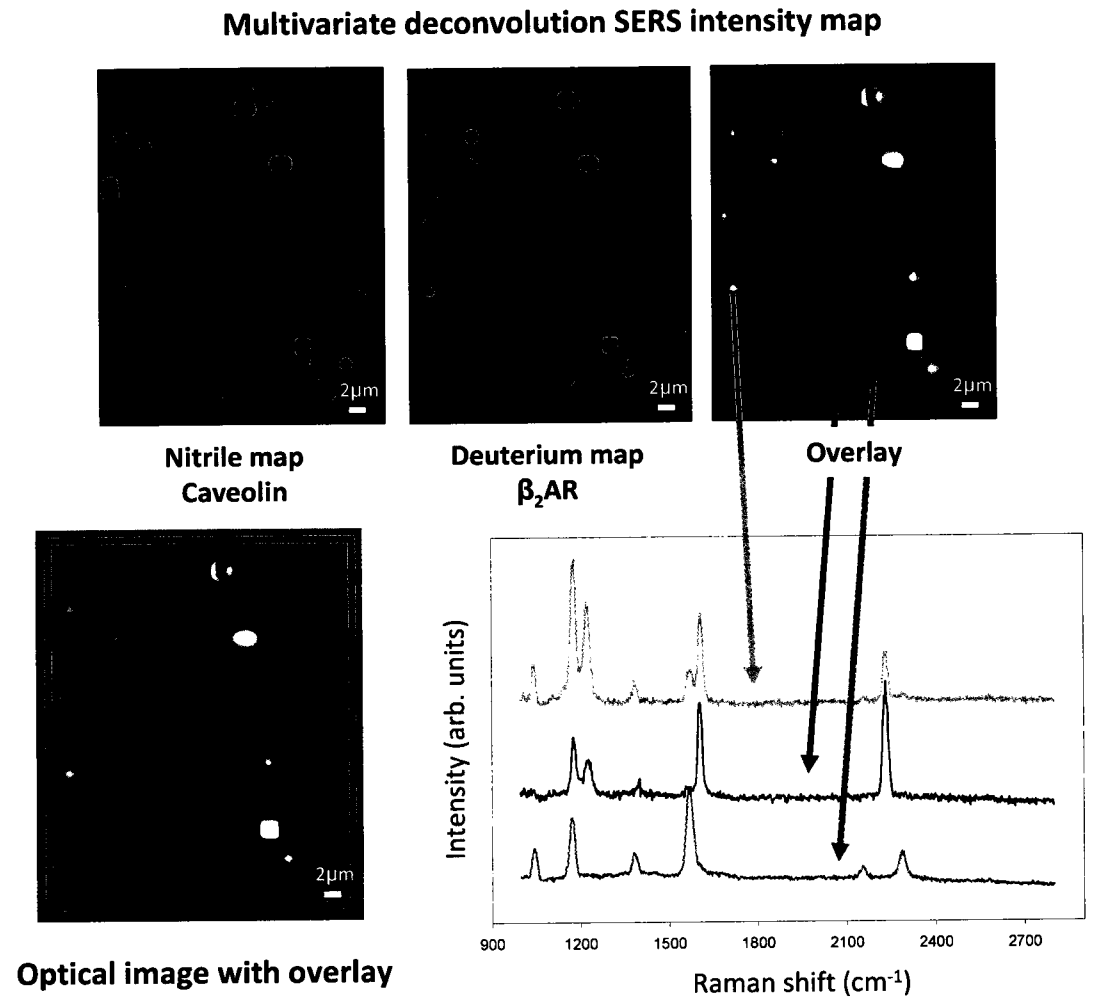

Figure 3.7 Multivarient deconvolution. Areas showing MMBN signature are depicted in red, DMMB signature are depicted in green and areas showing both MMBN and DMMB signatures are depicted in shades of organge (top). Also shown is the overlay plus optical of the same cell and represientive SERS spectra pulled from the image (bottom).

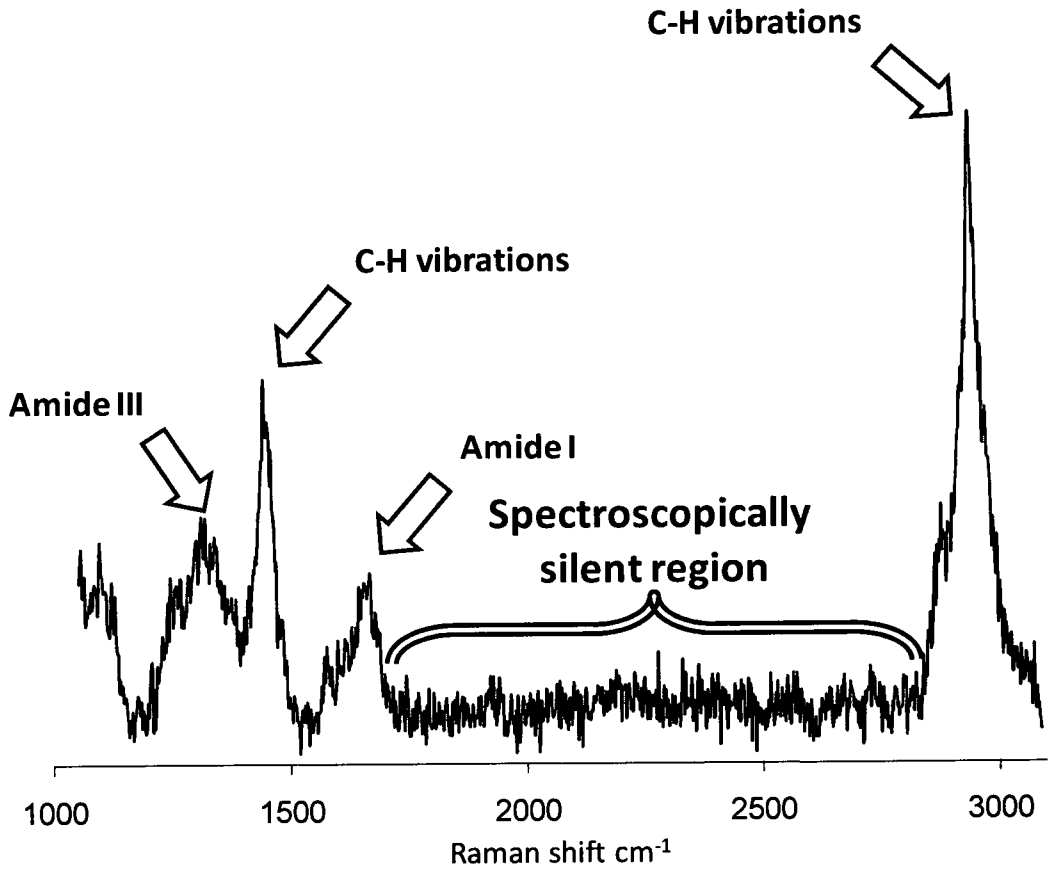

Figure 3.8 Raman spectrum of an H9c2 cell. Highlighted are the amide I and III vibration regions, the C–H vibration regions and the spectroscopically silent region.

unresolvable peaks in the regions between 3050cm^{-1} – 2850cm^{-1} where peaks corresponding to CH vibrations appear, and below 1700cm^{-1} where, among other things, the amide I and III peaks,[19] and peaks corresponding to CH_2 and CH_3 vibrations appear.[19] Fortunately the region between 2850cm^{-1} – 1700cm^{-1} is spectroscopically silent, and thus provides an excellent region for the detection of exogenous Raman reporter signals. Ideally, it is within this spectroscopically silent region that chosen Raman report groups should exhibit characteristic Raman active modes. Lastly, and most importantly, the whole ligand must be inert to the surrounding biological milieu, they must be bioorthogonal. The reporter groups that were chosen included cyano (C≡N), nitro (NO_2), alkyne (C≡C), deuterium (C-D) and boron (C-B).

Previous work from the Pezacki group and others has shown that the cyano reporter provides an good signal for SERS imaging.[15, 16, 20] Initial experiments by the Pezacki group used a ligand where the cyano reporter was located at approximately 3nm (calculated based on the addition of standard bond lengths of crystalline organic compounds[21]) assuming the ligand is protruding directly from the NP (Figure 3.9 A), generating a weak signal.[20] Recent experiments have shown that by using a ligand where the cyano reporter is located closer to the metal NP, such as the benzyl thiol ligands where the Raman reporter is located at a distance of approximately 1nm (Figure 3.9 C), the signal generated is much stronger.[15] This is to be expected since SERS intensity is distance dependant, and follows the following equation,[22]

$$I = \left(\frac{a+r}{a}\right)^{-10}$$

where I is the signal intensity of the Raman reporter, a is the radius of the NP and r is the distance of the Raman reporter from the surface. If this equation is applied to the two previously mentioned reporter ligands, the original 3nm ligand offers an Raman intensity of 0.1.

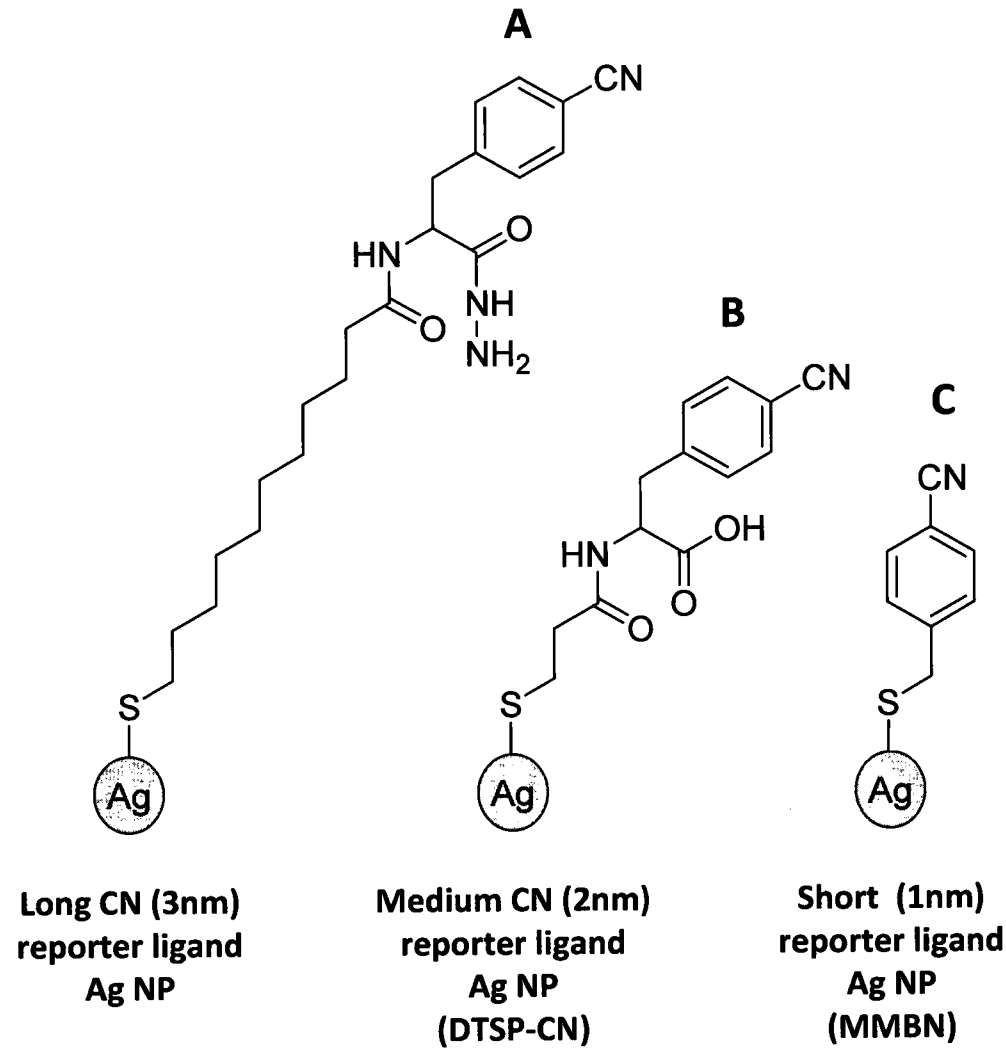

Figure 3.9 Length of different cyano Raman reporter ligands.

With the benzyl thiol ligands, which have the reporter group at a distance of approximately 1nm, the Raman intensity is now 0.5, a 5 fold improvement. Not surprisingly, NPs made with the DTSP based ligands, where the Raman reporter would be approximately 2nm from the metal surface (Figure 3.9 B), provided less intense signals then those made with the benzyl thiol based ligands, with a Raman intensity value of 0.2.

The DTSP based ligands were designed based on the ligands used in previous work. DTSP was used as a short tether and as a means to attach the ligand to the NP surface, through spontaneous reduction of the S–S bond by the NP and formation of a S–Ag bond at the surface.[23] The activated ester was reacted with an amino acid bearing the desired Ramon reporter (with the exception of DTSP-alkyne, which was reacted with propargyl amine) to yield the desired ligand. By using an amino acid, we anticipated being able to attach the Ab used for specific binding directly to the Raman reporter ligand though an amide bond by activating the free carboxylic acid once the ligand was bound the the NP surface. However, attempts to do this were unsuccessful and resulted in the NPs crashing out of solution. Additionally, while the Raman spectra of the DTSP based ligands all had easily resolvable reporter peaks, peaks in the SERS spectra of the NPs with the same ligands were broadened, making them difficult to resolve and diminishing the utility of these NPs for imaging. For the second set of ligands, the backbone structure was further simplified, loading the Raman reporter group closer to the NP surface. For this we used benzyl thiols, with the Raman reporter groups attached at the para position. The Raman spectra of the benzyl thiol based ligands had sharp easily resolvable reporter peaks, and the SERS spectra of the benzyl thiol NPs were equally well defined.

In addition to the Raman reporter ligands, coatings for NPs included DTSP and EG_3SH. DTSP was used as a means to attach the Ab to the NP through its activated carboxylic acid to

various lysine residues found within the Ab.[23] EG_3SH is a water soluble molecule, and was used to enhance the solubility of the NPs in aqueous solutions needed for cellular imaging.[24] The ideal ratio of ligands was determined to be 5:5:2 (EG_3SH : Raman reporter ligand : DTSP) for NPs to be water soluble, yet maintain the maximum Raman signal from the Raman reporter ligand. In addition to these three ligands, once the Ab was in place, to prevent non-specific binding of the NPs to the cell surface, it was necessary for the surface to be further protected using BSA. BSA is a common blocking agent used in many molecular biology techniques (eg. Western blots) to prevent non-specific binding of Abs to surfaces. For our purposes, BSA that was immunoglobulin G (IgG) free had to be used, since it was found that using normal BSA resulted in NPs crashing out of solution. This was attributed to the fact that the IgG found in BSA can cross react with some Abs, especially those derived in goats.

The size of the Ag NPs was also of important consideration. Typical NPs used with SERS range in size from 40-100nm.[25, 26] For single NP detection, 60nm Ag NPs have been shown to be comparable to larger arrays of NPs with respect to their SERS enhancement factors.[2] This large size becomes a problem when trying to image small receptors on the cell surface, since the large size of the NP may prevent binding of other NPs to adjacent receptors. SERS signals for single NPs smaller then 20nm are very difficult to detect as a result of their much weaker surface plasmons. However, if these small NPs become aggregated, coupling between neighboring particles produce an intense SERS signal arising from the plasmon intensity at the NP-NP interface.[27] (Figure 3.10) The Pezacki group has previously studied the β_2AR in cardiomyocytes (cell line H9c2 from rats).[28] These receptors, among other things, help to regulate the beat rate of the heart. Crystal structures of this receptor show that its diameter is roughly 4-5nm and form dimers spanning at least 10nm in diameter. Recently they have shown that small Ag NPs of approximately 15nm can be used to image the aggregation of β_2AR.[15] β_2AR is also known to

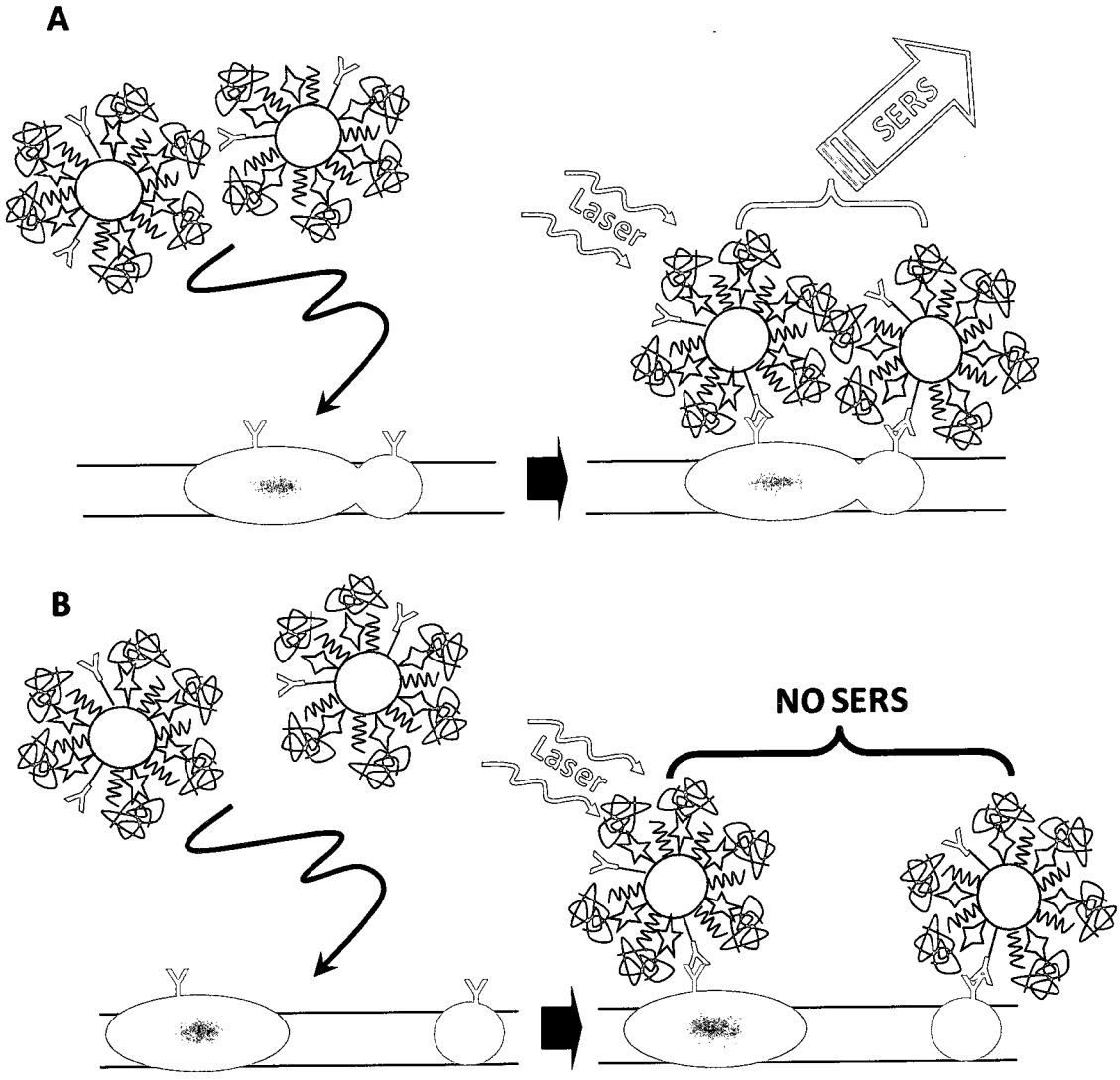

Figure 3.10 Schematic representation of SERS signal. **A** Representation of imaging of clustered receptors. SERS signal is visible because of enhancement gained from the coupling of neighboring NPs. **B** Representation of imaging of non-clustered receptors. SERS signal is negligible.

form signalling platforms with other proteins such as β_1 adrenergic receptors, calcium channels and caveolin. For the initial multiplex imaging experiments, the β_2AR and caveolin proteins were targeted using Ag NPs of approximately 25nm. This larger NP size was chosen in hopes of minimizing the detection of small clusters of these two proteins and only detect larger signalling platforms.

3.2.2 Imaging

The SERS intensity maps generated using the MMBN and DMMB signals, at 2230cm^{-1} and 1039cm^{-1} respectively, show good distribution of the NPs on the cell surface, indicating an even distribution of caveolin and β_2AR, in agreement to previous studies of β_2AR.[15, 28] Multivarient deconvolution using the full SERS spectrum generated by the NPs was used to pull out the weaker signals that are otherwise unresolvable from the background, and thus a more complete map of MMBN and DMMB NP distribution.

ImageJ was used to process the images further in order to try and quantify the amount of colocalization present between the two NPs. Using the multivarient deconvolution maps for MMBN and DMMB, the overlay map and colocalization map, pixel analysis (or voxel analysis) was performed to determine the amount of NPs present in each cell as previously published.[15] An example using the maps from the cell shown in figures 3.6 and 3.7 of the analysis is shown in Table 3.1, however these values vary from cell to cell and so a larger sample number is needed in order to gain any valuable information at the biological level. The total number of voxels assigned to NP signal, determined based on the overlay map, is 19737 which is assigned as 100% of the SERS signal generated by NPs. The number of voxels from the DMMB map is 6189 and from the MMBN map is 18444 relating to 31% and 93% of the SERS signal generate by NPs. Using the colocalization map generated by ImageJ, the number of voxels where both signal from

Table 3.1 Voxel analysis of a representative H9c2 cell

	Number of Voxels	% of Total SERS Signal
Overlay map	19,737	100%
MMBN map	18,444	93%
DMMB map	6,189	31%
Colocolization map	3,193	23%

MMBN and DMMB are present was determined to be 3193 which relates to 23% of the SERS signal generated by NPs.

3.4 Summary and Future Work

These initial experiments have demonstrated that Ag NPs functionalized with different Raman reporter ligands can be utilized to specifically tag and image different receptors within the same cell. Upon initial examination it is possible to see evidence of colocalization of the reporters. This is a promising preliminary result as the tagged receptors are known to associate. More extensive experimentation is currently underway, taking into account the different intensities of the Raman reporter molecules, in order to fully characterize the degree of colocalization determined by SERS. This technique promises to be a useful tool in the study of receptor aggregation.

3.5 References

1. Tripp, R. A.; Dluhy, R. A.; Zhao, Y. P., Novel nanostructures for SERS biosensing. *Nano Today* **2008,** 3, (3-4), 31-37.
2. Anker, J. N.; Hall, W. P.; Lyandres, O.; Shah, N. C.; Zhao, J.; Van Duyne, R. P., Biosensing with plasmonic nanosensors. *Nat. Mater.* **2008,** 7, (6), 442-453.
3. Durr, N. J.; Larson, T.; Smith, D. K.; Korgel, B. A.; Sokolov, K.; Ben-Yakar, A., Two-photon luminescence imaging of cancer cells using molecularly targeted gold nanorods. *Nano. Lett.* **2007,** 7, (4), 941-5.
4. Cao, Y. C.; Jin, R.; Mirkin, C. A., Nanoparticles with Raman Spectroscopic Fingerprints for DNA and RNA Detection. *Science* **2002,** 297, (5586), 1536-1540.
5. Brown, R. J. C.; Milton, M. J. T., Nanostructures and nanostructured substrates for surface - enhanced Raman scattering (SERS). *J. Raman Spectrosc* **2008,** 39, (10), 1313-1326.
6. Kneipp, K.; Wang, Y.; Kneipp, H.; Perelman, L. T.; Itzkan, I.; Dasari, R. R.; Feld, M. S., Single Molecule Detection Using Surface-Enhanced Raman Scattering (SERS). *Phys. Rev. Lett.* **1997,** 78, (9), 1667.
7. Norrod, K. L.; Sudnik, L. M.; Rousell, D.; Rowlen, K. L., Quantitative Comparison of Five SERS Substrates: Sensitivity and Limit of Detection. *Appl. Spectrosc.* **1997,** 51, 994-1001.
8. Weaver, M. J., Surface-enhanced Raman spectroscopy as a versatile *in situ* probe of chemisorption in catalytic electrochemical and gaseous environments. *J. Raman Spectrosc.* **2002,** 33, (5), 309-317.
9. Aroca, R. F.; Alvarez-Puebla, R. A.; Pieczonka, N.; Sanchez-Cortez, S.; Garcia-Ramos, J. V., Surface-enhanced Raman scattering on colloidal nanostructures. *Adv. Colloid Interface Sci.* **2005,** 116, (1-3), 45-61.
10. Sun, Y.; Xia, Y., Mechanistic Study on the Replacement Reaction between Silver Nanostructures and Chloroauric Acid in Aqueous Medium. *J. Am. Chem. Soc.* **2004,** 126, (12), 3892-3901.
11. Bell, S. E. J.; McCourt, M. R., SERS enhancement by aggregated Au colloids: effect of particle size. *Physical Chemistry Chemical Physics* **2009,** 11, (34), 7455-7462.
12. Shanmukh, S.; Jones, L.; Driskell, J.; Zhao, Y.; Dluhy, R.; Tripp, R. A., Rapid and Sensitive Detection of Respiratory Virus Molecular Signatures Using a Silver Nanorod Array SERS Substrate. *Nano Letters* **2006,** 6, (11), 2630-2636.
13. Qian, X. M.; Peng, X. H.; Ansari, D. O.; Yin-Goen, Q.; Chen, G. Z.; Shin, D. M.; Yang, L.; Young, A. N.; Wang, M. D.; Nie, S. M., In vivo tumor targeting and spectroscopic detection with surface-enhanced Raman nanoparticle tags. *Nature Biotechnology* **2008,** 26, (1), 83-90.
14. Michalet, X.; Pinaud, F. F.; Bentolila, L. A.; Tsay, J. M.; Doose, S.; Li, J. J.; Sundaresan, G.; Wu, A. M.; Gambhir, S. S.; Weiss, S., Quantum dots for live cells, in vivo imaging, and diagnostics. *Science* **2005,** 307, (5709), 538-544.
15. Kennedy, D. C.; Tay, L.-L.; Lyn, R. K.; Rouleau, Y.; Hulse, J.; Pezacki, J. P., Nanoscale Aggregation of Cellular β_2-Adrenergic Receptors Measured by Plasmonic Interactions of Functionalized Nanoparticles. *ACS Nano* **2009,** 3, (8), 2329-2339.
16. Skadtchenko, B. O.; Aroca, R., Surface-enhanced Raman scattering of p-nitrothiophenol: Molecular vibrations of its silver salt and the surface complex formed on silver islands and colloids. *Spectrochimica Acta Part A: Molecular and Biomolecular Spectroscopy* **2001,** 57, (5), 1009-1016.

17. Lin-Vien, D.; Colthup, N. B.; Fateley, W. G.; Grasselli, J. G., *The Handbook of infrared and raman characteristic frequencies of organic molecules* Academic Press: Boston :, 1991.
18. Jones, R. N.; Ripley, R. A., Raman Spectra of Deuterated Methyl Laurates and Related Compounds. *Can. J. Chem.* **1964,** 42, (2), 305-325.
19. Peticolas, W. L.; Patapoff, T. W.; Thomas, G. A.; Postlewait, J.; Powell, J. W., Laser Raman Microscopy of Chromosomes in Living Eukaryotic Cells: DNA Polymorphism *In Vivo*. *J. Raman Spectrosc.* **1996,** 27, (8), 571-578.
20. Hu, Q.; Tay, L. L.; Noestheden, M.; Pezacki, J. P., Mammalian cell surface imaging with nitrile-functionalized nanoprobes: biophysical characterization of aggregation and polarization anisotropy in SERS imaging. *J. Am. Chem. Soc.* **2007,** 129, (1), 14-5.
21. Bond Lengths in Crystalline Organic Compounds. In *Handbook of Chemistry and Physics, 89th Edition (internet version 2009)*
Lide, D. R., Ed. CRC Press/Taylor and Francis: Boca Raton, FL.
22. Kennedy, B. J.; Spaeth, S.; Dickey, M.; Carron, K. T., Determination of the distance dependence and experimental effects for modified SERS substrates based on self-assembled monolayers formed using alkanethiols. *J. Phys. Chem. B* **1999,** 103, (18), 3640-3646.
23. Friedrich, M. G.; Kirste, V. U.; Zhu, J.; Gennis, R. B.; Knoll, W.; Naumann, R. L. C., Activity of Membrane Proteins Immobilized on Surfaces as a Function of Packing Density. *J. Phys. Chem. B* **2008,** 112, (10), 3193-3201.
24. Zheng, M.; Davidson, F.; Huang, X., Ethylene glycol monolayer protected nanoparticles for eliminating nonspecific binding with biological molecules. *J. Am. Chem. Soc.* **2003,** 125, (26), 7790-1.
25. Qian, X. M.; Nie, S. M., Single-molecule and single-nanoparticle SERS: from fundamental mechanisms to biomedical applications. *Chemical Society Reviews* **2008,** 37, (5), 912-920.
26. Talley, C. E.; Huser, T. R.; Hollars, C. W.; Jusinski, L.; Laurence, T.; Lane, S. M., In *Nanoparticle Based Surface-Enhanced Raman Spectroscopy*, NATO Advanced Study Institute: Biophotonics, Ottawa, Canada, 2004.
27. Hao, E.; Schatz, G. C., Electromagnetic fields around silver nanoparticles and dimers. *J. Phys. Chem.* **2004,** 120, (1), 357-366.
28. Ianoul, A.; Grant, D. D.; Rouleau, Y.; Bani-Yaghoub, M.; Johnston, L. J.; Pezacki, J. P., Imaging nanometer domains of β-adrenergic receptor complexes on the surface of cardiac myocytes. *Nat. Chem. Biol.* **2005,** 1, (4), 196-202.

Chapter 4: Material and Methods

4.1 Characterization Techniques

4.1.1 Common Techniques

Nuclear Magnetic Resonance Spectroscopy (NMR). Characterization of novel compounds was done using NMR spectroscopy. All experiments were carried out on a Bruker DRX-400 using a frequency of 400.13 MHz for ^{1}H and 100.61 MHz for ^{13}C. Spectra were recorded using a broad band direct detection probe.

High Pressure Liquid Chromatography-Mass Spectrometry/Mass Spectrometry (HPLC-MS/MS). A Waters system consisting of a Waters 996 Photodiode Array Detector, an Alliance HT – Waters 2795 Separations Module, a Waters Micromass $Z_{Q\,2000}$ unit equipped with a pneumatically-assisted electrospray ionisation source was used for HPLC-MS analysis. Samples were run on a Water's Sunfire C18 (100mm x 2.10mm x 3.5µm) column. Standard conditions used, unless otherwise stated, were a gradient of 10-95% acetonitrile/0.1% formic acid in H_2O/0.1% formic acid over 15mins with a flow rate of 0.2mL/min. Eluent was directed first to the diode array detector and then to the mass spectrometer. The source temperature was set at 80°C, desolvation gas temperature was set at 200 C, and an electrospray capillary was set at 3.5kV with a cone voltage set at 10V. For MS analysis, the sample simply bypassed the column and was injected directly into the mass spectrometer. Data were collected in single ion recording mode and processed using Masslynx.

High Pressure Liquid Chromatography (HPLC). HPLC was used in order to follow the conversion of aldehyde to benzoin in solution optimization, as well as to optimize conditions for purification using preprative-HPLC. The system was an Agilent system consisting of quaternary pump, an Agilent 1100 degasser, an auto injector, and a UV/Vis detector set at 254nm. All samples were run on a NovaPak C18, 150mm x 3.9mm x 3.5μm column and data was processed using ChemStation. To follow the conversion of aldehyde to benzoin, a gradient of 10-95% acetonitrile/0.1% trifluroacetic acid in H_2O/0.1% trifluroacetic acid over 15mins with a flow rate of 1mL/min was used.

Gas Chromatography-Mass Spectrometry (GC-MS). GC-MS was used when LC-MS/MS failed to provide any conclusive data. Analysis was performed on an Agilent 6890GC/5975MSD instrument equipped with a HP-5 (Agilent) 30mm x 0.25mm x 0.25μm column. The carrier gas was helium with a constant flow of 1.5ml/min. An autosampler was used to inject 1 μl sample in methanol. The injector temperature was 250°C and split injection mode was used with split ratio 1:50. The CG oven temperature program was: initial temp. 100°C kept for 1 min. then temperature ramp of 10°C/min to 280°C. The MSD detector was working in scan mode with a mass range 40-550 mass units.

4.1.2 Techniques for Chapter 2

Attenuated Total Reflection Fourier Transform Infrared Spectroscopy (ATR-FTIR). ATR-FTIR spectra were recorded using a Nicolet MAGNA-IR 860 spectrometer at $4cm^{-1}$ resolution. The ATR crystals were mounted in a purged sample chamber with the light focused normal to one of the 45° bevels. Background spectra were obtained using a blank surface (oxide surface or H-terminated surface depending on experiment).

X-ray Photoelectron Spectroscopy (XPS). XPS spectra were recorded on a PHI 5500 instrument, using monochromated Al KR (1486eV) radiation with detection on the surface normal. The pressure during analysis was ~5×10^{-8} Torr. Spectra were fitted with Gaussian profiles using standard procedures. The positions of all peaks were normalized to C 1s at 285.0eV.

4.1.3 Techniques for Chapter 3

Cell Culture. H9c2 cells (ATCC, Manassas, VA) were grown in Dulbecco's modified Eagle's medium (Invitrogen, Burlington, ON) supplemented with 10% fetal bovine serum (FBS) (NorthBio, Toronto, ON) under standard culture conditions (37°C, 5% CO_2).

Surface Enhanced Raman Scattering Imaging and Spectroscopy (SERS). Raman spectroscopy and microscopy was acquired with a commercial microRaman system (LabRAM HR, Horiba Jobin Yvon) equipped with a software controlled XYZ stage and a thermal-electric cooled CCD detector. Samples were excited with 632.8nm radiation at a power density of ~10^3W/cm^2. Incident radiation was coupled into an Olympus BX51 optical microscope and focused to ~1μm diameter spot through a 100X objective. The same objective also collects the retro-reflected radiation and guides it to a notch filter which removes the Rayleigh radiation. In the Raman mapping experiments, a fine set of grid points within an area of interest is defined in the software and imaged by raster the sample under the tightly focused laser beam. At each of the grid point, a full Raman spectrum was acquired. The Raman spectra of ligands (Figure 3.2 A and 3.2 B) were generated with 4 second acquisition time (5 accumulation) with a power density of 10^5W/cm^2. The SERS spectra of the DTSP ligand NPs (Figure 3.4 A) were generated with 1 second acquisition time (2 accumulations) with a power density of 10^3W/cm^2 and for the benzyl thiol ligand NPs (Figure 3.4 B), with 10 second acquisition time (4 accumulations) with a power density of 10^3W/cm^2. The SERS image of the NP treated cell were generated with 1 second

acquisition time (2 accumulations) with a power density of $10^3 W/cm^2$ Upon completion of the mapping, Raman intensity map of the C≡N and C-D vibrational modes are generated by fitting and removing the associated background for each spectrum in the predefined spatial grid. The C≡N and C-D intensities are displayed as thermal maps (Figure 3.6). This is achieved by the Labspec 5.25 software (Horiba Jobin Yvon). Multivariate deconvolution (Figure 3.7) was achieved using the classic least square algorithm. This is done by first assigning the orthonormal model spectra (e.g. cyano and deuterium). Each spectrum in the map data set is then treated as the linear combination of the two model components. The algorism then assigns a different colour to each pure component. This is then displayed as a thermal map.

3.2 Synthetic Methods and Experimental Design

3.2.1 for Chapter 2

Silicon elements (H-terminated)

Cleaning and Hydrogen termination. ATR elements were cleaned with piranha solution (3:1 H_2SO_4, 96% : H_2O_2, 30%) at 120°C for 20 minutes, then rinsed with Milli-Q water. (*Warning: Piranha solutions should be handled with care and kept isolated from organic materials).* Samples were hydrogen terminated by etching in degassed ammonium fluoride for 15 minutes followed by a brief rinse in degassed Milli-Q water.

Direct attachment aldehyde: Monolayer Formation. A 0.2M solution of terephthalaldehyde in toluene was degassed by bubbling with argon in a glass Schlenck tube for 10 minutes the ATR element was added and the solution heated at 90°C for 1 hour. The solution was cooled to room temperature and the ATR element removed and washed with tetrachloroethylene in a Soxhlet Extractor for 15-20 minutes.

Amide linker: Monolayer Formation. Undecylenic acid was distilled and transferred to a Schlenck tube and degassed with argon. The hydrogen terminated ATR element was added to the Schlenck tube and degassed a further 10 minutes at which time it was reacted for 90 minutes under slow bubbling argon in a rayonnet photoreactor (300nm bulbs). The sample was removed and washed thoroughly with 1,1,2-trichloroethane and dried under a stream of nitrogen.

Amide linker: EDC Activation. EDC (120mg) and NHS (80mg) were dissolved in 10mL of Milli-Q water and the sample immersed in this solution for 1 hour. The ATR element was removed washed with Milli-Q water and 1,1,2-trichloroethane then dried under a stream of nitrogen.

Amide linker: Amide Formation. The NHS activated surface was immersed in a DMF solution of the amine for 2 hours, then rinsed with DMF and 1,1,2-trichloroethane and dried under a stream of nitrogen.

Amide linker: Acetal hydrolysis. The ATR element was placed in a solution of 10% sulfuric acid for 2 hours then washed with Milli-Q water and 1,1,2-trichloroethane then dried under a stream of nitrogen.

Silicon oxide elements

Cleaning. ATR elements were cleaned with piranha solution (3:1 H_2SO_4, 96% : H_2O_2, 30%) at 120°C for 20 minutes, then rinsed with Milli-Q water. (*Warning: Piranha solutions should be handled with care and kept isolated from organic materials).*

Imine linker: Functionalization with aldehyde. The ATR element was exposed to APTES for 10 minutes at room temperature. Once the free amine layer has been formed, the ATR element was washed by sonicating in ethanol for 10 seconds followed by rinsing with ethanol and placed in a 1mM solution of terephthalaldehyde in Milli-Q water for 30 minutes at room temperature.

The ATR element was then removed from solution and washed by sonicating in ethanol for 10 seconds followed by rinsing with ethanol.

Benzoin condensation on surface (general procedure). In 1mL of distilled water, 0.1mmol of catalyst was dissolved to which triethylamine (TEA) (27μL, 0.2mmol (with thiamine) or 18μL, 0.1mmol (with imidazolium catalyst)) was added. Para-substituted-benzaldehyde (0.1mmol) was added and the solution was thoroughly mixed to form an emulsion. The aromatic-aldehyde terminated ATR element was immersed in the solution and gently shaken. Reaction progression was monitored by ATR-FTIR. Gentle to vigorous washing was used as needed before scans to remove any non-covalently bound material.

Methoxybenzoins. Distributed among 4 1.5mL eppendorf vials, thiamine chloride hydrochloride (328mg, 0.984mmol) was dissolved in distilled water (2.4mL) along with triethylamine (280μL, 1.968mmol). *4*-methoxybenzaldehye (160μL, 0.984mmol) and benzaldehyde (120μL, 0.984mmol) were added to the solution and shaken vigorously to form an emulsion. The vials were then placed in a centrifuge and spun for 3 days at 1400rpm. The reactions were combined and 10mL of water and 10mL of ethyl acetate were added. The organic phase was isolate and the aqueous phase extracted and extracted 2 times with 10mL of ethyl acetate. The organic fractions were combined, dried with magnesium sulphate and concentrated. The resulting oil was purified by silica gel chromatography (SiO_2, 4 : 1 hexanes : ethyl acetate, Rf = 0.32) to isolate the desired benzoin product as a mixture of regioisomers (3:1 based on NMR). The isomers were then separated by preparative HPLC (NovaPak C18 19mm x 30mm, iso 30% MeCN in H_2O, 20 min) in 41 % total isolated yield.

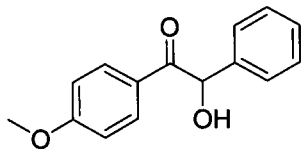

2-Hydroxy-1-(4-methoxy-phenyl)-2-phenyl-ethanone.[1] 20mg (33% yield). ^{1}H NMR (400 MHz, *CDCl$_3$*) δ ppm 7.93 (2 H, d, J 9.0), 7.39 – 7.25 (5 H, m), 6.88 (2 H, d, J 9.0), 5.91 (1 H, d, J 5.8), 4.67 (1 H, d, J 6.0), 3.84 (3 H, s). MS (pos. ESI, M+1) *m/z* 243.

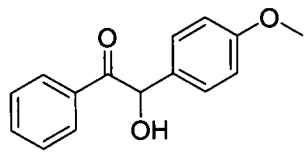

2-Hydroxy-2-(4-methoxy-phenyl)-1-phenyl-ethanone.[1] 8mg (8% yield). ^{1}H NMR (400 MHz, *CDCl$_3$*) δ ppm 8.00 – 7.86 (2 H, m), 7.54 (1 H, dd, J 4.3, 10.5), 7.42 (2 H, t, J 7.7), 7.30 – 7.24 (3 H, m), 6.87 (2 H, d, J 8.7), 5.93 (1 H, d, J 6.0), 4.50 (1 H, d, J 6.0), 3.78 (3 H, s). MS (pos. ESI, M+1) *m/z* 243.

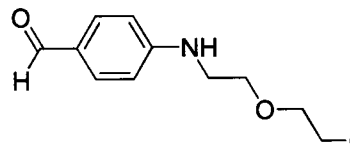

4-[2-(2-Hydroxy-ethoxy)-ethylamino]-benzaldehyde.[2] A mixture of 4-bromobenzaldehyde (925mg, 5mmol), 2-(2-amino-ethoxy)-ethanol (725µL, 7.5mmol), K_2CO_3 (1.38g, 10mmol), CuI (95mg, 0.5mmol), and L-proline (23mg, 1mmol) in 3mL of DMF (dry) was heated to 80°C for 48 hours in a sealed flask, under Ar. The cooled mixture was diluted with ethyl acetate and water. The organic layer was separated, and the aqueous layer was extracted with ethyl acetate. The combined organic layers were washed with brine, dried over Na_2SO_4, and concentrated. The residual oil was loaded on a silica gel column and eluted ethyl acetate to afford 200mg of the corresponding aniline (19% yield). ^{1}H (400 MHz, *CDCl$_3$*) δ ppm 9.75 (1 H, s), 7.72 (2 H, d, J 8.7), 6.66 (2 H, d, J 8.7), 4.80 (1 H, s), 3.80 (2 H, s), 3.78 – 3.72 (2 H, m), 3.69 – 3.57 (2 H, m), 3.44 (2 H, q, J 5.3), 2.01 (1 H, s). ^{13}C (100 MHz, *CDCl$_3$*) δ ppm 190.56

(CH), 153.45 (C), 132.54 (CH), 126.90 (C), 112.19 (CH), 72.49 (CH_2), 69.44 (CH_2), 62.01 (CH_2), 43.04 (CH_2). MS (pos. ESI, M+1) *m/z* 210.3, (neg. ESI, M-1) *m/z* 208.3.

4.3.2 for Chapter 3

General procedure for DTSP-based ligands.[3] In a 4ml vial, DTSP (1mol eq) was added to a mixture of the amine (2mol eq) and Na_2CO_3 (2mol eq) in acetonitrile/H_2O (1:1). The reaction was stirred at 50°C and monitored by LC-MS. Once complete (1 - 12 hours) the reaction was cooled to 0°C and acidified with HCl (1M aq). The resulting suspension was stirred at 0°C for 30 min and the precipitate collected and washed with water. If no precipitate was formed, the reaction was extracted twice with ethyl acetate and once with brine solution. The organic layers were combined, dried over magnesium sulphate and the solvent was removed by rotary evaporation to afford the product.

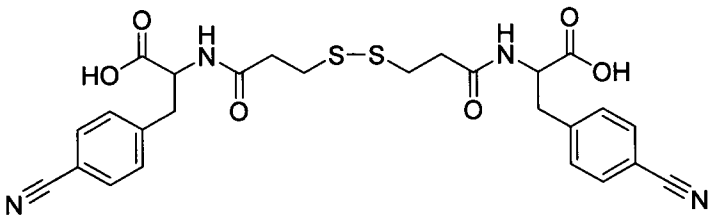

DTSP-PheCN. 32mg of white powder (26% yeild). ^{1}H NMR (400 MHz, *$CDCl_3$*) δ ppm 12.81 (s, 2 H), 8.34 (d, *J*=8.20 Hz, 2 H), 7.73 (d, *J*=8.17 Hz, 4 H), 7.42 (d, *J*=8.18 Hz, 4 H), 4.48 (dt, *J*=4.96, 9.09, 8.95 Hz, 2 H), 3.15 (dd, *J*=4.91, 13.71 Hz, 2 H), 2.93 (dd, *J*=9.62, 13.72 Hz, 2 H), 2.76 (t, *J*=7.01, 7.01 Hz, 4 H), 2.43 (dt, *J*=3.64, 7.18, 7.45 Hz, 4 H). ^{13}C NMR (101 MHz, *d_6DMSO*) δ ppm 172.46 (2 C), 169.95 (2 C) 143.59 (2 C), 131.92 (4 CH), 130.17 (4 CH), 118.82 (2 CN), 109.21 (2 C), 52.75 (2 C), 36.69 (2 CH_2), 34.58 (2 CH_2), 33.45 (2 CH_2). MS (pos. ESI, M+1) *m/z* 555, (neg ESI, M-1) *m/z* 553.

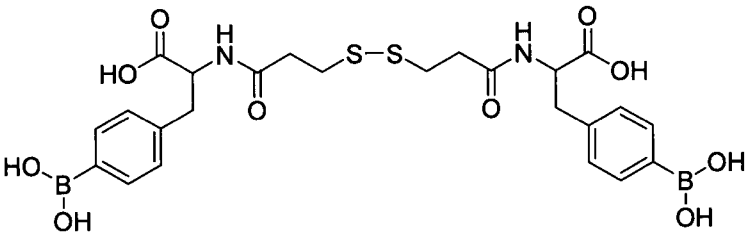

DTSP-boron$_2$. 97mg of white powder (66% yield). ^{1}H NMR (400 MHz, *d_6DMSO*) δ ppm 7.68 (d, *J*=8.00 Hz, 4 H), 7.29 (d, *J*=8.02 Hz, 4 H), 4.70 (m, 1 H), 3.29 (dd, *J*=4.82, 13.95 Hz, 2 H), 2.99 (dd, *J*=8.95, 12.97 Hz, 2 H), 2.69 (t, *J*=7.00, 7.00 Hz, 1 H), 2.54 (t, *J*=6.93, 6.93 Hz, 4 H). ^{13}C NMR (101 MHz, *d_6DMSO*) δ ppm 175.47 (2 C), 174.14 (2 C) 139.93 (2 C), 134.27(4 CH), 129.08(4 CH), 104.00(2 CB), 54.22 (2 C), 37.01 (2 CH_2), 34.63 (2 CH_2), 33.07 (2 CH_2). MS (neg. ESI, M-1) *m/z* 591.

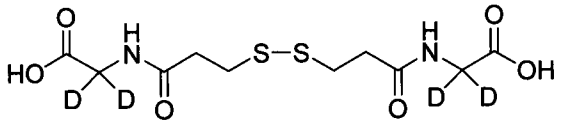

DTSP-d_2Gly. 28mg of white powder (34% yield). ^{1}H NMR (400 MHz, *d_6DMSO*) δ ppm 12.53 (s, 2 H), 8.27 (s, 2 H), 2.90 (t, *J*=7.23, 7.23 Hz, 4 H), 2.55 (d, *J*=7.23 Hz, 4 H). ^{13}C NMR (101 MHz, *d_6DMSO*) δ ppm 171.17 (2 C), 170.36 (2 C), 39.64 (m, 2 CD_2), 34.62 (2 CH_2), 33.57 (2 CH_2). MS (pos. ESI, M+1) *m/z* 329, (neg. ESI, M-1) *m/z* 327.

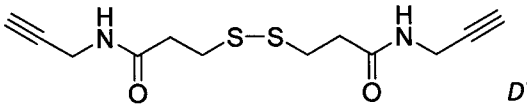

DTSP-alkyne. 3mg white powder (8% yield). ^{1}H NMR (400MHz, *d_6DMSO*) δ ppm 8.39 (t, J=5.12, 5.12 Hz, 2 H), 3.86 (dd, J=2.51, 5.44 Hz, 4 H), 3.11 (t, J=2.50, 2.50 Hz, 2 H), 2.88 (t, J=7.15, 7.15 Hz, 4 H), 2.48 (m, 4 H). ^{13}C NMR (100 MHz, *d_6DMSO*) δ ppm 172.56 (2 C), 80.97 (2 C), 72.93 (2 CH), 34.57 (2 CH_2), 33.50 (2 CH_2), 32.89 (2 CH_2). MS (neg. ESI, M-1) *m/z* 283.

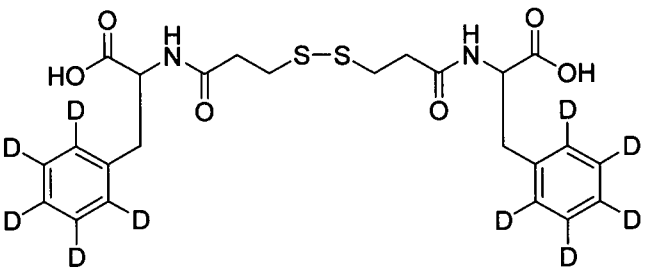

DTSP-d_5Phe. 100mg of yellow powder (77% yield). ^{1}H NMR (400 MHz, *d_6DMSO*) δ ppm 12.70 (s, 2 H), 8.29 (d, *J*=8.06 Hz, 2 H), 4.42 (dt, *J*=5.15, 8.72, 8.60 Hz, 2 H), 3.04 (dd, *J*=4.98, 13.78 Hz, 2 H), 2.85 (dd, *J*=9.48, 13.71 Hz, 2 H), 2.76 (t, *J*=7.06, 7.06 Hz, 4 H). ^{13}C NMR (101 MHz, *d_6DMSO*) δ ppm 172.86 (2 C), 169.94 (2 C), 137.27 (2 C), 128.57 (t, J_{CD}=24.45, 22.68 Hz,4 CD), 127.56 (t, J_{CD}=27.41, 21.28 Hz,4 CD), 125.83 (m, 2 CD), 53.36 (2 C), 36.62 (2 CH_2), 34.66 (2 CH_2), 33.55 (2 CH_2). MS (pos. ESI, M+1) *m/z* 515, (neg ESI, M-1) *m/z* 513.

General procedure for benzyl thiol based ligands.[4] In a small round bottom flask the benzyl chloride (1mol eq) was dissolved in ethanol and heated to 50°C. Thiourea (1mol eq) was added and the reaction as stirred vigorously overnight and left to cool to room temperature. The solid was filtered off and dissolved in water, if no precipitate was formed, the solvent was evaporated by rotary evaporation, and the resulting solid was dissolved in water. Na_2CO_3 was added until the reaction was basic (pH ~ 8). The resulting precipitate was then filtered and dissolved in 0.2M NaOH. The insoluble sulfide was filtered, and the filtrate was acidified with 1M HCl. The resulting precipitate was collected.

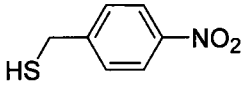

MMBNO.[5] 95mg of white powder (19% yield). ^{1}H NMR (400 MHz, *$CDCl_3$*) δ ppm 8.19 (d, J=8.72 Hz, 2 H), 7.50 (d, J=8.70 Hz, 2 H), 3.82 (d, J=6.62 Hz, 2 H), 1.83 (t, J=7.66, 7.66 Hz, 1 H). MS (neg ESI, M-1) *m/z* 168.

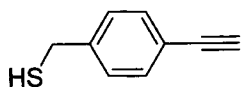

MMByne. 65mg of yellow oil (33% yield). ^{1}H NMR (400 MHz, *CDCl$_3$*) δ ppm 7.47 (d, *J*=8.11 Hz, 2 H), 7.20 (d, *J*=8.13 Hz, 2 H), 3.61 (s, 2 H), 3.11 (s, 1 H). MS (EI, M) *m/z* 148.

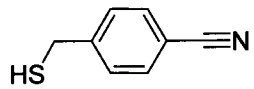

MMBN.[6] 44mg of white powder (90% yield). ^{1}H *NMR (400 MHz, CDCl$_3$)* δ ppm 7.61 (d, J=8.20 Hz, 2 H), 7.44 (d, J=8.17 Hz, 2 H), 3.77 (d, J=7.87 Hz, 2 H), 1.80 (t, J=7.87, 7.87 Hz, 1 H). MS (neg ESI, M-1) *m/z* 148.

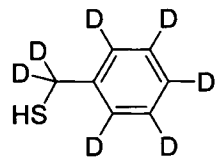

DMMB.[7] 13mg of yellow oil (32% yield). ^{2}H NMR (400 MHz, CH_2Cl_2) δ ppm 7.35 (m, 5H), 3.71 (s, 2H). MS (EI, M) *m/z* 131.

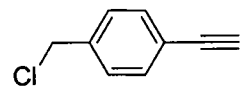

Ethynyl benzyl chloride.[8] Ethynylbenzyl alcohol (198mg, 1.5mmol) and pyridine (324μL, 4mmol) were combined in dichloromethane and slowly added to $SOCl_2$ (182μL, 2.5mmol) at 0°C. The reaction mixture was brought to room temperature and left to stir overnight. Once the reaction was complete, the solution was diluted with dichloromethane and washed twice with HCl (0.2M aq), twice with $NaHCO_3$ (saturated solution aq) and once with brine solution. The organic phase was dried over magnesium sulphate and concentrated by rotary evaporation. The resulting oil was purified by flash chromatography (9:1 hexanes : ethyl acetate) to afford the 35 mg (16% yield) of yellow oil. ^{1}H NMR (400 MHz, *CDCl$_3$*) δ ppm 7.49 (d, *J*=8.27 Hz, 2 H), 7.35 (d, *J*=8.33 Hz, 2 H), 4.57 (s, 2 H), 3.10 (s, 1 H). MS (EI, M) *m/z* 150.

Nanoparticle synthesis. To 1mL of Ag NP solution in a 4mL glass vial, was added 100μL of 50mM sodium borate buffer solution (pH 9). After mixing, the following was added sequentially: 2μL

DTSP 2mM solution, 5µL Raman reporter ligand 2mM solution and 5µL EG_3SH 2mM solution. The reaction was stirred vigorously at room temperature. After 4 hours, 40µL of secondary Ab (either donkey anti goat or donkey anti rabbit) and 100µL of 50mM sodium borate buffer solution (pH 9) was added and left over night (16 - 20 hours) at 4°C. After incubation with the secondary Ab, the solution was brought to room temperature and 30µL of 30% BSA (IgG and protease free) was added and left for 30 min. The solution was transferred to 1.5mL plastic eppendorf tubes and spun at 13.2Krpm for 10 min to form a pellet. The supernatant was removed and the pellet was resuspended in 1mL PBS. The NP solution was used as is for labelling experiments.

Sample preparation for labelling experiments. Silicon wafers with fixed H9c2 cells were distributed into wells of a 12 well plate. In one well, 1mL of PBS was followed by 4µL of each primary Ab (β_2AR and caveolin) and left to incubate for 24 hours at 4°C. After 24 hours, the solution was removed and the wafer rinsed twice with PBS. 500µL of mixed NP solution was added to wafer and left to incubate at 4°C for 24hrs. After 24 hours, the solution was removed and the wafer thoroughly rinsed with PBS. Three controls were also run. In the first the primary Ab treatment was omitted. In the second, treatment with the caveolin primary Ab (from goat) was omitted and the wafer was treated only with the NPs carrying the anti-rabbit secondary Ab. In the third, the opposite was carried out where treatment with the β_2AR primary Ab (from rabbit) was omitted and the wafer was treated only with the NPs carrying the anti-goat secondary Ab.

4. 4 Refrences

1. Linghu, X.; Potnick, J. R.; Johnson, J. S., Metallophosphites as Umpolung Catalysts: The Enantioselective Cross Silyl Benzoin Reaction. *Journal of the American Chemical Society* **2004,** 126, (10), 3070-3071.

2. Zhang, H.; Cai, Q.; Ma, D., Amino Acid Promoted CuI-Catalyzed Câˆ'N Bond Formation between Aryl Halides and Amines or N-Containing Heterocycles. *The Journal of Organic Chemistry* **2005,** 70, (13), 5164-5173.

3. Gong, Y.; Barbay, J. K.; Dyatkin, A. B.; Miskowski, T. A.; Kimball, E. S.; Prouty, S. M.; Fisher, M. C.; Santulli, R. J.; Schneider, C. R.; Wallace, N. H.; Ballentine, S. A.; Hageman, W. E.; Masucci, J. A.; Maryanoff, B. E.; Damiano, B. P.; Andrade-Gordon, P.; Hlasta, D. J.; Hornby, P. J.; He, W., Synthesis and Biological Evaluation of Novel Pyridazinone-Based α4 Integrin Receptor Antagonists. *Journal of Medicinal Chemistry* **2006,** 49, (11), 3402-3411.

4. Natarajan, J. K.; Alumasa, J. N.; Yearick, K.; Ekoue-Kovi, K. A.; Casabianca, L. B.; de Dios, A. C.; Wolf, C.; Roepe, P. D., 4-N-, 4-S-, and 4-O-Chloroquine Analogues: Influence of Side Chain Length and Quinolyl Nitrogen pKa on Activity vs Chloroquine Resistant Malaria. *Journal of Medicinal Chemistry* **2008,** 51, (12), 3466-3479.

5. Turos, E.; Revell, K. D.; Ramaraju, P.; Gergeres, D. A.; Greenhalgh, K.; Young, A.; Sathyanarayan, N.; Dickey, S.; Lim, D.; Alhamadsheh, M. M.; Reynolds, K., Unsymmetric aryl-alkyl disulfide growth inhibitors of methicillin-resistant Staphylococcus aureus and Bacillus anthracis. *Bioorganic & Medicinal Chemistry* **2008,** 16, (13), 6501-6508.

6. Szafranski, C. A.; Tanner, W.; Laibinis, P. E.; Garrell, R. L., Surface-Enhanced Raman Spectroscopy of Aromatic Thiols and Disulfides on Gold Electrodes. *Langmuir* **1998,** 14, (13), 3570-3579.

7. Hsu-Shan, H.; Wolfgang, W.; Klaus, K. M., Electron-impact Induced and Thermal Decomposition of Dithranol Derivatives, II: Multiple H-Rearrangements in 10-Benzylthio-dithranol Radical Cations *Arch. Pharm.* **1994,** 327, (11), 735-738.

8. Wu, L.-Y.; Yan, Z.-Y.; Xie, Y.-X.; Niu, Y.-N.; Liang, Y.-M., Ionic-liquid-supported organocatalyst for the enantioselective Michael addition of ketones to nitroolefins. *Tetrahedron: Asymmetry* **2007,** 18, (17), 2086-2090.

Appendix A

FT-IR of 4-methoxybenzaldehyde and therphthaldialdehyde on SiO_2.